Chapter 1

Introduction

In this introductory chapter, we present a brief overview on the current knowledge on neutrino physics. In section 1.1, we discuss the present status of neutrino physics. In section 1.2 and 1.3, we summarise the theory related to the neutrino masses and mixing. Then a short account of neutrino oscillations in vacuum as well as in medium, followed by a review on solar, atmospheric, accelerator and reactor type neutrino experiments, are presented in sections 1.4 – 1.7.

1.1 Present Status of Neutrino Physics

In the last 20 years of research in the field of neutrino physics, there has been an immense improvement in our knowledge of neutrino physics. Neutrino was first introduced by Wolfram Pauli in 1930 to explain the continuous electron energy distribution in nuclear beta decay. At first, it was assumed that neutrinos are massless. But, after the discovery of neutrino ocsillation phenomena by Pontecorvo in 1957 [1, 2], the neutrino physics has drastically changed. The osclillation phenomena provides that neutrinos are massive and they are mixed during propagation. In the year 1988, muon neutrinos were discovered in Kamiokande [3] and IMB experiments [4] and the

model-independent confirmation of atmospheric muon neutrinos oscillation was given by Super-Kamiokande experiment in 1998. At the end of 2002, the first result of the K2K long-baseline accelarator experiment [5] has provied the values of the neutrino mixing parameters that generate atmospheric neutrino oscillations [6].

In the year 2000, the combined results of the two experiments SNO [7] and Super-Kamiokande [8] gave the model-independent verification of the oscillations of solar electron neutrinos and the values of the solar neutrino mixing parameters were provied by the KamLAND very-long-baseline reactor experiment [9] at the end of 2002. This experiment measures a disappearance of electron anti-neutrinos due to oscillations.

In the Standard Model, the neutrinos were introduced as massless fermions. Thus, no gauge invariant renormalizable mass term can be formulated for neutrinos. Therefore, in the standard model there is no hope of either mixing or CP-violation in the leptonic sector. As a result, the experimental affirmation for neutrino masses and mixings hints towards a new kind of physics. In this chapter, we review the phenomenology of three neutrino masses and mixing based on neutrino oscillation phenomena and also discuss the theory to describe the neutrino masses.

1.2 Neutrino in the Standard Model

The Standard Model (SM) of particle physics is a spontaneously broken Yang-Mills quantum field theory describing the strong, weak and electromagnetic interactions connected by the gauge groups $SU(3), SU(2)$ and $U(1)$ [10]:

$$G_{SM} = SU(3)_C \times SU(2)_L \times U(1)_Y \tag{1.2.1}$$

with three matter fermion generations. The subscripts C, L, Y imply color, left-handed chiral group and the hypercharge.

Each generation comprises of five different representations of the gauge groups given by:

$$(1, 2, -\frac{1}{2}), \qquad (3, 2, \frac{1}{6}), \qquad (1, 1, -1), \qquad (3, 1, \frac{2}{3}), \qquad (3, 1, -\frac{1}{3}) \tag{1.2.2}$$

where the numbers in the parenthesis represent the transformation properties of the particles under G_{SM} (1.2.1). The matter content is listed in Table 1.1.

$L_L(1, 2, -\frac{1}{2})$	$Q_L(3, 2, \frac{1}{6})$	$E_R(1, 1, -1)$	$U_R(3, 1, \frac{2}{3})$	$D_R(3, 1, -\frac{1}{3})$
$\begin{pmatrix} \nu_e \\ e \end{pmatrix}_L$	$\begin{pmatrix} u \\ d \end{pmatrix}_L$	e_R	u_R	d_R
$\begin{pmatrix} \nu_\mu \\ \mu \end{pmatrix}_L$	$\begin{pmatrix} c \\ s \end{pmatrix}_L$	μ_R	c_R	s_R
$\begin{pmatrix} \nu_\tau \\ \tau \end{pmatrix}_L$	$\begin{pmatrix} t \\ b \end{pmatrix}_L$	τ_R	t_R	b_R

Table 1.1: SM matter contents [10]

Furthermore, the model also contains a single Higgs boson doublet H, whose transformation properties are given as:

$$H = \begin{pmatrix} H^+ \\ H^0 \end{pmatrix} \sim (1, 2, \frac{1}{2}) \tag{1.2.3}$$

The vacuum expectation value of this Higgs field breaks the gauge symmetry,

$$\langle H \rangle = \begin{pmatrix} 0 \\ \frac{v}{\sqrt{2}} \end{pmatrix} \Longrightarrow G_{SM} \longrightarrow SU(3)_C \times U(1)_{EM} \tag{1.2.4}$$

The Higgs boson was the only missing piece of the SM. But, in March 2013, the LHC experiment has confirmed the existence of Higgs boson [11] for which Peter Higgs and François Englert, were awarded the Nobel Prize in Physics.

It can be clearly seen from Table 1.1 that the neutrinos which are categorized as fermions do not undergo strong or electromagnetic interactions. Only active neutrinos show weak interactions i.e. they are singlets of $SU(3)_C \times U(1)_{EM}$ whereas they are not singlets of $SU(2)_L$.

As mentioned above, the SM has three active neutrinos ν_e, ν_μ and ν_τ with their anti-partners. The e, μ and τ are called as the charged-lepton mass eigenstates and ν_e, ν_μ and ν_τ are the $SU(2)$ partners of these mass eigenstates. The weak charged current (CC) interactions between the neutrinos and their corresponding charged leptons are given by,

$$-\mathscr{L}_{CC} = \frac{g}{\sqrt{2}} \sum_l \bar{\nu_{Ll}} \gamma_\mu l_L^- W_\mu^+ + H.C. \tag{1.2.5}$$

Beside this, the SM neutrinos have neutral-current (NC) interactions,

$$-\mathscr{L}_{NC} = \frac{g}{2cos\theta_W} \sum_l \bar{\nu_{Ll}} \gamma_\mu \nu_{Ll} Z_\mu^0 \tag{1.2.6}$$

These two Eqs. (1.2.5) and (1.2.6) are sufficient to describe all the neutrino interactions within the SM. From Eq. (1.2.6), we can easily determine the decay width of the Z^0 boson into neutrinos. This decay width is proportional to the number of light left-handed neutrinos which indicates the existence of only three light active neutrinos in the SM.

Another salient feature of the SM is that the SM with the gauge symmetry of Eq. (1.2.1) and the particle content of Table 1.1 follows an accidental global symmetry:

$$G_{SM}^{global} = U(1)_B \times U(1)_{L_e} \times U(1)_{L_\mu} \times U(1)_{L_\tau} \tag{1.2.7}$$

Here $U(1)_B$ is the symmetry in th baryon number and $U(1)_{L_{(e,\mu,\tau)}}$ are the symmetries of the three lepton flavor with total lepton number $L = \sum_i L_i$, where $i = e, \mu, \tau$. This symmetry is termed as accidental symmetry because nobody is imposing this symmetry. It is a result of the gauge symmetry and the representations of the physical states.

In the SM, fermions get masses from the Yukawa interactions in which a right-handed fermion couples with its left-handed doublet and Higgs field. The Yukawa Lagrangian is given by,

$$-\mathscr{L}_{Yukawa} = Y^d_{ij}\bar{Q_{Li}}HD_{Rj} + Y^u_{ij}\bar{Q_{Li}}\tilde{H}U_{Rj} + Y^l_{ij}\bar{L_{Li}}HE_{Rj} + H.C. \tag{1.2.8}$$

where $\tilde{H} = i\tau_2 H^*$. After spontaneous symmetry breaking , the fermions get masses

$$m^f_{ij} = Y^f_{ij}\frac{v}{\sqrt{2}} \tag{1.2.9}$$

Since there is no right-handed neutrinos in this model and hence the Yukawa term (1.2.8) leave the neutrinos massless.

Thus it could be understood that in the SM, the neutrinos remain massless. In order to get mass of the neutrino, one should go beyond the SM.

1.3 Extension of Standard Model and Neutrino Mass

As discussed in section (1.2), the SM of particle physics is capable of describing nearly all the fundamental particles and their interactions except gravity. Moreover, the SM fails to explain many observed phenomena of nature like the origin of tiny neutrino mass and matter-antimatter asymmetry of the Universe. To explain the mass of the neutrino, the particle contents of the SM must be extended.

If we add an arbitrary "m" number of right handed neutrinos along with the particle contents of the SM, then there will be two types of mass terms in the Lagrangian which arises from gauge invariant renormalizable operators [10]:

$$-\mathscr{L}_{M_\nu} = M_{Dij}\bar{\nu_{si}}\nu_{Lj} + \frac{1}{2}M_{Nij}\bar{\nu_{si}}\nu^c_{si} + H.C. \tag{1.3.1}$$

where $\nu^c = C\bar{\nu^T}$ is a charge conjugated field and C is the charge conjugation matrix. M_D is a complex $m \times 3$ matrix and M_N is a symmetric matrix of dimension $m \times m$.

The first term in Eq.(1.3.1) is the Dirac mas term generated from spontaneous electroweak symmetry breaking from Yukawa interactions

$$Y^{\nu}_{ij}\bar{\nu_{si}}\tilde{H}^{\dagger}L_{Lj} \Rightarrow M_{Dij} = Y^{\nu}_{ij}\frac{v}{\sqrt{2}} \tag{1.3.2}$$

The second term in Eq.(1.3.1)is the Majorana mass term which is singlet under the SM gauge group. Hence, it can appear as a bare mass term.

Eq.(1.3.1) can also be written as:

$$-\mathscr{L}_{M_\nu} = \frac{1}{2}\bar{\vec{\nu^c}}M_\nu\vec{\nu} + H.C. \tag{1.3.3}$$

where,

$$M_\nu = \begin{pmatrix} 0 & {M_D}^T \\ M_D & M_N \end{pmatrix} \tag{1.3.4}$$

and $\vec{\nu} = (\vec{\nu_L}, \vec{\nu_s^c})$ is a 6-dimensional vector. The matrix M_ν is complex and symmetric which can be diagonalized by a unitary matrix V of dimension 6 as

$$V^T M_\nu V = \text{diag}(m_1, m_2, ..., m_6) \tag{1.3.5}$$

In terms of resulting 6-mass eigenstates,

$$\vec{\nu}_{\text{mass}} = V^{\dagger}\vec{\nu}, \tag{1.3.6}$$

Eq.(1.3.3) can be rewritten as:

$$-\mathscr{L}_{M_\nu} = \frac{1}{2}\sum_{k=1}^{6} m_k(\bar{\nu}^c_{\text{mass},k}\ \nu_{\text{mass},k} + \bar{\nu}_{\text{mass},k}\ {\nu^c}_{\text{mass},k}) = \frac{1}{2}\sum_{k=1}^{6} m_k\bar{\nu}_{Mk}\ \nu_{Mk} \tag{1.3.7}$$

where,

$$\nu_{Mk} = \nu_{\text{mass},k} + \nu^c_{\text{mass},k} = (V^{\dagger}\vec{\nu})_k + (V^{\dagger}\vec{\nu})^c_k \tag{1.3.8}$$

which obey the Majorana condition

$$\nu_M = \nu^c_M \tag{1.3.9}$$

and are introduced as the Majorana neutrinos. Thus the Majorana condition suggests only one field to describe both the neutrino and anti-neutrino states i.e. a Majorana neutrino can be described by a two-component spinor apart from the charged fermions, which are Dirac particles and are represented by four-component spinors.

1.4 Three-Neutrino Mixing

As we have discussed earlier, there are three active neutrinos from the experimental evidences and they take part in standard charged current (CC) and neutral current (NC) weak interactions. Let us denote the neutrino mass eigenstates by $(\nu_1, \nu_3,$ $\nu_3)$, the charged lepton mass eigenstates by (e, μ, τ), the corresponding interaction eigenstates by (e^I, μ^I, τ^I) and $\bar{\nu} = (\nu_{Le}, \nu_{L\mu}, \nu_{L\tau})$ respectively. Thus the leptonic charged current interactions are given by

$$-\mathscr{L}_{CC} = \frac{g}{\sqrt{2}}(\bar{e}_L, \bar{\mu}_L, \bar{\tau}_L)\gamma^\mu U \begin{pmatrix} \nu_1 \\ \nu_2 \\ \nu_3 \end{pmatrix} W_\mu^+ + H.C. \tag{1.4.1}$$

where U is a (3×3) unitary matrix.

The charged lepton and the neutrino mass terms and the neutrino mass in the interaction basis are given by:

$$-\mathscr{L}_M = \left[(\bar{e}_L^I, \bar{\mu}_L^I, \bar{\tau}_L^I) M_l \begin{pmatrix} e_R^I \\ \mu_R^I \\ \tau_R^I \end{pmatrix} + H.C.\right] - \mathscr{L}_{M_\nu} \tag{1.4.2}$$

The term $-\mathscr{L}_{M_\nu}$ is already defined in Eq.(1.3.3).

Thus we can write

$$\begin{aligned} V_L^{l\dagger} M_l V_R^l &= \text{diag}(m_e, m_\mu, m_\tau) \\ V_L^{\nu\dagger} M_\nu V_R^\nu &= \text{diag}(m_1, m_2, m_3) \end{aligned} \tag{1.4.3}$$

where V^l and V^ν are the two 3×3 unitary diagonalizing matrices for the charged leptons and the neutrinos. Thus, the mixing matrix $U_{\rm PMNS}$ can be derived from these two diagonalizing matrices:

$$U_{\rm PMNS} = \begin{pmatrix} c_{12}c_{13} & s_{12}c_{13} & s_{13}e^{-i\delta} \\ -s_{12}c_{23} - c_{12}s_{23}s_{13}e^{i\delta} & c_{12}c_{23} - s_{12}s_{23}s_{13}e^{i\delta} & s_{23}c_{13} \\ s_{12}s_{23} - c_{12}c_{23}s_{13}e^{i\delta} & -c_{12}s_{23} - s_{12}c_{23}s_{13}e^{i\delta} & c_{23}c_{13} \end{pmatrix} \text{diag}(1, e^{i\alpha}, e^{i(\beta+\delta)}). \tag{1.4.4}$$

where $c_{ij} = \cos\theta_{ij}$, $s_{ij} = \sin\theta_{ij}$. δ is the Dirac CP phase and α, β are the Majorana phases. The mixing matrix $U_{\rm PMNS}$ is a 3×3 matrix analogous to the CKM matrix for the quarks [12, 13] except the two extra phases. Due to the Majorana nature of the neutrinos, the matrix $U_{\rm PMNS}$ depends on six independent parameters: three mixing angles and three phases (one for Dirac and two for Majorana).

1.5 Neutrino Oscillation

Neutrino oscillation is a quantum mechanical phenomena in which a neutrino that is created with a specific flavor (e, μ or τ) can change to a different flavor. This is possible only when the neutrinos are massive and the mass difference is not so large. If in any charged-current interaction, there involves an electron then a ν_e will be produced. When this neutrino propagates, it is the physical state that propagates with time. After some time, it has a probability to change into a different flavor state. As stated above, the basic criteria for neutrino oscillation is that there should be a mass difference between the neutrino states and the mass eigenstates should be different from the flavor eigenstates. The reason behind it is that if the two states have the same mass then both will propagate in the same way and there will be no oscillation. In the next subsections, these things will be discussed in brief.

1.5.1 Neutrino Oscillation in Vacuum

The flavor eigenstate of neutrino can be written as $\begin{pmatrix} \nu_e \\ \nu_\mu \\ \nu_\tau \end{pmatrix}$ and the mass eigenstate can be written as $\begin{pmatrix} \nu_1 \\ \nu_2 \\ \nu_3 \end{pmatrix}$ with mass eigenvalues (m_1, m_2, m_3). The flavor eigenstate and the mass eigenstate can be co-related by 3×3 rotation matrix [15]

$$\begin{pmatrix} \nu_e \\ \nu_\mu \\ \nu_\tau \end{pmatrix} = (U_{\text{PMNS}}) \begin{pmatrix} \nu_1 \\ \nu_2 \\ \nu_3 \end{pmatrix}. \tag{1.5.1}$$

where

$$U_{\text{PMNS}} = \begin{pmatrix} U_{e1} & U_{e2} & U_{e3} \\ U_{\mu 1} & U_{\mu 2} & U_{\mu 3} \\ U_{\tau 1} & U_{\tau 2} & U_{\tau 3} \end{pmatrix}. \tag{1.5.2}$$

If we consider only two generation neutrino then we can write

$$\begin{pmatrix} \nu_e \\ \nu_\mu \end{pmatrix} = \begin{pmatrix} cos\theta & sin\theta \\ -sin\theta & cos\theta \end{pmatrix} \begin{pmatrix} \nu_1 \\ \nu_2 \end{pmatrix}. \tag{1.5.3}$$

At time t

$$\begin{aligned} \nu_e(t) &= \nu_1 cos\theta e^{-iE_1 t} + \nu_2 sin\theta e^{-iE_2 t}, \\ \nu_\mu(t) &= -\nu_1 sin\theta e^{-iE_1 t} + \nu_2 cos\theta e^{-iE_2 t}. \end{aligned} \tag{1.5.4}$$

Therefore, at time $t = 0$, the above equation reduces to

$$\begin{aligned} \nu_e(0) &= \nu_1 cos\theta + \nu_2 sin\theta, \\ \nu_\mu(0) &= -\nu_1 sin\theta + \nu_2 cos\theta. \end{aligned} \tag{1.5.5}$$

Substituting ν_1 and ν_2 from eq. (1.5.5) into eq. (1.5.4) we get

$$\nu_e(t) = \nu_e(0)[cos^2\theta e^{-iE_1 t} + sin^2\theta e^{-iE_2 t}] + \nu_\mu(0)[e^{-iE_2 t} - e^{-iE_1 t}] cos\theta sin\theta. \tag{1.5.6}$$

Now here we take the approximations, $E_1 = \sqrt{m_1^2 + p_1^2} \cong p + m_1^2/2p$ and $E_2 = \sqrt{m_2^2 + p_2^2} \cong p + m_2^2/2p$. We also consider that the momentum of the neutrino is high enough so that $p_1 = p_2 = p$.

Thus the probability of $\nu_e \rightarrow \nu_\mu$ oscillation in time t is given by

$$P(t)_{\nu_e \rightarrow \nu_\mu} = sin^2\theta cos^2\theta[e^{-iE_2t} - e^{-iE_1t}]^2 = sin^2 2\theta . 2sin^2(\frac{t.\Delta m_{21}^2}{4E}), \tag{1.5.7}$$

where $t = \frac{L}{C}$. The term L is the oscillation distance and $\Delta m_{21}^2 = |m_2^2 - m_1^2|$. From eq. (1.5.6) it is clearly seen that the probability of oscillation ($P(t)_{\nu_e \rightarrow \nu_\mu}$) in vacuum depends on the following parameters:

- The mixing angle θ.
- The mass squared difference Δm_{21}^2.
- The oscillation distance L.

Thus from eq. (1.5.6) one can find out that the vital condition to occur neutrino oscillation in vacuum are:

- Δm_{21}^2 cannot be zero i,e, the neutrino cannot be massless and also they can not be degenerate.
- There should be a finite mixing between the different flavors of neutrino in the neutrino beam.
- There must be lepton flavor violation so that the different neutrino types as defined by the weak charged current, are mixtures of the mass eigenstates.

1.5.2 Neutrino Oscillation in Matter (MSW effect)

The oscillation pattern of neutrino will be exceptionally changed if one considers the presence of matter. Moreover, under certain conditions, the presence of matter can

lead to resonant amplification of the transition between given types of neutrino (ν_e, ν_μ, ν_τ) even when the same transitions are strongly suppressed in vacuum due to small mixing. If a neutrino is produced in some reactions at time $t = 0$, then after time t it should have a non-zero amplitude to be found as ν_e or ν_μ. The neutrino state can be defined as

$$|\nu_e(t) >= a_e(t)|\nu_e > +a_\mu(t)|\nu_\mu > . \tag{1.5.8}$$

The evolution of $a_e(t)$ and $a_\mu(t)$ are governed by the free particle Hamiltonian given by [14]

$$i\frac{d}{dt}\begin{pmatrix} a_e \\ a_\mu \end{pmatrix} = \frac{1}{4E}\begin{pmatrix} \Delta m^2_{21} cos2\theta & \Delta m^2_{21} sin2\theta \\ \Delta m^2_{21} sin2\theta & -\Delta m^2_{21} cos2\theta \end{pmatrix}\begin{pmatrix} a_e \\ a_\mu \end{pmatrix}, \tag{1.5.9}$$

where $\Delta m^2_{21} = m^2_2 - m^2_1$ and θ is the mixing angle defined by

$$\nu_e = cos\theta\nu_1 + sin\theta\nu_2, \qquad \nu_\mu = -sin\theta\nu_1 + cos\theta\nu_2. \tag{1.5.10}$$

Since the neutrino travels through solar matter and hence they will undergo neutral current interactions with the matter. However, only the ν_e interaction is more effective to consider and hence the eq. (1.5.9) turns out to be

$$i\frac{d}{dt}\begin{pmatrix} a_e \\ a_\mu \end{pmatrix} = \frac{1}{4E}\begin{pmatrix} A - \Delta m^2_{21} cos2\theta & \Delta m^2_{21} sin2\theta \\ \Delta m^2_{21} sin2\theta & \Delta m^2_{21} cos2\theta - A \end{pmatrix}\begin{pmatrix} a_e \\ a_\mu \end{pmatrix}, \tag{1.5.11}$$

where $A = 2\sqrt{2}G_F\eta_e E$ gives the effective mass square difference gained by the neutrino pairs due to the interactions in the Sun. η_e is the electron number density inside the Sun and is a function of the distance from the Sun's core. As the neutrino travels inside the Sun A changes. At some point, the diagonal terms in eq . (1.5.11) become equal and the effective neutrino mixing also become maximal. This resonance enhancement of the mixing due to the presence of matter with varying density is known as "Mikheyev-Smirnov-Wolfenstein (MSW)" effect. Hence the resonance condition can be written as

$$A = \Delta m^2_{21} cos2\theta. \tag{1.5.12}$$

The evolution equation (1.5.11) has the structure of a Schrödinger equation with the effective Hamiltonian matrix in the flavor basis

$$\mathcal{H} = \frac{1}{4E}\begin{pmatrix} A - \Delta m^2_{21} cos2\theta & \Delta m^2_{21} sin2\theta \\ \Delta m^2_{21} sin2\theta & \Delta m^2_{21} cos2\theta - A \end{pmatrix}, \tag{1.5.13}$$

which can be diagonalized by a unitary matrix

$$U_M = \begin{pmatrix} cos\theta_M & sin\theta_M \\ -sin\theta_M & cos\theta_M \end{pmatrix} \tag{1.5.14}$$

Equation (1.5.14) is the effective mixing matrix in matter and

$$\Delta m^2_M = \sqrt{(\Delta m^2_{21} cos2\theta - A)^2 + (\Delta m^2_{21} sin2\theta)^2} \tag{1.5.15}$$

is the effective squared-mass difference. The effective mixing angle in matter θ_M is given by

$$tan2\theta_M = \frac{tan2\theta}{1 - \frac{A}{\Delta m^2_{21} cos2\theta}} \tag{1.5.16}$$

Using the condition given in eq. (1.5.12) we get from eq. (1.5.16) $tan2\theta_M \longrightarrow \infty$ or $\theta_M \longrightarrow \frac{\pi}{4}$. This implies that it is possible to have $\theta_M = \frac{\pi}{4}$ even if the vacuum mixing angle is small. The oscillation length at the resonance can be derived as

$$L^{\text{res}} = \frac{4\pi p}{\Delta m^2_{21} sin2\theta} \tag{1.5.17}$$

If $sin2\theta_M = 1$ then $L = \frac{4\pi p}{\Delta m^2_{21}}$ which corresponds to large oscillation probabilities.

If $A = 0$ and the mixing angle in vacuum θ is very small then eq. (1.5.16) gives rise to same mass eigenstates as oscillation in matter.

1.6 Neutrino Mass Hierarchy

As stated above, neutrinos travel as a mixture of three flavor states and hence we can not predict the mass of ν_e, ν_μ, ν_τ separately but one can predict their mass squared

difference. On the basis of present knowledge, one can not decide whether the mass eigenstate ν_3 is heavier or lighter than the mass eigenstates ν_1 and ν_2. This is commonly referred as neutrino mass hierarchy and is divided into two categories [16]

- Normal Hierarchy (NH): The scenario, in which the mass eigenstate ν_3 is heavier, is referred to as the normal mass hierarchy (NH). For NH patters, we can simply write that

$$m_3 > m_2 > m_1,$$

where m_3, m_2, m_1 are the mass eigenvalues respectively.

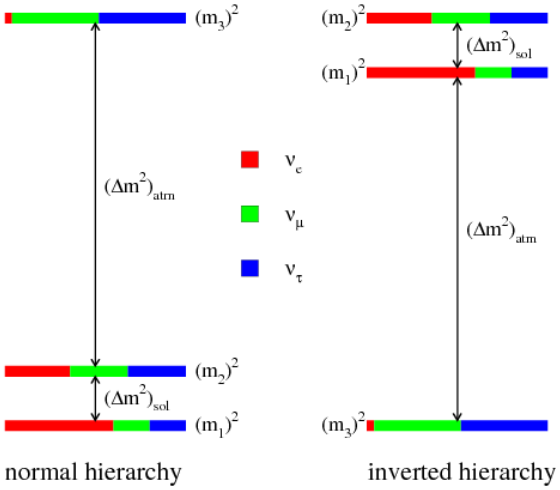

Figure 1.1: Possible neutrino mass hierarchies [17]

- Inverted Hierarchy (IH): The scenario, in which the mass eigenstate ν_3 is lighter, is referred to as the inverted mass hierarchy (IH). For IH patters, we can similarly write as

$$m_2 > m_1 > m_3$$

These two mass orderings are illustrated in fig:1.1. This thesis is mainly based on these two mass hierarchy patterns on different aspects.

1.7 Different Neutrino Oscillation Experiments

In this section we briefly outline the various neutrino oscillation experiments connected to both solar and atmospheric neutrinos. We also manifest the experimental data of those experiments within the framework of three neutrino mixings.

1.7.1 Neutrino Detection Method

The basic principle of neutrino detection is based on the β-transformations which can be written as

$$\begin{aligned} n &\to p + e^- + \bar{\nu_e} \\ p &\to n + e^+ + \nu_e \end{aligned} \tag{1.7.1}$$

or equivalently as

$$\begin{aligned} n + \nu_e &\to p + e^- \\ p + \bar{\nu_e} &\to n + e^+ \end{aligned} \tag{1.7.2}$$

We can see that in eqs. (1.7.1) and (1.7.2) lepton number is conserved. The specific properties of the neutrino ($Z_\nu = 0,\ m_\nu \cong 0,\ \mu_\nu = 0$) make the experimental detection of this particle very difficult. The estimated value of the interaction cross section of the neutrino with the nucleus is equal to 10^{-44} cm^2. Thus the mean free path in a condensed medium ($n = 10^{22}$ cm^{-3}) will be

$$l = \frac{1}{n\sigma} = \frac{1}{10^{22} \times\ 10^{-44}}\ \text{cm} = 10^{22}\ \text{cm} = 10^{17}\ \text{km}, \tag{1.7.3}$$

while the corresponding value in the nuclear matter ($n = 10^{38}$ cm^{-3}) is

$$l = \frac{1}{n\sigma} = \frac{1}{10^{38} \times\ 10^{-44}}\ \text{cm} = 10^{6}\ \text{cm} = 10\ \text{km}, \tag{1.7.4}$$

i.e. 10^8 times more than the nuclear dimension. Hence the existence of neutrino was confirmed only when there is a high intensity flux of neutrinos.

There are mainly three methods of detecting neutrinos which are briefly described as follows:

- **Water Detector (Elastic Scattering):**

  The basic principle of water detector is that in water, neutrino can hit electrons out of atoms with so much force that the electrons emit characteristic Cherenkov light. Physicists can then detect this light with the help of photo-tubes surrounding the detector.

$$\nu_e + e^- \rightarrow \nu_e + e^- \tag{1.7.5}$$

  This principle was used in Super-Kamiokande experiment.

- **Radio-Chemical Method:**

  The principle used in radio-chemical method is reverse β decay in which neutrino can change proton in atomic nuclei into neutrons, which can be detected through their reactions.

$$\begin{aligned} \bar{\nu_e} + p &\rightarrow \ n + e^+ \\ \nu_e + {}^{37}\mathrm{Cl} &\rightarrow {}^{37}\mathrm{Ar} + e^- \\ \nu_e \ + \ {}^{71}\mathrm{Ga} \ &\rightarrow \ {}^{71}\mathrm{Ge} + \ e^- \end{aligned} \tag{1.7.6}$$

  The first one was employed in Homestake experiment and the second one in GALLEX, SAGE, GNO experiments.

- **Heavy Water Detector:**

  The general principle of heavy water detector is mainly based on charged current interaction through ν_e and neutral current interaction through $\nu_x; x = e, \mu, \tau$.

$$\begin{aligned} \nu_e + {}^2\mathrm{H} &\rightarrow \ p + p + e^- \\ \nu_x + {}^2\mathrm{H} &\rightarrow \ p + n + \nu_x \ (x = \mu, \tau) \end{aligned} \tag{1.7.7}$$

The above principle was employed in SNO.

1.7.2 Solar Neutrino Oscillation Experiments

There are several solar neutrino experiments which are successful in observing the solar neutrinos. The list of those experiments are listed below with the year of confirmation and the country in which the experiments were implemented.

- Homestake experiment (1970, Lead, South Dakota) (Radio-chemical method).
- SAGE (Russia), GALLEX (Gran Sasso) (1998) (Radio-chemical method).
- Gallium Neutrino Observatory (GNO) (2003, Gran Sasso)(Radio-chemical Method).
- KAMIOKANDE (1987, Japan)(water detector which produces Cherenkov radiation).
- Super-KAMIOKANDE (2002, Japan)(water detector).
- SNO(1999, Canada)(Heavy water detector).
- KamLAND (2003, Japan).

Homestake Experiment (Davis's Experiment)

The first pioneering experiment to detect solar neutrino was introduced by Davis and his collaborators at Homestake using $^{37}\mathrm{Cl} - ^{37}\mathrm{Ar}$ method which was proposed by Pontecorvo [18]. In this experiment, ^{37}Cl absorbs a ν_e followed by the produced ^{37}Ar decay through orbital e^- capture,

$$\nu_e + ^{37}\mathrm{Cl} \rightarrow ^{37}\mathrm{Ar} + e^- (\text{thresold 814 keV}). \tag{1.7.8}$$

Since the threshold of the above reaction is 814 keV, hence the detector is sensitive to all neutrinos generated in the Sun except the p-p neutrinos.

Reaction	Abbr.	Flux ($cm^{-2}s^{-1}$)
$pp \rightarrow\ de^{+}\nu$	*pp*	$5.97(1 \pm 0.006) \times 10^{10}$
$pe^{-}p \rightarrow\ d\nu$	*pep*	$1.41(1 \pm 0.011) \times 10^{8}$
$^{3}\mathrm{He}\ p \rightarrow\ ^{4}\mathrm{He}\ e^{+}\ \nu$	*hep*	$7.90(1 \pm 0.015) \times 10^{3}$
$^{7}\mathrm{Be}\ e^{-} \rightarrow\ ^{7}\mathrm{Li}\ \nu + \gamma$	^{7}Be	$5.07(1 \pm 0.06) \times 10^{9}$
$^{8}\mathrm{B} \rightarrow\ ^{8}\mathrm{Be}^{*}\ e^{+}\ \nu$	^{8}B	$5.94(1 \pm 0.11) \times 10^{6}$
$^{13}\mathrm{N} \rightarrow\ ^{13}\mathrm{C}\ e^{+}\ \nu$	^{13}N	$2.88(1 \pm 0.15) \times 10^{8}$
$^{15}\mathrm{O} \rightarrow\ ^{15}\mathrm{N}\ e^{+}\ \nu$	^{15}O	$2.15(1^{+0.17}_{-0.16}) \times 10^{8}$
$^{17}\mathrm{F} \rightarrow\ ^{17}\mathrm{O}\ e^{+}\ \nu$	^{17}F	$5.82(1^{+0.19}_{-0.17}) \times 10^{6}$

Table 1.2: The Standard Solar Model (SSM) neutrino fluxes predicted by the BPS08 (GS) model [19]

The energy of the neutrino and their flux from the different processes in the Sun are given in Table 1.2.

Thus it is clear from Table 1.2 that the dominant contribution in the $^{37}\mathrm{Cl} - ^{37}\mathrm{Ar}$ experiment came from ^{8}B neutrinos, but ^{7}B, *pep*, ^{13}N and ^{15}O neutrinos also have contribution as well. It is necessary to comment that the observed flux is significantly smaller than the SSM calculation [20].

Gallium Experiments

In gallium experiments (GALLEX and GNO at Gran Sasso in Italy and SAGE at Baskan in Russia), they use the following reaction

$$\nu_e\ +\ ^{71}\mathrm{Ga}\ \rightarrow\ ^{71}\mathrm{Ge} + \ e^{-}\quad \text{(threshold 233 keV)} \tag{1.7.9}$$

The SSM calculation predicts that more than 80% of the capture rate in gallium arises due to low energy *pp*. The results of GALLEX, GNO, GNO + GALLEX and

SAGE experiments are shown in Table 1.3.

Experiment	^{71}Ga $-$ ^{71}Ge (SNU)
GALLEX [21]	$77.5 \pm 6.2^{+4.3}_{-4.7}$
GNO [22]	$62.9^{+5.5}_{-5.3} \pm 2.5$
GNO+GALLEX [22]	$69.3 \pm 4.1 \pm 3.6$
SAGE [23]	$65.4^{+3.1+2.6}_{-3.0-2.8}$
SSM [BPS08(GS)] [19]	$127.9^{+8.1}_{-8.2}$

Table 1.3: The results of radio-chemical solar neutrino experiments. The predictions of a recent SSM BPS08(GS) [19] are also listed in the last row. SNU (Solar Neutrino Unit) is defined as 10^{-36} neutrino captures per atom per second.

Kamiokande Experiment

The Kamiokande experiment was started in 1987 in Japan which utilizes ν_e scattering,

$$\nu_x \ + \ e^- \ \rightarrow \ \nu_x \ + \ e^-, \tag{1.7.10}$$

in a large water-Cherenkov detector. It was the first experiment which gave the direct evidence that neutrinos come from the direction of the Sun [24]. The above reaction is sensitive to all active neutrinos, $x = e, \mu$ and τ. The results of Kamiokande experiment is shown in Table 1.4.

Super-Kamiokande Experiment

The Super-Kamiokande experiment [25–28] was mainly started taking data from 1996 in which a 50-kton water Cherenkov detector was used to replace the Kamiokande experiment. Due to the high threshold (recoil-electron total energy of 7 MeV in Kamiokande and 5 MeV in Super-Kamiokande), this experiment was successful in observing pure ^{8}B solar neutrinos.

Experiment	Reaction	^{8}B ν flux (10^6cm^{-2}s^{-1})
Kamiokande [29]	ν_e	$2.80 \pm 0.19 \pm 0.33$
Super-K I [26, 28]	ν_e	$2.38 \pm 0.02 \pm 0.08$
Super-K II [27, 28]	ν_e	$2.41 \pm 0.05^{+0.16}_{-0.15}$
Super-K III [28]	ν_e	$2.32 \pm 0.04 \pm 0.05$
SNO (Pure D_2O) [30]	CC	$1.76^{+0.06}_{-0.05} \pm 0.09$
	ν_e	$2.39^{+0.24}_{-0.23} \pm 0.12$
	NC	$5.09^{+0.44+0.46}_{-0.43-0.43}$
Borexino [31]	ν_e	$2.4 \pm 0.4 \pm 0.1$
SSM[BPS08(GS)] [19]	-	$5.94(1 \pm 0.11)$

Table 1.4: ^{8}B solar neutrino results obtained from different experiments. The predictions of a recent SSM BPS08(GS) [19] are also listed in the last row.

Sudbury Neutrino Observatory (SNO)

Another solar neutrino experiment SNO in Canada had started observation in 1999 in which they used 1000 tons of ultar-pure heavy water (D_2O) contained in a spherical acrylic vessel, surrounded by an ultra-pure H_2O shield. SNO measured ^{8}B solar neutrinos via the charged-current (CC) and neutral-current (NC) reactions [32–40]

$$\nu_e \ + \ d \rightarrow e^- \ + \ p \ + \ p \qquad \text{(CC)}, \tag{1.7.11}$$

and

$$\nu_x \ + \ d \rightarrow \nu_x \ + \ p \ + \ n \qquad \text{(NC)}, \tag{1.7.12}$$

as well as ν_e scattering as defined in eq. (1.7.10). The CC reaction is sensitive to ν_e only, while the NC is sensitive to all active neutrinos. The results of SNO are shown in Table 1.4.

Borexino Experiment

In 2007 at Gran Sasso in Italy, a new solar neutrino experiment Borexino started observation. This experiment measures solar neutrinos via ν_e scattering in 300 tons of ultra-pure liquid scintillator.

Experiment	Reaction	^{7}Be ν flux ($10^9 \mathrm{cm}^{-2}\mathrm{s}^{-1}$)
Borexino [42]	ν_e	3.10 ± 0.15
SSM[BPS08(GS)] [19]	-	$5.07(1 \pm 0.06)$

Table 1.5: ^{7}Be solar neutrino result from Borexino. The predictions of a recent SSM BPS08(GS) [19] are also listed in the last row.

Experiment	Reaction	*pep* ν flux ($10^8 \mathrm{cm}^{-2}\mathrm{s}^{-1}$)
Borexino [42]	ν_e	1.0 ± 0.2
SSM[BPS08(GS)] [19]	-	$1.41(1 \pm 0.011)$

Table 1.6: *pep* solar neutrino result from Borexino. The predictions of a recent SSM BPS08(GS) [19] are also listed in the last row.

The experiment was successful in observing ^{7}Be solar neutrinos with an energy threshold 250 keV [41–49] and ^{8}B solar neutrinos with threshold value of 3 MeV [31]. The results are depicted in Table 1.4, 1.5 and 1.6.

1.7.3 Atmospheric Neutrino Experiments

The Kamiokande experiment in Japan and the IMB experiment in the US were the pioneering experimental projects to develop large volume water Cherenkov detector with the primary goal of detecting nucleon decay, as predicted by GUT developed in 1970's. It was observed that in both the experiments, the ratio of ν_μ induced events to ν_e induced events subsequently get reduced from the expected value of 2. The flux obtained from Kamiokande and IMB experiments are shown in Table 1.7.

Experiment	Flux
Kamiokande [50]	$0.06 \pm 0.07 \pm 0.05$
IMB [4]	$0.54 \pm 0.05 \pm 0.12$

Table 1.7: Experimental data from Kamiokande and IMB.

1.7.4 Reactor Experiments

The most elegant way to measure θ_{13} is through kilometre-baseline reactor neutrino oscillation experiments. The main advantage of it is that the generation of non-zero θ_{13} will cause a deficit of $\bar{\nu_e}$ flux at $\sim 1-2$ km baseline which is proportional to the value of $\sin^2 2\theta_{13}$ [51]. Since the reactor measurements are independent of CP-phase and θ_{23}, therefore a high precision measurement can be achieved.

In order to measure θ_{13}, the two first generated kilometre-baseline reactor experiments, CHOOZ [52] and PALO VERDE [53–55] were constructed. The CHOOZ detector was built at a distance of $\sim 1,050$m from the two reactors of the CHOOZ power plant of Electricite de France in the Ardennes region of France while the PALO VERDE detector was built at distances of 750, 890 and 890 m from the three reactors of the Palo Verde Nuclear Generating Station in the Arizona desert of the United States. More interestingly, both the experiments had failed to observe the $\bar{\nu_e}$ deficit from θ_{13} but they had succeded in giving an upper limit of $\sin^2 2\theta_{13} < 0.10$ at 90% confidence level [52].

Due to the importance of knowing the precise value of θ_{13} and the failure of CHOOZ and PALE VERDE experiments, a series of worldwide second-generation kilometre-baseline reactor experiments were started in the 21st century. Among those, Double Chooz [56–58] in France, RENO [60] in Korea and Daya Bay [61,62] in China were the most famous experiments which tried to push the sensitivity to θ_{13} considerably below 10°.

In the Double Chooz experiment, they measured ν_es from two 4.25 GW_{th} reactors with a far detector placed in 1050 m from the two reactor cores. With the 101 days of data, they initially reported $\sin^2 2\theta_{13} = 0.086 \pm 0.041 \pm 0.030$ [56]. Recently, they recorded $\sin^2 2\theta_{13} = 0.109 \pm 0.030 \pm 0.025$ [59] with 227.93 live days of running. Double Chooz was also successful in measuring θ_{13} using inverse β-decay interactions with neutrons capture on hydrogen [63] or from combined fit Gd-capture and H-capture rate+spectrum etc [64].

The RENO experiment consists of six 2.8 GW_{th} reactors at Yonggwang Nuclear Power Plant in Korea with two identical detectors located at 294 m and 1383 m from the reactor array center. Their initial result includes $\sin^2 2\theta_{13} = 0.113 \pm 0.013 \pm 0.019$ with 229 days of running time [60]. In September 2013, RENO reported a new result of $\sin^2 2\theta_{13} = 0.100 \pm 0.010 \pm 0.012$ with 403 live days of data [65].

The Daya Bay experiment measured the ν_es from the Daya Bay nuclear power complex in China which includes six 2.9 GW_{th} reactors with six identical detectors positioned in two near (470 m and 576 m) and one far (1648 m) underground hall. The initial results of Daya Bay gave the evidence of non-zero θ_{13} in 5.2σ confidence level with a value of $\sin^2 2\theta_{13} = 0.0.089 \pm 0.010 \pm 0.005$ (139 days of data) [61]. Later, they repoted their latest results for $\sin^2 2\theta_{13} = 0.090^{+0.008}_{-0.009}$ based on 217 days of live running [66].

[9] Eguchi, K., et al. First results from kamLAND: Evidence for reactor antineutrino disappearance, *Phys. Rev. Lett.*, **90**(2), 2003.

[10] Gonzalez-Garcia, M.C. & Maltoni, M. Phenomenology with massive neutrinos, *Phys. Reports*, **460**(1), 1–129, 2008.

[11] Cho, A. Higgs boson makes its debut after decades-long search, *Science*, **337**(6091), 141–143, 2012.

[12] Nir, Y. CP violation: The CKM matrix and new physics, *Nuclear Physics B-Proceedings Supplements*, **117**, 111–126, 2003.

[13] Barger, V., et al. Universal evolution of CKM matrix elements, arXiv:hep-ph/9210260, 1992.

[14] Wolfenstein, L. Neutrino oscillations in matter, *Phys. Rev. D*, **17**(9), 2369, 1978.

[15] King, S. F. Neutrino mass models, *Rep. Prog. Phys.*, **67**(2), 107, 2004.

[16] Qian, X., & Vogel, P. Neutrino mass hierarchy, *Prog. Part. Nucl. Phys.*, **83**, 1–30, 2015.

[17] Cahn, R. N., et al. White Paper: Measuring the Neutrino Mass Hierarchy, arXiv:1307.5487, 2013.

[18] Pontecorvo, B. *Chalk River Lab. Report* PD **205**, 1946.

[19] Pena-Garay, C. & Serenelli, A.M. Solar neutrinos and the solar composition problem, arXiv:0811.2424.

[20] Davis. R., et al. Search for Neutrinos from the Sun, *Phys. Rev. Lett.*, **20**(21), 1205–1209, 1968.

[21] Hampel, W., et al. GALLEX solar neutrino observations: results for GALLEX IV, *Phys. Lett. B*, **447**(1), 127–133, 1999.

[22] Altmann, M., et al. Complete results for five years of GNO solar neutrino observations. *Physics Letters B*, **616**(3), 174–190, 2005.

[23] Abdurashitov, J.N., et al. Measurement of the solar neutrino capture rate with gallium metal. III. Results for the 2002–2007 data-taking period, *Physical Review C*, **80**(1), 15807, 2009.

[24] Hirata, K.S., et al. Observation of ^{8}B solar neutrinos in the Kamiokande-II detector, *Phys. Rev. Lett.*, **63**(1), 16–19, 1989.

[25] Fukuda, Y., et al. Measurements of the solar neutrino flux from Super-Kamiokande's first 300 days, *Phys. Rev. Lett.*, **81**(6), 1158–1162, 1998.

[26] Hosaka, J., et al. Solar neutrino measurements in Super-Kamiokande-I, *Phys. Rev. D*, **73**, 112001, 2005.

[27] Cravens, J. P., et al. Solar neutrino measurements in Super-Kamiokande-II, *Phys. Rev. D*, **78**(3), 032002, 2008.

[28] Abe, K., et al. Solar neutrino results in Super-Kamiokande-III, *Phys. Rev. D*, **83**(5), 052010, 2011.

[29] Fukuda, Y., et al. Solar neutrino data covering solar cycle 22, *Phys. Rev. Lett.*, **77**(9), 1683-1686, 1996.

[30] Ahmad, Q. R., et al. Direct evidence for neutrino flavor transformation from neutral-current interactions in the Sudbury Neutrino Observatory, *Phys. Rev. Lett.*, **89**(1), 011301, 2002.

[31] Bellini, G., et al. Measurement of the solar ^{8}B neutrino rate with a liquid scintillator target and 3 MeV energy threshold in the Borexino detector, *Phys. Rev. D*, **82**(3), 033006, 2010.

[32] Aharmim, B., et al. Electron energy spectra, fluxes, and day-night asymmetries of ^{8}B solar neutrinos from measurements with NaCl dissolved in the heavy-water detector at the Sudbury Neutrino Observatory, *Phys. Rev. C*, **72**(5), 055502, 2005.

[33] Aharmim, B., et al. Independent Measurement of the Total Active ^{8}B Solar Neutrino Flux Using an Array of ^{3}He Proportional Counters at the Sudbury Neutrino Observatory, *Phys. Rev. Lett.*, **101**(11), 111301, 2008.

[34] Aharmim, B., et al. Measurement of the ν_e and total ^{8}B solar neutrino fluxes with the Sudbury Neutrino Observatory phase-III data set, *Phys. Rev. C*, **87**(1), 015502, 2013.

[35] Aharmim, B., et al. Low-energy-threshold analysis of the Phase I and Phase II data sets of the Sudbury Neutrino Observatory, *Phys. Rev. C* **81**(5), 055504, 2010.

[36] Aharmim, B., et al. Combined analysis of all three phases of solar neutrino data from the Sudbury Neutrino Observatory, *Phys. Rev. C*, **88**(2), 025501, 2013.

[37] McDonald, A. B., et al. First neutrino observations from the Sudbury Neutrino Observatory, *Nucl. Phys. B-Proceedings Supplements*, **91**(1), 21–28, 2001.

[38] Klein, J.R. Solar neutrino results from the Sudbury Neutrino Observatory, *International Journal of Modern Physics A*, **17**(24),3378-3392, 2002.

[39] Ahmed, S. N., et al. Measurement of the Total Active ^{8}B Solar Neutrino Flux at the Sudbury Neutrino Observatory with Enhanced Neutral Current Sensitivity, *Phys. Rev. Lett.*, **92**(18), 181301, 2004.

[40] Poon, A. W. Recent results from the sudbury neutrino observatory, *EPJC*, 33(1), 823-825, 2004.

[41] Arpesella, C., et al. Direct Measurement of the ^{7}Be Solar Neutrino Flux with 192 Days of Borexino Data, *Phys. Rev. Lett.*, **101**(9), 091302, 2008.

[42] Bellini, G., et al. Precision measurement of the ^{7}Be solar neutrino interaction rate in Borexino, *Phys. Rev. Lett.*, **107**(14), 141302, 2011.

[43] Bellini, G., et al. Absence of a day–night asymmetry in the ^{7}Be solar neutrino rate in Borexino, *Phys. Lett. B*, **707**(1), 22–26, 2012.

[44] Bellini, G., et al. First Evidence of *pep* Solar Neutrinos by Direct Detection in Borexino, *Phys. Rev. Lett.*, **108**(5), 051302, 2012.

[45] Smirnov, O., et al. Solar neutrino with Borexino: results and perspectives, *Phys. of Particles and Nuclei*, **46**(2), 166–173, 2015.

[46] Irgaziev, B., et al. The estimation of the neutrino flux produced by pep reactions in the Sun, *Physica Scripta*, **89**(8), 084010, 2014.

[47] Bellini, G., et al. Final results of Borexino Phase-I on low-energy solar neutrino spectroscopy, *Phys. Rev. D*, **89**(11), 112007, 2014.

[48] Back, H., et al. Borexino calibrations: hardware, methods, and results, *Journal of Instrumentation*, **7**(10), 10018, 2012.

[49] Pallavicini, M., et al. Solar neutrino results from Borexino and main future perspectives, *Nuclear Instruments and Methods in Physics Research Section A:*

Accelerators, Spectrometers, Detectors and Associated Equipment, **630**(1), 210–213, 2011.

[50] Hirata, K. S., et al. Experimental study of the atmospheric neutrino flux, *Phys. Lett. B*, **205**(2), 416–420, 1988.

[51] Vogel, P., et al. Neutrino oscillation studies with reactors, *Nature communications*, **6**, 1–12, 2015.

[52] Apollonio, M., et al. Limits on neutrino oscillations from the CHOOZ experiment, *Phys. Lett. B*, **466**(2), 415-430, 1999.

[53] Boehm, F., et al. Search for neutrino oscillations at the Palo Verde nuclear reactors, *Phys. Rev. Lett.*, **84**(17), 3764–3767, 2000.

[54] Boehm, F., et al. Final results from the Palo Verde neutrino oscillation experiment, *Phys. Rev. D*, **64**(11), 112001, 2001.

[55] Boehm, F., et al. Results from the Palo Verde neutrino oscillation experiment, *Phys. Rev. D*, **62**(7), 072002, 2000.

[56] Abe, Y., et al. Indication of reactor ν_e disappearance in the Double Chooz experiment, *Phys. Rev. Lett.*, **108**(13), 131801, 2012.

[57] Abe, Y., et al. Improved measurements of the neutrino mixing angle θ_{13} with the Double Chooz detector, *JHEP* **2014**(10), 1–44, 2014.

[58] Abe, Y., et al. Background-independent measurement of θ_{13} in Double Chooz, *Phys. Lett. B*, **735**, 51–56, 2014.

[59] Abe, Y., et al. Reactor ν_e disappearance in the Double Chooz experiment, *Physical Review D*, **86**(5), 052008, 2012.

[60] Ahn, J. K., et al. Observation of reactor electron antineutrinos disappearance in the RENO experiment, *Phys. Rev. Lett.*, **108**(19), 191802, 2012.

[61] An, F. P., et al. Observation of electron-antineutrino disappearance at Daya Bay, *Phys. Rev. Lett.*, **108**(17), 171803, 2012.

[62] An, F. P., et al. Improved measurement of electron antineutrino disappearance at Daya Bay, *Chinese Physics C*, **37**(1), 011001, 2013.

[63] Abe, Y., et al. First measurement of θ_{13} from delayed neutron capture on hydrogen in the Double Chooz experiment, *Phys. Lett. B*, **723**(1), 66–70, 2013.

[64] Buck, C. talk at the EPS HEP 2013 Conference, Stockholm, July 18-24, 2013.

[65] Kim, S. Review on θ_{13} Measurements From Reactor Experiments, *16th Lomonosov Conference on Elementary Particle Physics*, Moscow, Russia, 30–35, 2013.

[66] An, F. P., et al. Spectral measurement of electron antineutrino oscillation amplitude and frequency at Daya Bay, *Phys. Rev. Lett.*, **112**(6), 061801, 2014.

Bibliography

[1] Pontecorvo, B. Mesonium and antimesonium, *Sov. Phys. JETP*, **33**, 549–551, 1957.

[2] Pontecorvo, B. Inverse beta processes and nonconservation of lepton charge, *Sov. Phys. JETP*, **34**, 247–249, 1958.

[3] Fukuda, Y., et al. Evidence for oscillation of atmospheric neutrinos, *Phys. Rev. Lett.*, **81**(8), 1562–1567, 1998.

[4] Bionta, R.M., et al. Contained neutrino interactions in an underground water detector, *Phys.Rev. D* **38**(3), 768–775, 1988.

[5] Ahn, M.H., et al. Indications of neutrino oscillation in a 250 km long-baseline experiment, *Phys. Rev. Lett.*, **90**(4), 2003.

[6] Guinti, C. & Laveder, M. Neutrino mixing, arXiv:hep-ph/0310238, 2003.

[7] Ahmed, Q.R., et al. Measurement of the rate of $\nu_e + d \rightarrow p + p + e^-$ interactions produced by ^{8}B solar neutrinos at the sudbury neutrino observatory, *Phys. Rev. Lett.*, **87**(7), 2001.

[8] Fukuda, S., et al. Solar ^{8}B and *hep* neutrino measurements from 1258 days of data, *Phys. Rev. Lett.*, **86**(25), 5651–5655, 2001.

Chapter 2

Perturbations to $\mu - \tau$ Symmetry and Leptogenesis with Type II Seesaw

---

In this chapter, we study the different $\mu - \tau$ symmetric neutrino mass matrices originating from type I seesaw mechanism which give rise to zero values of θ_{13}. We then apply a perturbative term originates from type II seesaw which breaks the $\mu - \tau$ symmetry and calculate the neutrino oscillation parameters as a function of type II seesaw strength. We also extend our study to get baryogenesis by incorporating the origin of nontrivial leptonic CP phase in the charged lepton sector.

2.1 Introduction

The standard model (SM) of particle physics have been established as the most successful theory describing all fundamental particles and their interactions except gravity, specially after the discovery of its last missing piece, the Higgs boson in 2012. In spite of its huge phenomenological success, the SM fails to explain many observed

phenomena in nature. Origin of tiny neutrino mass and matter-antimatter asymmetry are two of such phenomena which can be explained only within the framework of some beyond standard model (BSM) physics. Neutrinos which remain massless in the SM, have been shown to have tiny but non-zero mass (twelve order of magnitude smaller than the electroweak scale) by several neutrino oscillation experiments [1–5]. Recent neutrino oscillation experiments T2K [6], Double ChooZ [7], Daya-Bay [8] and RENO [9] have not only made the earlier predictions for neutrino parameters more precise, but also predicted non-zero value of the reactor mixing angle θ_{13} as given below.

Experimental Data	$\sin^2 2\theta_{13}$	$\sin^2 \theta_{13}$
T2K [6]	$0.11^{0.11}_{-0.05}$ $\left(0.14^{0.12}_{-0.06}\right)$	$0.028^{0.019}_{-0.024}$ $\left(0.036^{0.022}_{-0.030}\right)$
Double ChooZ [7]	$0.086 \pm 0.041 \pm 0.030$	$0.022^{0.019}_{-0.018}$
Daya-Bay [8]	$0.092 \pm 0.016 \pm 0.005$	0.024 ± 0.005
RENO [9]	$0.113 \pm 0.013 \pm 0.019$	0.029 ± 0.006

Table 2.1: Experimental value of reactor mixing angle from recent neutrino oscillation experiments.

Oscilation Parameters	Within 3σ range (*Schwetz et al.* [10])	within 3σ range (*Fogli et al.* [11])
Δm^2_{21} [10^{-5} eV^2]	7.00-8.09	6.99-8.18
$\lvert\Delta m^2_{31}$ (NH) [10^{-3} eV^2]	2.27-2.69	2.19-2.62
$\lvert\Delta m^2_{23}$ (IH) [10^{-3} eV^2]	2.24-2.65	2.17-2.61
$\sin^2 \theta_{12}$	0.27-0.34	0.259-0.359
$\sin^2 \theta_{23}$	0.34-0.67	0.331-0.637
$\sin^2 \theta_{13}$	0.016-0.030	0.017-0.031

Table 2.2: The global fit values for the mass squared differences and mixing angles as reported by Ref. [10] presented by 2nd column and by Ref. [11] by third column.

Recent global fits for different oscillation parameters within their 3σ range taken from Ref. [10] and Ref. [11] are presented below in table 2.2.

Several BSM frameworks have been proposed to explain the origin of tiny neutrino mass and the pattern of neutrino mixing. Tiny neutrino mass can be explained by seesaw mechanisms which broadly fall into three types : type I [12–15], type II [16–21] and type III [22] whereas the pattern of neutrino mixing can be understood by incorporating additional flavor symmetries.

The neutrino oscillation data before the discovery of non-zero θ_{13} were in perfect agreement with $\mu-\tau$ symmetric neutrino mass matrix. Four different neutrino mixing pattern which can originate from such a $\mu-\tau$ symmetric neutrino mass matrix are: Bimaximal Mixing (BM) [23–25], Tri-bimaximal Mixing (TBM) [26–31], Hexagonal Mixing (HM) [32] and Golden Ratio Mixing (GRM) [33–38]. All these scenarios predict $\theta_{23} = 45^o, \theta_{13} = 0$ but different values of solar mixing angle $\theta_{12} = 45^o$ (BM), $\theta_{12} = 35.3^o$ (TBM), $\theta_{12} = 30^o$ (HM), $\theta_{12} = 31.71^o$ (GRM). However, in view of the fact that the latest experimental data have ruled out $\sin^2\theta_{13} = 0$, one needs to go beyond these $\mu-\tau$ symmetric frameworks. Since the experimental value of θ_{13} is still much smaller than the other two mixing angles, $\mu-\tau$ symmetry can still be a valid approximation and the non-zero θ_{13} can be accounted for by incorporating the presence of small perturbations to $\mu-\tau$ symmetry coming from different sources like charged lepton mass diagonalization, for example. Several such scenarios have been widely discussed in [39–48] and the latest neutrino oscillation data can be successfully predicted within the framework of many interesting flavor symmetry models.

Apart from the origin of neutrino mass and mixing, the observed matter anti-matter asymmetry also remains unexplained within the SM framework. The observed baryon asymmetry in the Universe is encoded in the baryon to photon ratio measured by dedicated cosmology experiments like Wilkinson Mass Anisotropy Probe (WMAP), Planck etc. The latest data available from Planck mission constrain the baryon to

photon ratio [49] as

$$Y_B \simeq (6.065 \pm 0.090) \times 10^{-10} \tag{2.1.1}$$

Leptogenesis is one of the most widely studied mechanism of generating this observed baryon asymmetry in the Universe by generating an asymmetry in the leptonic sector first and later converting it into baryon asymmetry through electroweak sphaleron transitions [50]. As pointed out first by Fukugita and Yanagida [51], the out of equilibrium CP violating decay of heavy Majorana neutrinos provides a natural way to create the required lepton asymmetry. The salient feature of this mechanism is the way it relates two of the most widely studied problems in particle physics: the origin of neutrino mass and the origin of matter-antimatter asymmetry. This idea has been implemented in several interesting models in the literature [52–65]. Recently such a comparative study was done to understand the impact of mass hierarchies, Dirac and Majorana CP phases on the predictions for baryon asymmetry in [66] within the framework of left-right symmetric models.

In the present chapter, we propose a common mechanism which can generate the desired neutrino mass and mixing including non-zero θ_{13} and also the matter antimatter asymmetry. We extend the SM by three right handed singlet neutrinos and one Higgs triplet such that both type I and type II seesaw can contribute to neutrino mass. Type I seesaw is assumed to give rise to a $\mu - \tau$ symmetric neutrino mass matrix with $\theta_{13} = 0$ whereas type II seesaw acts as a perturbation which breaks the $\mu - \tau$ symmetry resulting in non-zero θ_{13}. Similar works have been done recently where type II seesaw was considered to be the origin of θ_{13} [67, 68] as well as non-zero Dirac CP phase δ [69] by assuming the type I seesaw giving rise to TBM type mixing. Some earlier works studying neutrino masses and mixing by using the interplay of two different seesaw mechanisms can be found in [70–75]. In this work we generalize earlier studies on TBM type mixing to most general $\mu-\tau$ symmetric neutrino mass matrices and check whether a minimal form of $\mu-\tau$ symmetry breaking type II seesaw can give

rise to correct value of reactor mixing angle θ_{13}. We then calculate the predictions for other neutrino parameters as well as observables like sum of absolute neutrino masses $\sum_i |m_i|$ and effective neutrino mass $m_{ee} = |\sum_i U_{ei}^2 m_i|$. We check whether the sum of absolute neutrino masses obey the cosmological upper bound $\sum_i |m_i| < 0.23$ eV [49] and whether the effective neutrino mass m_{ee} lies within the bounds coming from neutrinoless double beta decay experiments. We also calculate the lepton asymmetry by considering the source of leptonic Dirac CP violation in the charged lepton sector. From the requirement of generating correct neutrino parameters and baryon asymmetry we constrain type II seesaw strength, Dirac CP phase and at the same time discriminate between neutrino mass hierarchies, different lightest neutrino masses and different $\mu - \tau$ symmetric mass matrices.

The plan of the chapter is sketched as following manner. In section 2.2 we discuss the methodology of type I and type II seesaw mechanisms. In section 2.3, we discuss the parametrization of different $\mu - \tau$ symmetric neutrino mass matrices. We then discuss deviations from $\mu - \tau$ symmetry using type II seesaw in section 2.4. In section 2.5, we discuss CP violation and outline the mechanism of leptogenesis in the presence of type I and type II seesaw. In section 2.6 we discuss our numerical analysis and results and then finally conclude in section 2.7.

2.2 Seesaw Mechanism: Type I and Type II

Type I seesaw [12–15] mechanism is the simplest possible realization of the dimension five Weinberg operator [76] for the origin of neutrino masses within a renormalizable framework. This mechanism is implemented in the standard model by the inclusion of three additional right handed neutrinos ($\nu_R^i, i = 1, 2, 3$) as $SU(2)_L$ singlets with zero $U(1)_Y$ charges. Being singlet under the gauge group, bare mass terms of the right handed neutrinos M_{RR} are allowed in the Lagrangian. On the other hand, in

type II seesaw [16–21] mechanism, the standard model is extended by inclusion of an additional $SU(2)_L$ triplet scalar field Δ having $U(1)_Y$ charge twice that of lepton doublets with its 2×2 matrix representation as

$$\Delta = \begin{pmatrix} \Delta^+/\sqrt{2} & \Delta^{++} \\ \Delta^0 & -\Delta^+/\sqrt{2} \end{pmatrix} .$$

Thus, the gauge invariant lagrangian relevant for type I plus type II seesaw mechanism is given below

$$\mathcal{L} = (D_\mu \Phi)^\dagger (D^\mu \Phi) + \mathrm{Tr}(D_\mu \Delta)^\dagger (D^\mu \Delta) - \mathcal{L}_Y^{\mathrm{lept}} - V(\Phi, \Delta) \ , \tag{2.2.1}$$

with the leptonic interaction terms,

$$\mathcal{L}_Y = y_{ij} \ell_i \tilde{\Phi} \nu_R + f_{ij} \ell_i^T C (i\tau_2) \Delta \ell_j + \frac{1}{2} \nu_R^T C^{-1} M_R \nu_R + \mathrm{h.c.} \tag{2.2.2}$$

Here $\ell_L \equiv (\nu, \ e)_L^T$, $\Phi \equiv (\phi^0, \phi^-)^T$ and C is the charge conjugation operator. The scalar potential of the model using SM Higgs doublet Φ and Higgs triplet scalar Δ_L is

$$\begin{aligned} \mathcal{V}(\Phi, \Delta) = \mu_\Phi^2 \Phi^\dagger \Phi + \lambda_1 \left(\Phi^\dagger \Phi\right)^2 + \mu_\Delta^2 \mathrm{Tr}\left(\Delta^\dagger \Delta\right) + \lambda_2 \left[\mathrm{Tr}\left(\Delta^\dagger \Delta\right)\right]^2 \\ + \lambda_3 \mathrm{Det}\left(\Delta^\dagger \Delta\right) + \lambda_4 \left(\Phi^\dagger \Phi\right) \mathrm{Tr}\left(\Delta^\dagger \Delta\right) + \lambda_5 \left(\Phi^\dagger \tau_i \Phi\right) \mathrm{Tr}\left(\Delta^\dagger \tau_i \Delta\right) \\ + \frac{1}{\sqrt{2}} \mu_{\Phi\Delta} \left(\Phi^T i\tau_2 \Delta \Phi\right) + \mathrm{h.c.} \end{aligned}$$

With vacuum expectation value of the SM Higgs $\langle \Phi^0 \rangle = v/\sqrt{2}$, the trilinear mass term $\mu_{\Phi\Delta}$ generates an induced VEV for Higgs triplet as $\langle \Delta^0 \rangle = v_\Delta/\sqrt{2}$ where $v_\Delta \simeq \mu_{\Phi\Delta} v^2/\sqrt{2}\mu_\Delta^2$, the resulting in 6×6 neutrino mass matrix after electroweak symmetry breaking reads as

$$\mathcal{M}_\nu = \begin{pmatrix} m_{LL} & m_{LR} \\ m_{LR}^T & M_{RR} \end{pmatrix} , \tag{2.2.3}$$

where $m_{LR} = y_\nu \, v$ is the Dirac neutrino mass, $m_{LL} = f_\nu \, v_\Delta$ is the Majorana mass for light active neutrinos and m_{RR} is the bare mass term for heavy sterile Majorana

neutrinos. Within the mass hierarchy $M_{RR} \gg m_{LR} \gg m_{LL}$, the seesaw formula for light neutrino mass is given by

$$m_\nu \equiv m_{LL} = m^I_{LL} + m^{II}_{LL} \tag{2.2.4}$$

where the formula for type I seesaw contribution is presented below,

$$m^I_{LL} = -m_{LR} M^{-1}_{RR} m^T_{LR}. \tag{2.2.5}$$

where m_{LR} is the Dirac mass term of the neutrinos which is typically of electroweak scale. Demanding the light neutrinos to be of eV scale one needs M_{RR} to be as high as 10^{14} GeV without any fine-tuning of Dirac Yukawa couplings. Whereas the type II seesaw contribution to light neutrino mass is given by

$$m^{II}_{LL} = f_\nu v_\Delta \,, \tag{2.2.6}$$

where the analytic formula for induced VEV for neutral component of the Higgs scalar triplet, derived from the minimization of the scalar potential, is

$$v_\Delta \equiv \langle \Delta^0 \rangle = \frac{\mu_{\Phi\Delta} v^2}{\mu^2_\Delta} \,. \tag{2.2.7}$$

In the low scale type II seesaw mechanism operative at TeV scale, barring the naturalness issue, one can consider a very small value of trilinear mass parameter to be

$$\mu_{\Phi\Delta} \simeq 10^{-8}\,\text{GeV}\,,$$

where the Higgs scalar triplet mass lie within TeV range which give interesting phenomenological possibility of being produced in pairs at LHC. The sub-eV scale light neutrino mass with type II seesaw mechanism contrains the corresponding Majorana Yukawa coupling as

$$f^2_\nu < 1.4 \times 10^{-5} \left(\frac{\mu_\Delta}{1\ \text{TeV}}\right) .$$

Within reasonable value of $f_\nu \simeq 10^{-2}$, the triplet Higgs scalar VEV is $v_\Delta \simeq 10^{-7}$ GeV which is in agreement with the oscillation data. It is worth to note here that the tiny trilinear mass parameter $\mu_{\Phi\Delta}$ controls the neutrino overall mass scale, but does not play any role in the couplings with the fermions and thereby, making the lepton flavour violaion studies more viable.

2.3 $\mu - \tau$ Symmetric Neutrino Mass Matrix

$\mu - \tau$ symmetric neutrino mass matrix is one of the most widely studied neutrino mixing scenario in the literature. In this work, we consider four different types of $\mu - \tau$ symmetric neutrino mass matrix: Bimaximal mixing (BM), Tri-bimaximal mixing (TBM), Hexagonal mixing (HM) and Golden Ratio mixing (GRM). These scenarios predict $\theta_{13} = 0, \theta_{23} = \frac{\pi}{4}$ whereas the value of θ_{12} depends upon the particular model. Since $\theta_{13} = 0$ has been ruled out by latest neutrino oscillation experiments, the $\mu-\tau$ symmetry has to be broken appropriately in order to account for the correct neutrino oscillation data. We assume these four different $\mu - \tau$ symmetric neutrino mass matrices to originate from type I seesaw mechanism whereas type II seesaw term acts as a perturbation which breaks $\mu - \tau$ symmetry in order to produce the correct neutrino oscillation parameters.

The $\mu - \tau$ symmetric BM type neutrino mass matrix originating from type I seesaw can be parametrised as

$$m_{LL} = \begin{pmatrix} A+B & F & F \\ F & A & B \\ F & B & A \end{pmatrix} \tag{2.3.1}$$

This has eigenvalues $m_1 = A+B+\sqrt{2}F, m_2 = A+B-\sqrt{2}F, m_3 = A-B$. It predicts the mixing angles as $\theta_{23} = \theta_{12} = 45^o$ and $\theta_{13} = 0$. It clearly shows that only the first mixing angle θ_{23} is still allowed from oscillation data whereas $\theta_{12} = 45^o$ and $\theta_{13} = 0$

have been ruled out experimentally.

The $\mu - \tau$ symmetric TBM type neutrino mass matrix originating from type I seesaw can be parametrized as

$$m_{LL} = \begin{pmatrix} A & B & B \\ B & A+F & B-F \\ B & B-F & A+F \end{pmatrix} \tag{2.3.2}$$

which is clearly $\mu - \tau$ symmetric with eigenvalues $m_1 = A - B,\ m_2 = A + 2B,$ $m_3 = A - B + 2F$. It predicts the mixing angles as $\theta_{12} \simeq 35.3^o,\ \theta_{23} = 45^o$ and $\theta_{13} = 0$. Although the prediction for first two mixing angles are still allowed from oscillation data, $\theta_{13} = 0$ has been ruled out experimentally at more than 9σ confidence level.

In the same way, the $\mu - \tau$ symmetric Hexagonal mixing (HM) type neutrino mass matrix can be written as

$$m_{LL} = \begin{pmatrix} A & B & B \\ B & \frac{1}{2}(A + 2\sqrt{\frac{2}{3}}B + F) & \frac{1}{2}(A + 2\sqrt{\frac{2}{3}}B - F) \\ B & \frac{1}{2}(A + 2\sqrt{\frac{2}{3}}B - F) & \frac{1}{2}(A + 2\sqrt{\frac{2}{3}}B + F) \end{pmatrix} \tag{2.3.3}$$

This has eigenvalues $m_1 = \frac{1}{3}(3A - \sqrt{6}B), m_2 = A + \sqrt{6}B$ and $m_3 = F$. This predicts the mixing angles to be $\theta_{23} = 45^o, \theta_{12} = 30^o$ and $\theta_{13} = 0$. Oscilation data still allow $\theta_{23} = 45^o$ and $\theta_{12} = 30^o$ whereas $\theta_{13} = 0$ is ruled out. For GRM pattern, the $\mu - \tau$ symmetric neutrino mass matrix can be written as

$$m_{LL} = \begin{pmatrix} A & B & B \\ B & F & A + \sqrt{2}B - F \\ B & A + \sqrt{2}B - F & F \end{pmatrix}, \tag{2.3.4}$$

giving the eigenvalues equal to $m_1 = \frac{1}{2}(2A + \sqrt{2}B - \sqrt{10}B), m_2 = \frac{1}{2}(2A + \sqrt{2}B + \sqrt{10}B)$, and $m_3 = -A - \sqrt{2}B + 2F$. This gives rise to neutrino mixing angles as $\theta_{23} = 45^o$, $\theta_{12} = 31.71^o$ and $\theta_{13} = 0$. Apart from θ_{13}, the other two mixing angles are still within the 3σ range of neutrino mixing angles.

2.4 Deviations from $\mu - \tau$ Symmetry

For simplicity, we assume the type II seesaw mass matrix to be of minimal form while ensuring, at the same time, that it breaks the $\mu - \tau$ symmetry in order to generate non-zero θ_{13}. The form of the neutrino mass matrix arising from type II seesaw only is taken as

$$m_{LL}^{II} = \begin{pmatrix} 0 & -w & w \\ -w & w & 0 \\ w & 0 & -w \end{pmatrix} \tag{2.4.1}$$

The structure of this mass matrix although looks ad-hoc, can however, be explained within generic flavor symmetry models like A_4. Within the framework of seesaw mechanism, neutrino mass and mixing have been extensively studied by many authors using discrete flavor symmetries [77–100] available in the literature. Among the different discrete flavor symmetry groups, the group of even permutations on four elements A_4 can naturally explain the $\mu - \tau$ symmetric mass matrix obtained from type I seesaw mechanism. Without going into the details of generating a $\mu - \tau$ symmetric mass matrix within A_4 models, an exercise performed already by several authors, here we briefly outline one possible way of generating the type II seesaw mass matrix (2.4.1) within an A_4 model. This group has 12 elements having 4 irreducible representations, with dimensions n_i, such that $\sum_i n_i^2 = 12$. The characters of 4 representations are shown in table 4.1. The complex number ω is the cube root of unity. The group A_4 has four irreducible representations namely, $\mathbf{1}, \mathbf{1}', \mathbf{1}''$ and $\mathbf{3}$. In generic A_4 models, the $SU(2)_L$ lepton doublets $l = (l_e, l_\mu, l_\tau)$ are assumed to transform as triplet $\mathbf{3}$ under A_4 whereas the $SU(2)_L$ singlet charged leptons e^c, μ^c, τ^c transform as $\mathbf{1}, \mathbf{1}', \mathbf{1}''$ respectively. In type I seesaw scenarios, the $SU(2)_L$ singlet right handed neutrinos ν^c transform as a triplet under A_4. Since we are trying to explain the structure of type II term only, we confine our discussion to the lepton doublets only. We introduce three scalars $\zeta_1, \zeta_2, \zeta_3$ transforming as $\mathbf{1}, \mathbf{1}', \mathbf{1}''$ under A_4. The $SU(2)_L$

triplet Higgs field Δ_L is assumed to be a singlet under A_4. Thus the type II seesaw term can be written as

$$\mathcal{L}^{II} = fll(\zeta_1 + \zeta_2 + \zeta_3)\Delta_L/\Lambda$$

where Λ is the cutoff scale and f is a dimensionless coupling constant.

The decomposition of the $ll\zeta_{1,2,3}$ terms into A_4 singlet gives

$$ll\zeta_1 = (l_e l_e + l_\mu l_\tau + l_\tau l_\mu)\zeta_1$$

$$ll\zeta_2 = (l_\mu l_\mu + l_e l_\tau + l_\tau l_e)\zeta_2$$

$$ll\zeta_3 = (l_\tau l_\tau + l_e l_\mu + l_\mu l_e)\zeta_3$$

Assuming the vacuum alignments of the scalars as $\langle\zeta_1\rangle = 0, \langle\zeta_2\rangle = \Lambda, \langle\zeta_3\rangle = -\Lambda$, we obtain the type II seesaw contribution to neutrino mass as

$$m_{LL}^{II} = \begin{pmatrix} 0 & -f\langle\delta_L^0\rangle & f\langle\delta_L^0\rangle \\ -f\langle\delta_L^0\rangle & f\langle\delta_L^0\rangle & 0 \\ f\langle\delta_L^0\rangle & 0 & -f\langle\delta_L^0\rangle \end{pmatrix} \tag{2.4.2}$$

which has the same form as (2.4.1) if we denote $f\langle\delta_L^0\rangle = fv_L$ as w. We adopt this minimal structure of the type II seesaw mass matrix for our numerical analysis.

Class	$\chi^{(1)}$	$\chi^{(2)}$	$\chi^{(3)}$	$\chi^{(4)}$
C_1	1	1	1	3
C_2	1	ω	ω^2	0
C_3	1	ω^2	ω	0
C_4	1	1	1	-1

Table 2.3: Character table of A_4

2.5 CP violation and Leptogenesis

Leptogenesis is one of the most widely studied mechanisms to generate the observed baryon asymmetry of the Universe by creating an asymmetry in the leptonic sector first, which subsequently gets converted into baryon asymmetry through $B + L$ violating sphaleron processes during electroweak phase transition. Since quark sector CP violation is not sufficient for producing observed baryon asymmetry, a framework explaining non-zero θ_{13} and leptonic CP phase could not only give a better picture of leptonic flavor structure, but also the origin of matter-antimatter asymmetry.

In a model with both type I and type II seesaw mechanisms at work, there are two possible sources of lepton asymmetry: either the CP violating decay of the lightest right handed neutrino or that of scalar triplet. Recently, such a work was performed in [66] where the contributions of type I and type II seesaw to baryon asymmetry were calculated without assuming any specific symmetries in the type I or type II seesaw matrices. In another work [69], type II seesaw was considered to be the origin of non-zero θ_{13} and non-trivial Dirac CP phase simultaneously and baryon asymmetry was calculated taking contribution only from the type II seesaw term. In the present work, both type I and type II seesaw mass matrices are real and hence the diagonalizing matrix U_ν of neutrino mass matrix is also real giving rise to trivial values of Dirac CP phase. Thus, the only remaining source of CP violation in leptonic sector is the charged lepton sector.

We note that the Pontecorvo-Maki-Nakagawa-Sakata (PMNS) leptonic mixing matrix is related to the diagonalizing matrices of neutrino and charged lepton mass matrices U_ν, U_l respectively, as

$$U_{\rm PMNS} = U_l^\dagger U_\nu \tag{2.5.1}$$

The PMNS mixing matrix can be parametrized as

$$U_{\rm PMNS} = \begin{pmatrix} c_{12}c_{13} & s_{12}c_{13} & s_{13}e^{-i\delta} \\ -s_{12}c_{23} - c_{12}s_{23}s_{13}e^{i\delta} & c_{12}c_{23} - s_{12}s_{23}s_{13}e^{i\delta} & s_{23}c_{13} \\ s_{12}s_{23} - c_{12}c_{23}s_{13}e^{i\delta} & -c_{12}s_{23} - s_{12}c_{23}s_{13}e^{i\delta} & c_{23}c_{13} \end{pmatrix} \tag{2.5.2}$$

where $c_{ij} = \cos\theta_{ij},\ s_{ij} = \sin\theta_{ij}$ and δ is the Dirac CP phase. Our goal is to generate correct values of neutrino mixing angles including non-zero θ_{13} with the combination of type I and type II seesaw. Since, neutrino mass matrix is real without any phase, its diagonalizing matrix U_ν is also real and takes the form of $U_{\rm PMNS}$ after setting δ to zero. Thus, the charged lepton mass diagonalizing matrix U_l, the only source of non-zero CP phase δ can be written as

$$U_l = \begin{pmatrix} c_{13}^2 + e^{i\delta}s_{13}^2 & (1-e^{-i\delta})c_{13}s_{13}s_{23} & (1-e^{-i\delta})c_{13}s_{13}c_{23} \\ (-1+e^{i\delta})c_{13}s_{13}s_{23} & c_{13}^2 + s_{13}^2(c_{23}^2 + e^{-i\delta}s_{23}^2) & (-1+e^{-i\delta})c_{23}s_{13}^2 s_{23} \\ (-1+e^{i\delta})c_{13}s_{13}c_{23} & (-1+e^{-i\delta})c_{23}s_{13}^2 s_{23} & c_{13}^2 + s_{13}^2(s_{23}^2 + e^{-i\delta}c_{23}^2) \end{pmatrix} \tag{2.5.3}$$

We derive this form of U_l such that $U_l^\dagger U_\nu$ gives the desired form of PMNS mixing matrix (2.5.2). If we assume that this matrix U_l also diagonalizes the Dirac neutrino mass matrix m_{LR}, the CP phase originating in the charged lepton sector can affect the lepton asymmetry as we discuss below.

In our work we are considering CP-violating out of equilibrium decay of heavy RH neutrinos in to Higgs and lepton within the framework of dominant type I and sub-dominant type II seesaw mechanism. In principle, the decay of Higgs triplet having masses few hundred GeV can contribute to the CP-asymmetry in the lepton sector having prominent gauge interaction along with the as usual CP-asymmetry due to heavy ($> 10^9$ GeV) right-handed neutrino decays without having any gauge interaction. The wash-out factors in case of CP-asymmetry due to Triplet decay is large and thus, the net CP-asymmetry is negligible. For simplicity we consider only the right handed neutrino decay as a source of lepton asymmetry and neglect the

contribution coming from triplet decay. The lepton asymmetry from the decay of right handed neutrino into leptons and Higgs scalar is given by

$$\epsilon_{N_k} = \sum_i \frac{\Gamma(N_k \to L_i + H^*) - \Gamma(N_k \to \bar{L}_i + H)}{\Gamma(N_k \to L_i + H^*) + \Gamma(N_k \to \bar{L}_i + H)} \tag{2.5.4}$$

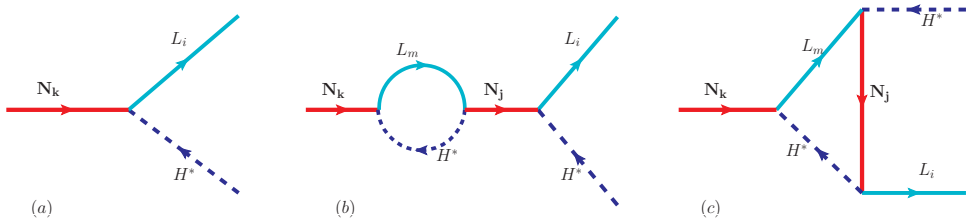

Figure 2.1: Right handed neutrino decay

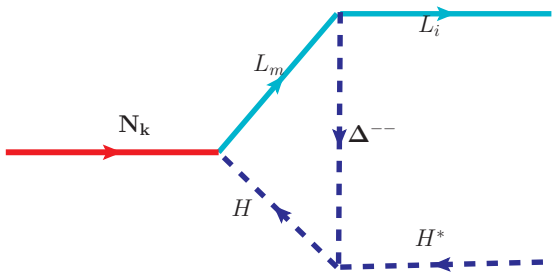

Figure 2.2: Right handed neutrino decay

In a hierarchical pattern for right handed neutrinos $M_{2,3} \gg M_1$, it is sufficient to consider the lepton asymmetry produced by the decay of lightest right handed neutrino N_1 decay. In a type I seesaw framework where the particle content is just the standard model with three additional right handed neutrinos, the lepton asymmetry is generated through the decay processes shown in figure 2.1. In the presence of type II seesaw, N_1 can also decay through a virtual triplet as can be seen in figure 2.2. Following the notations of [64], the lepton asymmetry arising from the decay of N_1

in the presence of type I seesaw only can be written as

$$\begin{aligned}\epsilon_1^\alpha &= \frac{1}{8\pi v^2}\frac{1}{(m_{LR}^\dagger m_{LR})_{11}}\sum_{j=2,3}\mathrm{Im}[(m_{LR}^*)_{\alpha 1}(m_{LR}^\dagger m_{LR})_{1j}(m_{LR})_{\alpha j}]g(x_j) \\ &+\frac{1}{8\pi v^2}\frac{1}{(m_{LR}^\dagger m_{LR})_{11}}\sum_{j=2,3}\mathrm{Im}[(m_{LR}^*)_{\alpha 1}(m_{LR}^\dagger m_{LR})_{j1}(m_{LR})_{\alpha j}]\frac{1}{1-x_j} \quad (2.5.5)\end{aligned}$$

where $v = 174$ GeV is the vev of the Higgs doublet responsible for breaking the electroweak symmetry,

$$g(x) = \sqrt{x}\left(1+\frac{1}{1-x}-(1+x)\ln\frac{1+x}{x}\right)$$

and $x_j = M_j^2/M_1^2$. The second term in the expression for ϵ_1^α above vanishes when summed over all the flavors $\alpha = e, \mu, \tau$. The sum over flavors is given by

$$\epsilon_1 = \frac{1}{8\pi v^2}\frac{1}{(m_{LR}^\dagger m_{LR})_{11}}\sum_{j=2,3}\mathrm{Im}[(m_{LR}^\dagger m_{LR})_{1j}^2]g(x_j) \quad (2.5.6)$$

After determining the lepton asymmetry ϵ_1, the corresponding baryon asymmetry can be obtained by

$$Y_B = c\kappa\frac{\epsilon}{g_*} \quad (2.5.7)$$

through electroweak sphaleron processes [50]. Here the factor c is measure of the fraction of lepton asymmetry being converted into baryon asymmetry and is approximately equal to -0.55. κ is the dilution factor due to wash-out process which erase the produced asymmetry and can be parametrized as [101–103]

$$\begin{aligned}-\kappa &\simeq \sqrt{0.1K}\exp[-4/(3(0.1K)^{0.25})], \text{ for } K \geq 10^6 \\ &\simeq \frac{0.3}{K(\ln K)^{0.6}}, \text{ for } 10 \leq K \leq 10^6 \\ &\simeq \frac{1}{2\sqrt{K^2+9}}, \text{ for } 0 \leq K \leq 10. \quad (2.5.8)\end{aligned}$$

where K is given as

$$K = \frac{\Gamma_1}{H(T=M_1)} = \frac{(m_{LR}^\dagger m_{LR})_{11}M_1}{8\pi v^2}\frac{M_{Pl}}{1.66\sqrt{g_*}M_1^2}$$

Here Γ_1 is the decay width of N_1 and $H(T = M_1)$ is the Hubble constant at temperature $T = M_1$. The factor g_* is the effective number of relativistic degrees of freedom at $T = M_1$ and is approximately 110.

We note that the lepton asymmetry shown in equation (2.5.6) is obtained by summing over all the flavors $\alpha = e, \mu, \tau$. A non-vanishing lepton asymmetry is generated only when the right handed neutrino decay is out of equilibrium. Otherwise both the forward and the backward processes will happen at the same rate resulting in a vanishing asymmetry. Departure from equilibrium can be estimated by comparing the interaction rate with the expansion rate of the Universe. At very high temperatures ($T \geq 10^{12}$GeV) all charged lepton flavors are out of equilibrium and hence all of them behave similarly resulting in the one flavor regime. However at temperatures $T < 10^{12}$ GeV ($T < 10^9$GeV), interactions involving tau (muon) Yukawa couplings enter equilibrium and flavor effects become important [104–107]. Taking these flavor effects into account, the final baryon asymmetry is given by

$$Y_B^{2flavor} = \frac{-12}{37g^*}[\epsilon_2\eta\left(\frac{417}{589}\tilde{m_2}\right) + \epsilon_1^\tau\eta\left(\frac{390}{589}\tilde{m_\tau}\right)]$$

$$Y_B^{3flavor} = \frac{-12}{37g^*}[\epsilon_1^e\eta\left(\frac{151}{179}\tilde{m_e}\right) + \epsilon_1^\mu\eta\left(\frac{344}{537}\tilde{m_\mu}\right) + \epsilon_1^\tau\eta\left(\frac{344}{537}\tilde{m_\tau}\right)]$$

where $\epsilon_2 = \epsilon_1^e + \epsilon_1^\mu, \tilde{m_2} = \tilde{m_e} + \tilde{m_\mu}, \tilde{m_\alpha} = \frac{(m_{LR}^*)_{\alpha 1}(m_{LR})_{\alpha 1}}{M_1}$. The function η is given by

$$\eta(\tilde{m_\alpha}) = \left[\left(\frac{\tilde{m_\alpha}}{8.25\times10^{-3}\text{eV}}\right)^{-1} + \left(\frac{0.2\times10^{-3}\text{eV}}{\tilde{m_\alpha}}\right)^{-1.16}\right]^{-1}$$

In the presence of an additional scalar triplet, the right handed neutrino can also decay through a virtual triplet as shown in figure 2.2. The contribution of this diagram to lepton asymmetry can be estimated as [108, 109]

$$\epsilon_{\Delta 1}^\alpha = -\frac{M_1}{8\pi v^2}\frac{\sum_{j=2,3}\text{Im}[(m_{LR})_{1j}(m_{LR})_{1\alpha}(M_\nu^{II*})_{j\alpha}]}{\sum_{j=2,3}|(m_{LR})_{1j}|^2} \tag{2.5.9}$$

For the calculation of baryon asymmetry, we go to the basis where the right handed Majorana neutrino mass matrix is diagonal

$$U_R^* M_{RR} U_R^\dagger = \text{diag}(M_1, M_2, M_3) \tag{2.5.10}$$

In this diagonal M_{RR} basis, the Dirac neutrino mass matrix also changes to

$$m_{LR} = m_{LR}^0 U_R \tag{2.5.11}$$

where m_{LR}^0 is the Dirac neutrino mass matrix given by

$$m_{LR}^0 = U_l m_{LR}^d U_l^\dagger \tag{2.5.12}$$

Here m_{LR}^d is the diagonal form of the Dirac neutrino mass matrix in our calculation given by

$$m_{LR}^d = \begin{pmatrix} \lambda^m & 0 & 0 \\ 0 & \lambda^n & 0 \\ 0 & 0 & 1 \end{pmatrix} m_f \tag{2.5.13}$$

where $\lambda = 0.22$ is the standard Wolfenstein parameter, (m, n) are positive integers and $m_f = m_\tau \; tan\beta = 80.43\text{GeV}$. As mentioned earlier, U_l is the matrix which is assumed to diagonalize both the charged lepton and Dirac neutrino mass matrices.

2.6 Numerical Analysis

To begin with, we write down the light neutrino mass matrix m_{LL} in terms of (complex) mass eigenvalues m_1, m_2, m_3 and PMNS mixing matrix $U_{\text{PMNS}} \equiv U$, working in a basis where charged lepton mass matrix is already diagonal, as

$$m_\nu = U^* \text{diag}(m_1, m_2, m_3) U^\dagger \,. \tag{2.6.1}$$

The mixing matrix U is parametrized in terms of three neutrino mixing angle θ_{23}, θ_{12}, θ_{13} and a Dirac phase δ. The two Majorana phases are absorbed in mass eigenvalues

m_i instead in the mixing matrix U. Here the two Majorana phases are simply taken to be zero for subsequent numerical analysis.

At the first step of numerical analysis, we have considered particularly four choices of U and m_ν so that $\theta_{13} = 0$ and θ_{23} is maximal with the general form of the mixing matrix at leading order as

$$U = \begin{pmatrix} c_{12} & s_{12} & 0 \\ -s_{12}/\sqrt{2} & c_{12}/\sqrt{2} & -1/\sqrt{2} \\ -s_{12}/\sqrt{2} & c_{12}/\sqrt{2} & 1/\sqrt{2} \end{pmatrix} \tag{2.6.2}$$

We start writing the relevant matrix form for light neutrino mass satisfying $\mu-\tau$ symmetry and corresponding mixing matrix having different values of θ_{12} but consistent with our earlier assumptions, i.e. $\theta_{13} = 0$ and maximal θ_{23}, as

$$m_\nu^{(0)}\big|_{\rm BM} = \begin{pmatrix} A+B & F & F \\ F & A & B \\ F & B & A \end{pmatrix}, \qquad U_{\rm BM} = \begin{pmatrix} 1/\sqrt{2} & 1/\sqrt{2} & 0 \\ -1/2 & 1/2 & -1/\sqrt{2} \\ -1/2 & 1/2 & 1/\sqrt{2} \end{pmatrix}, \tag{2.6.3}$$

with $m_1 = A + B + \sqrt{2}F, m_2 = A + B - \sqrt{2}F, m_3 = A - B$.

$$m_\nu^{(0)}\big|_{\rm TBM} = \begin{pmatrix} A & B & B \\ B & A+F & B-F \\ B & B-F & A+F \end{pmatrix}, \qquad U_{\rm TBM} = \begin{pmatrix} 2/\sqrt{6} & 1/\sqrt{3} & 0 \\ -1/\sqrt{6} & 1/\sqrt{3} & -1/\sqrt{2} \\ -1/\sqrt{6} & 1/\sqrt{3} & 1/\sqrt{2} \end{pmatrix} \tag{2.6.4}$$

with $m_1 = A - B,\ m_2 = A + 2B,\ m_3 = A - B + 2F$. It is clear from the BM and TBM-type of mixing matrices

$$\tan^2\theta_{23} = |U_{\mu 3}|^2/|U_{\tau 3}|^2 = 1\,.$$

Similarly, there are other two other types of mass matrix and mixing matrix which can reproduce $\theta_{13} = 0$ and maximal θ_{23} and they are: (i) Hexagonal type predicting

$\theta_{12} = \pi/6$, (ii) Golden ratio type for which $\theta_{12} \tan^{-1}(1/\varphi)$ with $\phi = (1+\sqrt{5})/2$.

$$m_\nu^{(0)}\big|_{\mathrm{HM}} = \begin{pmatrix} A & B & B \\ B & \frac{1}{2}(A + 2\sqrt{\frac{2}{3}}B + F) & \frac{1}{2}(A + 2\sqrt{\frac{2}{3}}B - F) \\ B & \frac{1}{2}(A + 2\sqrt{\frac{2}{3}}B - F) & \frac{1}{2}(A + 2\sqrt{\frac{2}{3}}B + F) \end{pmatrix},$$
$$U_{\mathrm{HM}} = \begin{pmatrix} \frac{\sqrt{3}}{2} & \frac{1}{2} & 0 \\ -\frac{\sqrt{2}}{4} & \frac{\sqrt{6}}{4} & -\frac{1}{\sqrt{2}} \\ -\frac{\sqrt{2}}{4} & -\frac{\sqrt{6}}{4} & \frac{1}{\sqrt{2}} \end{pmatrix} \tag{2.6.5}$$

with $m_1 = \frac{1}{3}(3A - \sqrt{6}B), m_2 = A + \sqrt{6}B$ and $m_3 = F$.

$$m_\nu^{(0)}\big|_{\mathrm{GRM}} = \begin{pmatrix} A & B & B \\ B & F & A + \sqrt{2}B - F \\ B & A + \sqrt{2}B - F & F \end{pmatrix},$$
$$U_{\mathrm{GRM}} = \begin{pmatrix} \frac{\sqrt{2}}{\sqrt{5-\sqrt{5}}} & \frac{\sqrt{2}}{\sqrt{5+\sqrt{5}}} & 0 \\ -\frac{\sqrt{2}}{\sqrt{5+\sqrt{5}}} & \frac{\sqrt{2}}{\sqrt{5-\sqrt{5}}} & -1/\sqrt{2} \\ -\frac{\sqrt{2}}{\sqrt{5+\sqrt{5}}} & \frac{\sqrt{2}}{\sqrt{5-\sqrt{5}}} & 1/\sqrt{2} \end{pmatrix} \tag{2.6.6}$$

with $m_1 = \frac{1}{2}(2A + \sqrt{2}B - \sqrt{10}B), m_2 = \frac{1}{2}(2A + \sqrt{2}B + \sqrt{10}B)$, and $m_3 = -A - \sqrt{2}B + 2F$.

Parameters (BM)	IH	NH	IH	NH
A	0.023946	0.015114	0.0731646	0.0741
B	0.024946	0.0141142	0.00816462	0.00409996
F	0.00027118	0.0145033	0.000163019	0.00542086
m_3	0.001	0.0497393	0.065	0.0858662
m_2	0.0492747	0.0087178	0.0815598	0.0705337
m_1	0.0485077	0.001	0.0810987	0.07
$\sum_i m_i$	0.0987824	0.0594571	0.22766	0.22639

Table 2.4: Parametrization of the neutrino mass matrix for BM

Parameters (TBM)	IH	NH	IH	NH
A	0.0487942	0.0035726	0.0812524	0.07017789
B	0.0002555	0.0025726	0.000153696	0.00017789
F	-0.023769	0.0243546	-0.00804935	0.007798948
m_3	0.001	0.0497092	0.065	0.0855979
m_2	0.0493052	0.0087178	0.0815598	0.0705337
m_1	0.0485387	0.001	0.0810987	0.07
$\sum_i m_i$	0.098844	0.059427	0.227657	0.226132

Table 2.5: Parametrization of the neutrino mass matrix for TBM

Parameters (HM)	IH	NH	IH	NH
A	0.048699	0.00292945	0.081214	0.0701334
B	0.00023485	0.00236308	0.000141179	0.000163405
F	0.001	0.0497393	0.065	0.0858662
m_3	0.001	0.0497393	0.065	0.0858662
m_2	0.0492747	0.0087178	0.0815598	0.0705337
m_1	0.0485077	0.001	0.0810987	0.07
$\sum_i m_i$	0.0987824	0.0594571	0.227658	0.2261957

Table 2.6: Parametrization of the neutrino mass matrix for HM

For normal hierarchy, the diagonal mass matrix of the light neutrinos can be written as $m_{\text{diag}} = \text{diag}(m_1, \sqrt{m_1^2 + \Delta m_{21}^2}, \sqrt{m_1^2 + \Delta m_{31}^2})$ whereas for inverted hierarchy it can be written as $m_{\text{diag}} = \text{diag}(\sqrt{m_3^2 + \Delta m_{23}^2 - \Delta m_{21}^2}, \sqrt{m_3^2 + \Delta m_{23}^2}, m_3)$. We choose two possible values of the lightest mass eigenstate m_1, m_3 for normal and inverted hierarchies respectively. First we choose m_{lightest} as large as possible such that the sum of the absolute neutrino masses fall just below the cosmological upper bound. For normal and inverted hierarchies, this turns out to be 0.07 eV and 0.065 eV respectively. Then we allow moderate hierarchy to exist between the mass eigenvalues and choose

the lightest mass eigenvalue to be 0.001 eV to study the possible changes in our analysis and results. The parametrization for all these possible cases are shown in table 2.4, 2.5, 2.6 and 2.7.

Parameters (GRM)	IH	NH	IH	NH
A	0.0487197	0.00305254	0.0812261	0.0701377
B	0.0002425	0.00234835	0.000145813	0.000157545
F	0.0250314	0.0270146	0.0732162	0.0775182
m_3	0.001	0.047655	0.065	0.0846759
m_2	0.0492747	0.0084262	0.0815598	0.0704982
m_1	0.0485077	0.001	0.0810987	0.07
$\sum_i m_i$	0.0987824	0.057081	0.227658	0.225174

Table 2.7: Parametrization of the neutrino mass matrix for GRM

Parameters	TBM(IH)	TBM(NH)	BM(IH)	HEX (NH)
w	0.004435	0.004575	0.00461	0.00461
$\sin^2\theta_{13}$	0.01621	0.01672	0.01622	0.01621
$\sin^2\theta_{23}$	0.4105	0.5918	0.4102	0.5937

Table 2.8: Parameters used in the calculation of baryogenesis

Model	δ for 1 flavor(in radian)	δ for 2 flavor(in radian)
TBM(IH), $m_3 = 0.001$	0.00329867-0.0043982297, 3.1376656-3.13860814	3.14190681
TBM(NH), $m_1 = 0.001$	3.14269221-3.14300637, 6.282085749-6.282242829	-
BM(IH), $m_3 = 0.001$	0.000314159, 1.40711935, 4.8754376	0.0001570769
HEX(NH), $m_1 = 0.001$	3.182276-3.1981413, 6.28020079-6.2808291	-

Table 2.9: Values of δ giving rise to correct baryon asymmetry

For our numerical analysis, we adopt the minimal structure (2.4.1) of the type II seesaw term as

$$m_{LL}^{II} = \begin{pmatrix} 0 & -w & w \\ -w & w & 0 \\ w & 0 & -w \end{pmatrix} , \tag{2.6.7}$$

where ω denotes the strength of perturbation coming from type II seesaw mechanism.

We first numerically fit the leading order $\mu - \tau$ symmetric neutrino mass matrix (2.3.2) by taking the central values of the global fit neutrino oscillation data [10]. We also incorporate the cosmological upper bound on the sum of absolute neutrino masses [49] reported by the Planck collaboration recently. In the second step, we have to diagonalize the complete mass matrix

$$m_\nu = m_\nu^{(0)} + m_\nu^{(pert.)} = m_\nu^I + m_\nu^{II} ,$$

and as a result, there is a corresponding mixing matrix whose elements are related to the parameters of the model plus the strength of the type II perturbation term.

After fitting the type I seesaw contribution to neutrino mass with experimental data, we introduce the type II seesaw contribution as a perturbation to the $\mu - \tau$ symmetric neutrino mass matrix.

The strength of the type II seesaw perturbation in order to generate the correct value of non-zero θ_{13} can be seen from figure 2.3, 2.4, 2.5 and 2.6. We also calculate other neutrino parameters by varying the type II seesaw strength and show our results as a function of $\sin^2\theta_{13}$ in figure 2.7, 2.8, 2.9, 2.10 for BM mixing, figure 2.11, 2.12, 2.13, 2.14 for TBM mixing, figure 2.15, 2.16, 2.17, 2.18 for Hexagonal mixing and figure 2.19, 2.20, 2.21, 2.22 for GR mixing. We also calculate the sum of the absolute neutrino masses $\sum_i |m_i|$ to check whether it lies below the Planck upper bound. Finally, we calculate the effective neutrino mass $m_{ee} = |\sum_i U_{ei}^2 m_i|$ which can play a great role in neutrino-less double beta decay. These are shown as a function of $\sin^2\theta_{13}$ in figure 2.23, 2.24, 2.25, 2.26, 2.27, 2.28, 2.29 and 2.30.

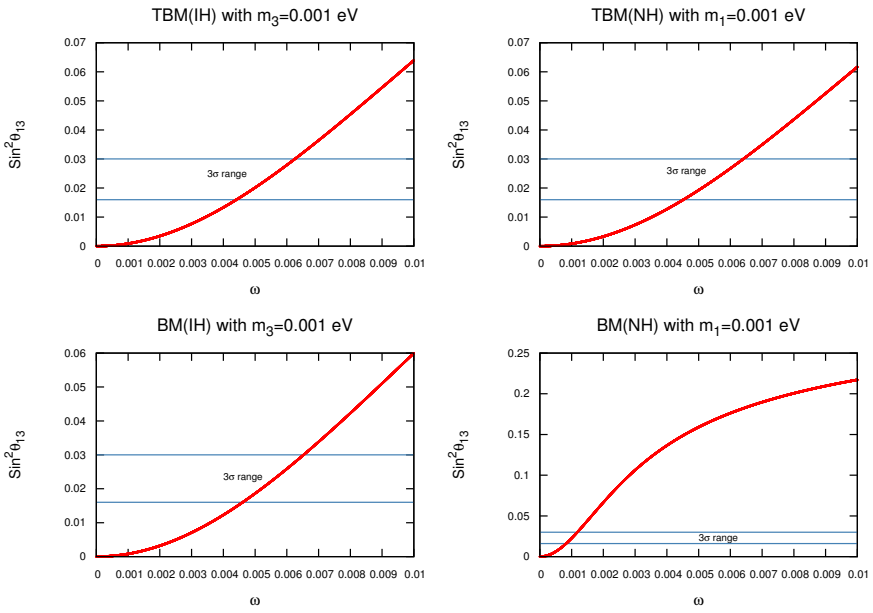

Figure 2.3: Variation of $\sin^2\theta_{13}$ with type II seesaw strength w for BM and TBM with $m_1(m_3) = 0.07(0.065)$ eV.

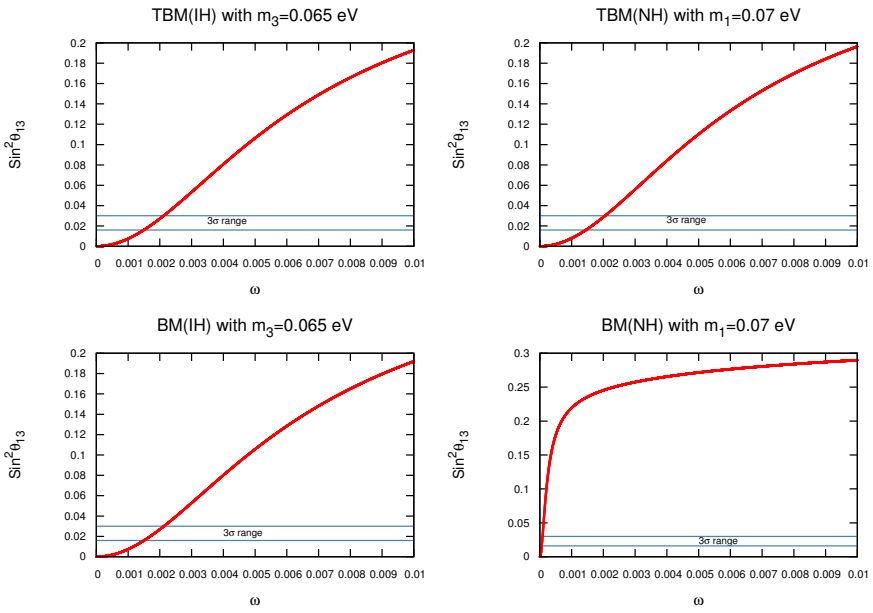

Figure 2.4: $\sin^2\theta_{13}$ with type II seesaw strength w for BM and TBM with $m_1(m_3) = 0.07(0.065)$ eV.

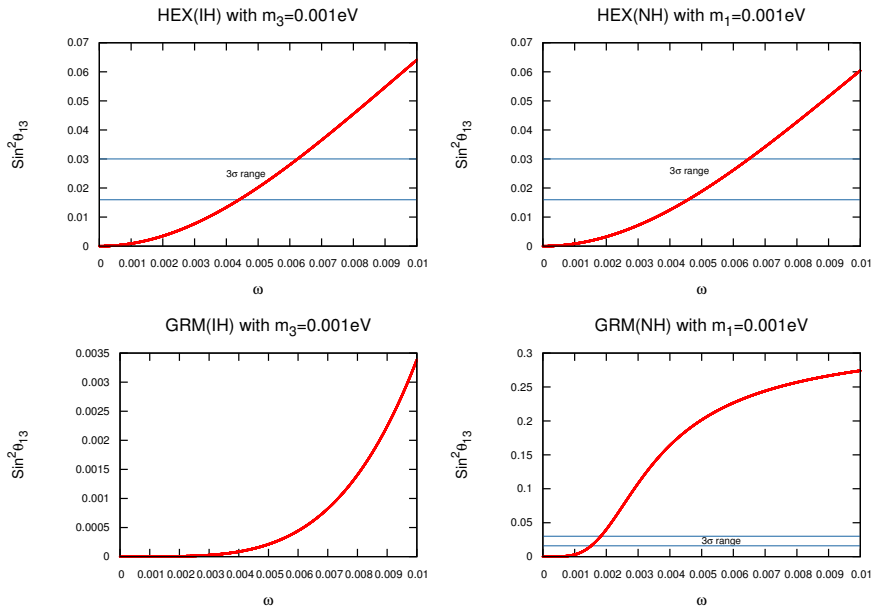

Figure 2.5: $\sin^2\theta_{13}$ with type II seesaw strength w for HM and GRM with $m_1(m_3) = 0.001$ eV.

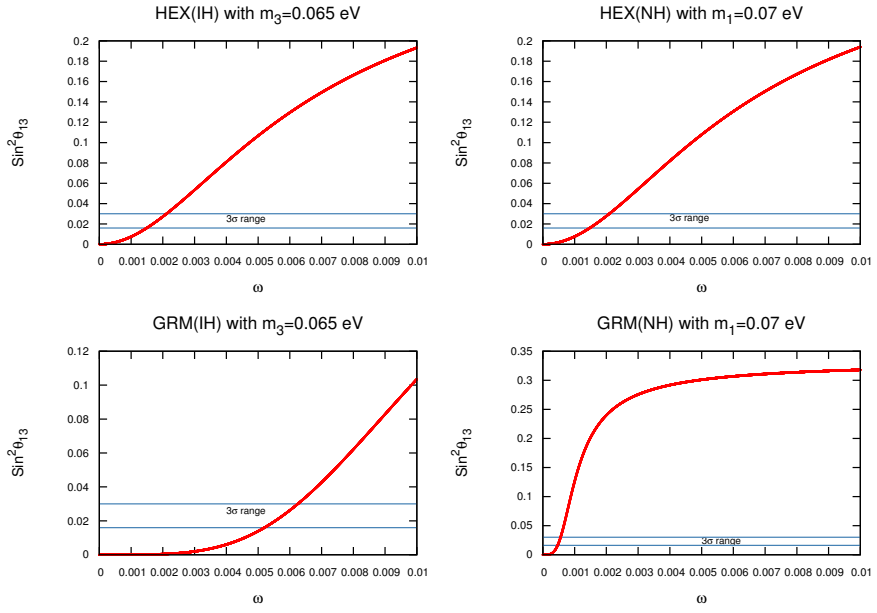

Figure 2.6: $\sin^2\theta_{13}$ with type II seesaw strength w for HM and GRM with $m_1(m_3) = 0.07(0.065)$ eV.

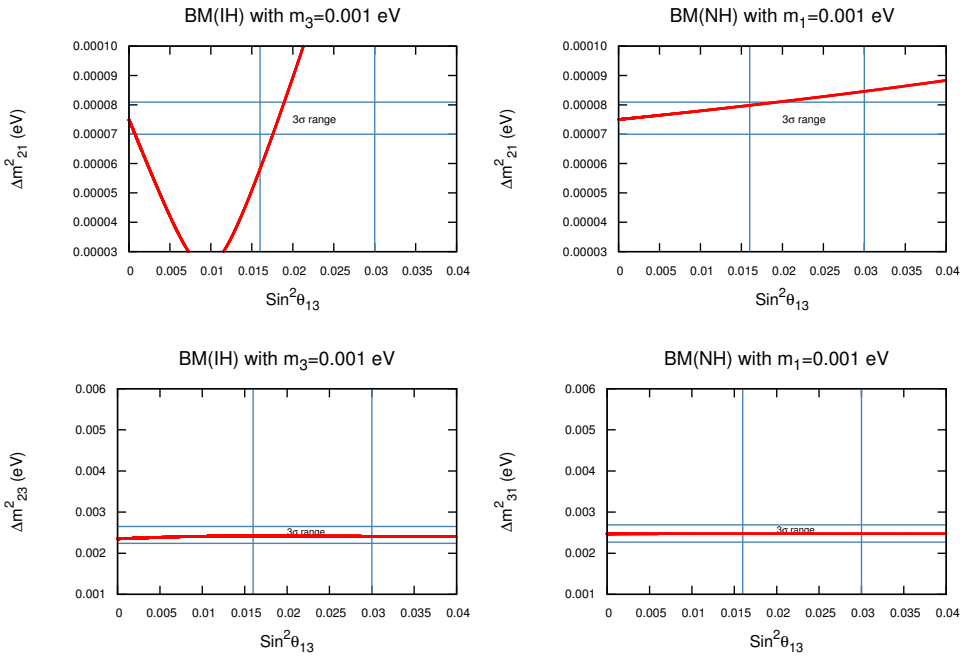

Figure 2.7: Δm^2_{21}, Δm^2_{23}, Δm^2_{31} with $\sin^2\theta_{13}$ for BM with $m_1(m_3) = 0.001$ eV.

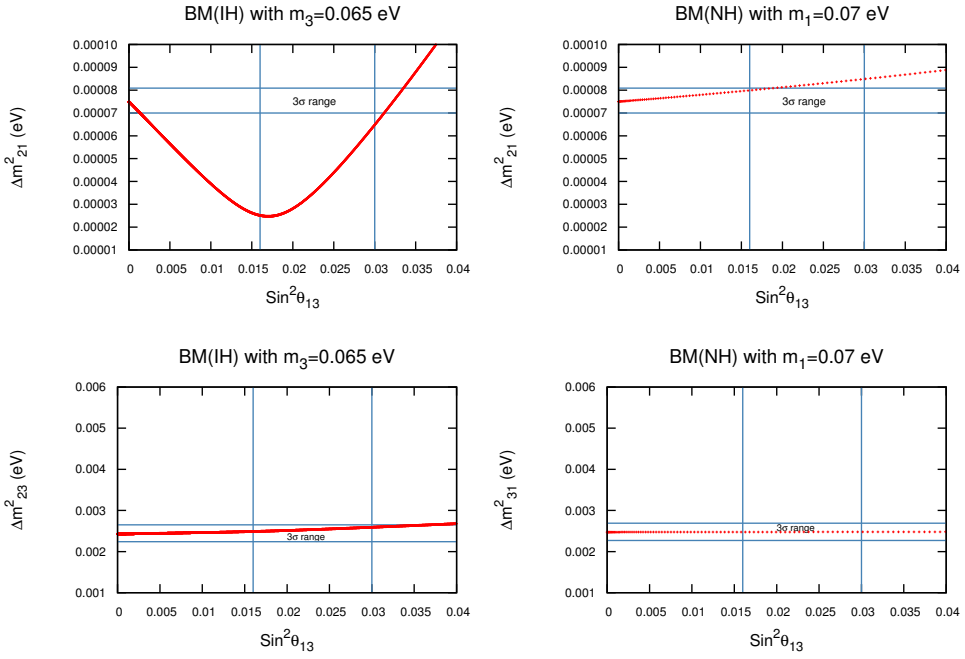

Figure 2.8: Δm^2_{21}, Δm^2_{23}, Δm^2_{31} with $\sin^2\theta_{13}$ for BM with $m_1(m_3) = 0.07(0.065)$ eV.

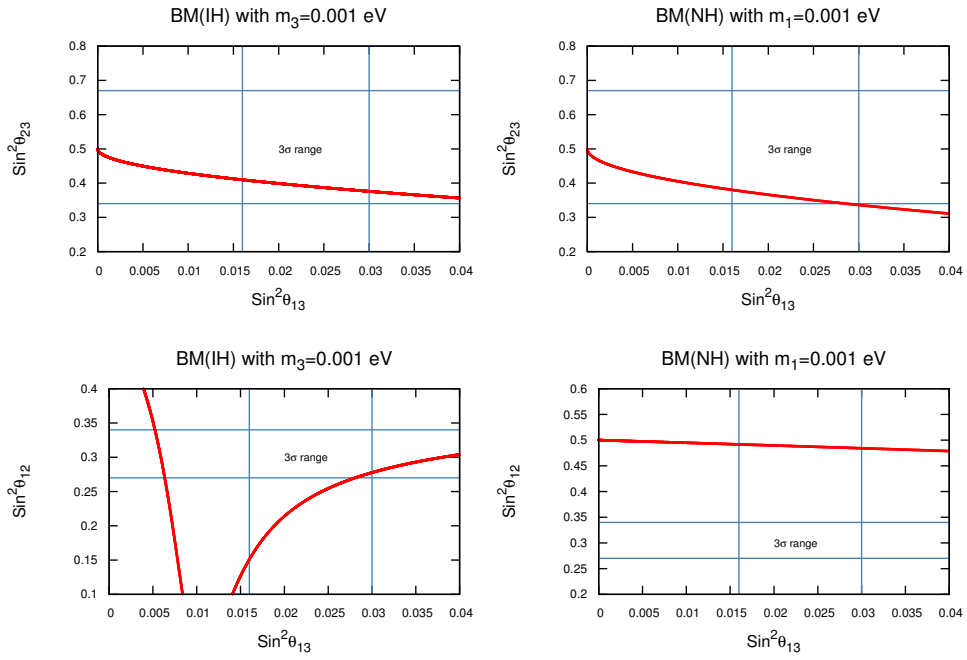

Figure 2.9: $\sin^2\theta_{23}$, $\sin^2\theta_{12}$ with $\sin^2\theta_{13}$ for BM with $m_1(m_3) = 0.001$ eV.

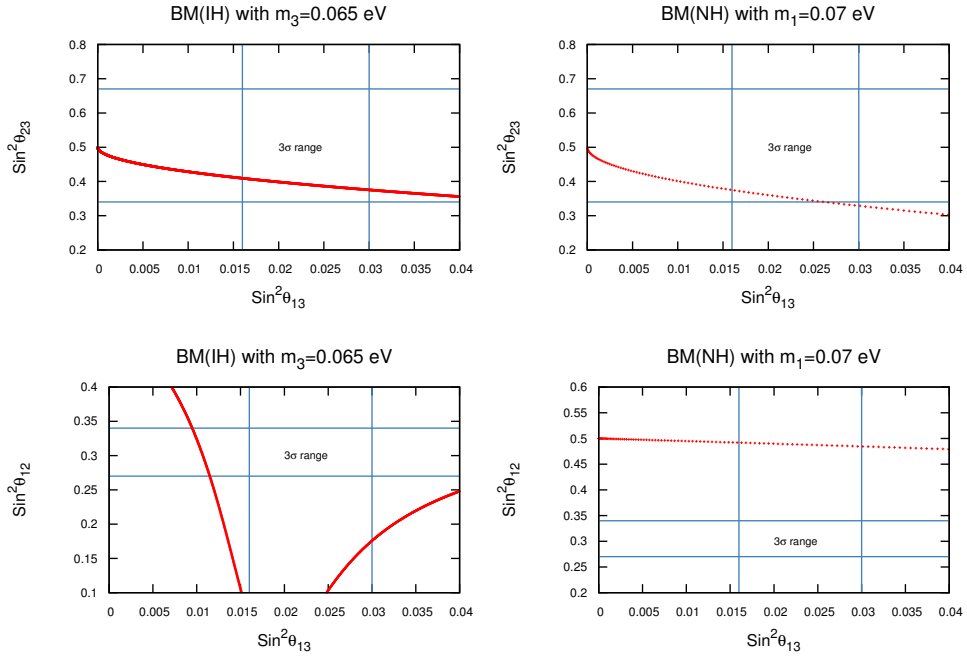

Figure 2.10: $\sin^2\theta_{23}$, $\sin^2\theta_{12}$ with $\sin^2\theta_{13}$ for BM with $m_1(m_3) = 0.07(0.065)$ eV.

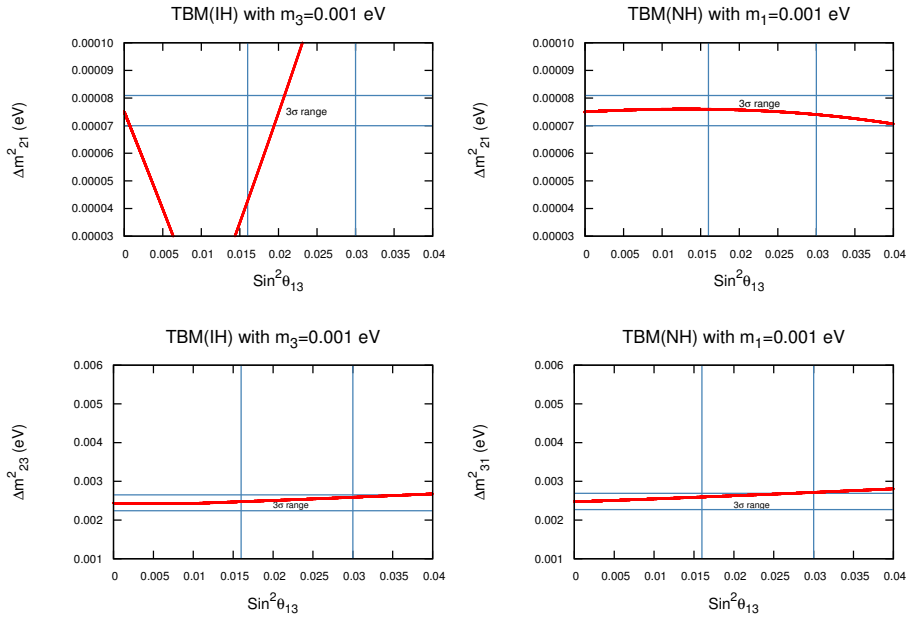

Figure 2.11: Δm^2_{21}, Δm^2_{23}, Δm^2_{31} with $\sin^2\theta_{13}$ for TBM with $m_1(m_3) = 0.001$ eV.

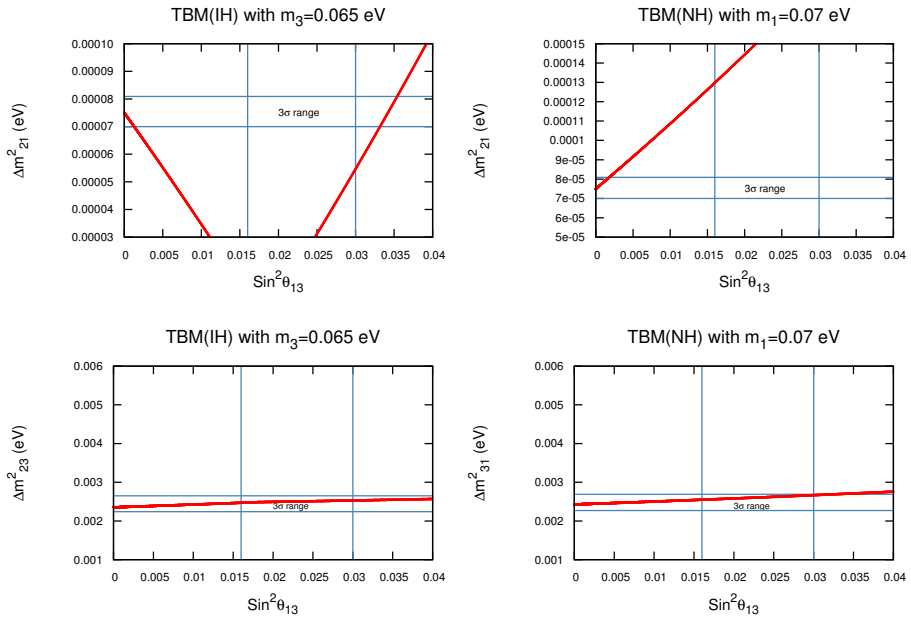

Figure 2.12: Δm^2_{21}, Δm^2_{23}, Δm^2_{31} with $\sin^2\theta_{13}$ for TBM with $m_1(m_3) = 0.07(0.065)$ eV.

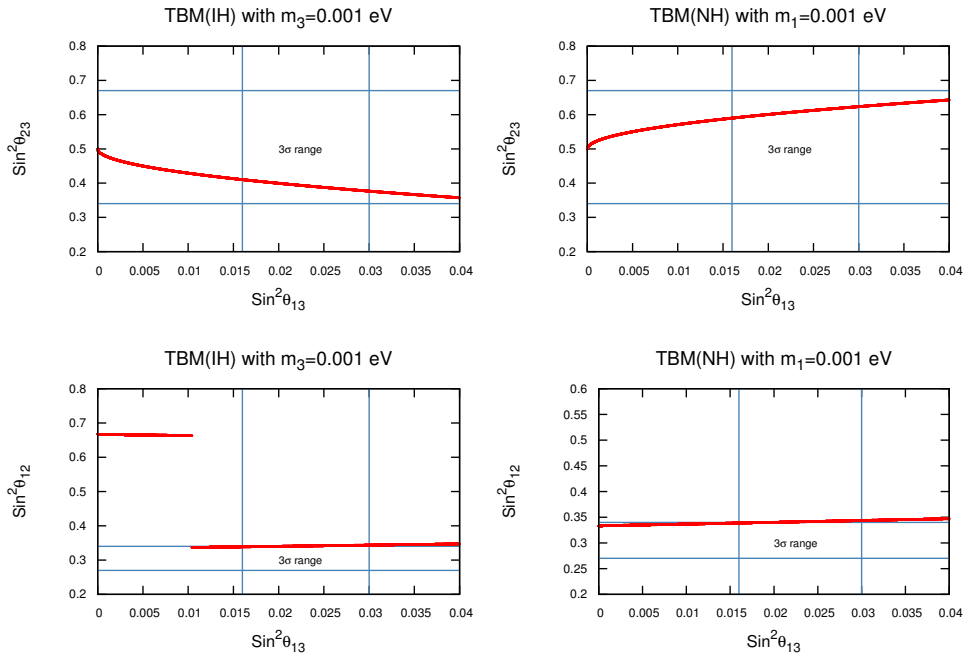

Figure 2.13: $\sin^2\theta_{23}$, $\sin^2\theta_{12}$ with $\sin^2\theta_{13}$ for TBM with $m_1(m_3) = 0.001$ eV.

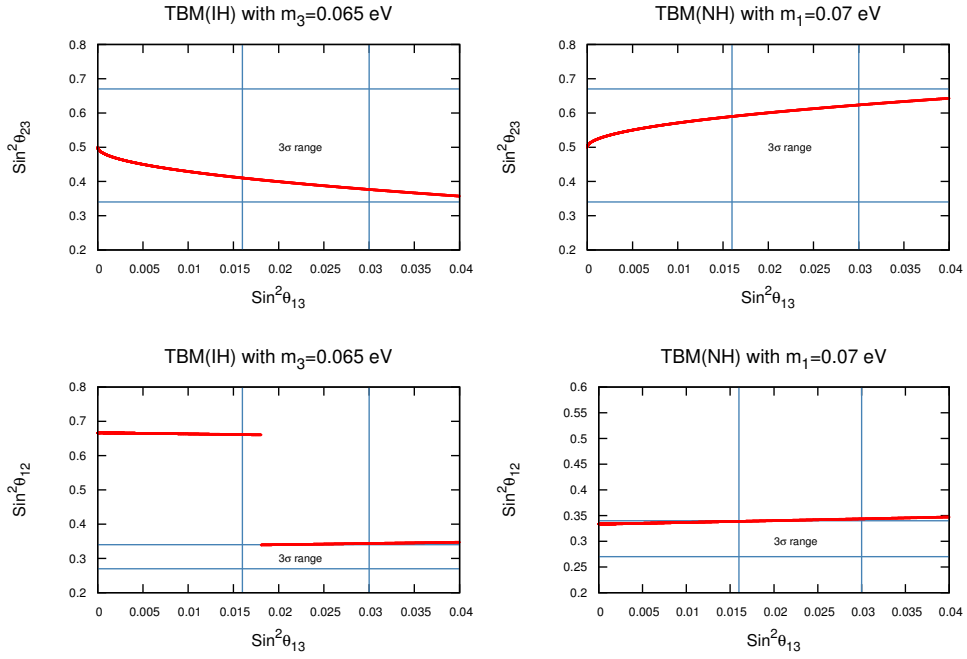

Figure 2.14: $\sin^2\theta_{23}$, $\sin^2\theta_{12}$ with $\sin^2\theta_{13}$ for TBM with $m_1(m_3) = 0.07(0.065)$ eV.

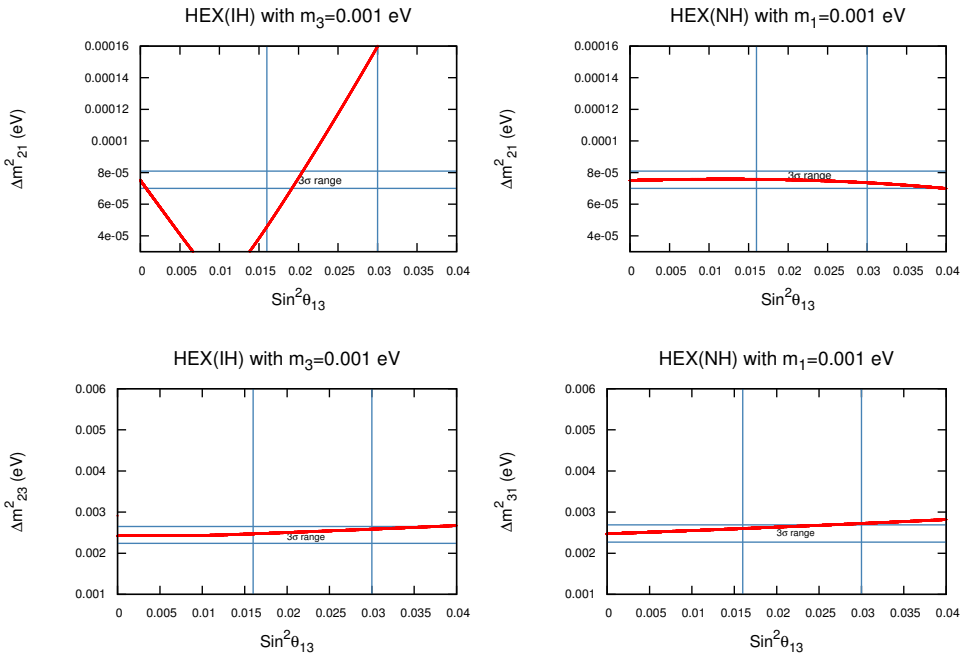

Figure 2.15: Δm^2_{21}, Δm^2_{23}, Δm^2_{31} with $\sin^2\theta_{13}$ for HM with $m_1(m_3) = 0.001$ eV.

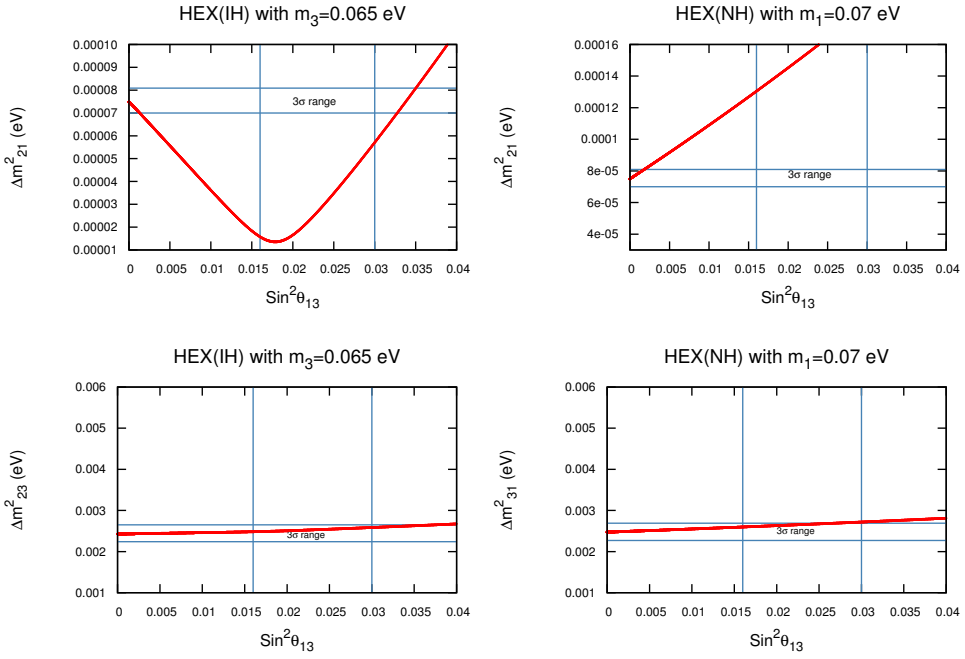

Figure 2.16: Δm^2_{21}, Δm^2_{23}, Δm^2_{31} with $\sin^2\theta_{13}$ for HM with $m_1(m_3) = 0.07(0.065)$ eV.

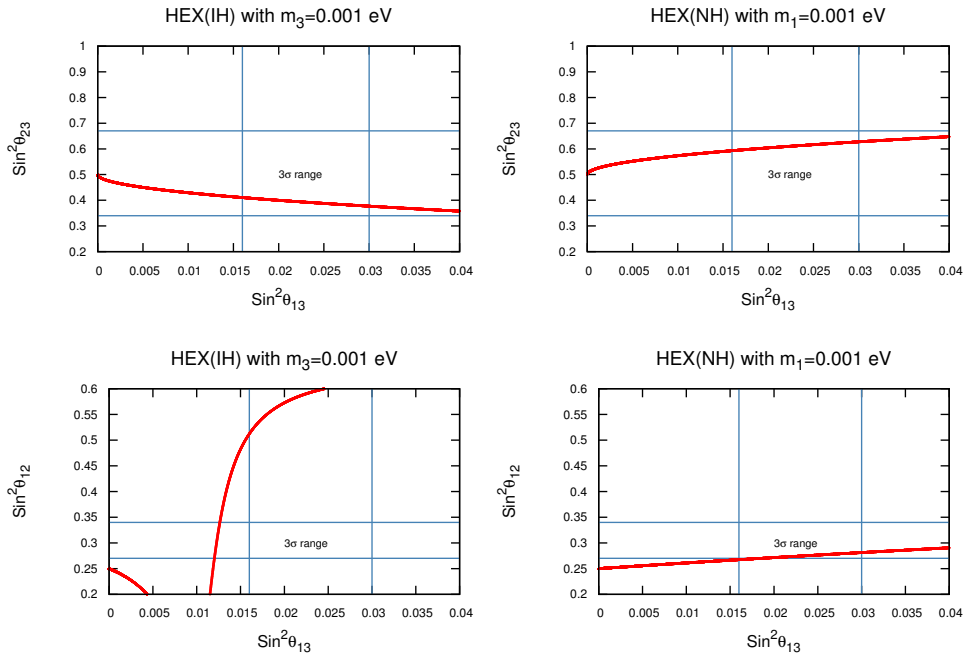

Figure 2.17: $\sin^2\theta_{23}$, $\sin^2\theta_{12}$ with $\sin^2\theta_{13}$ for HM with $m_1(m_3) = 0.001$ eV.

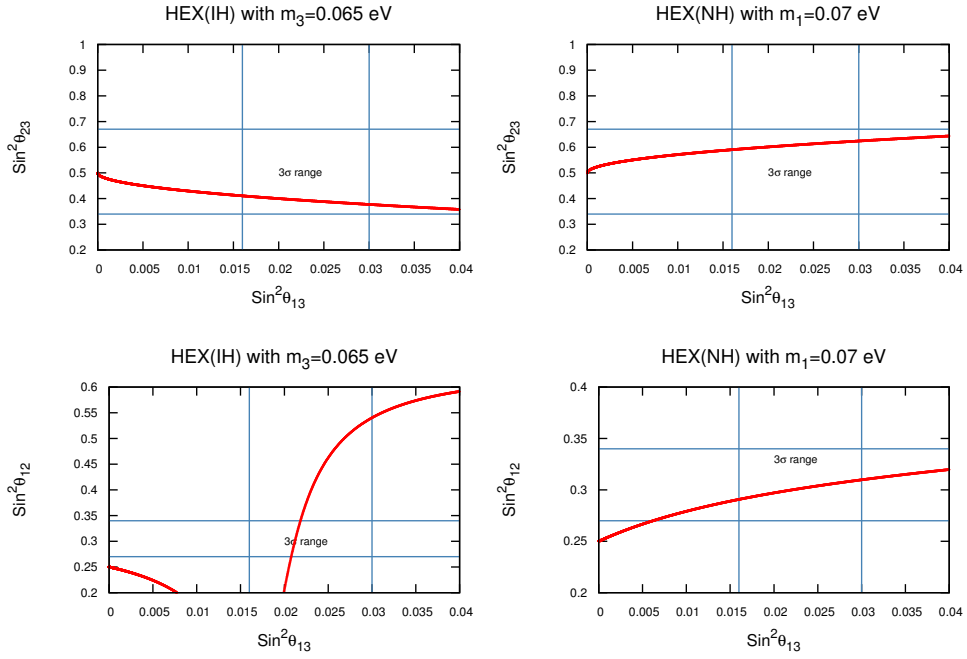

Figure 2.18: $\sin^2\theta_{23}$, $\sin^2\theta_{12}$ with $\sin^2\theta_{13}$ for HM with $m_1(m_3) = 0.07(0.065)$ eV.

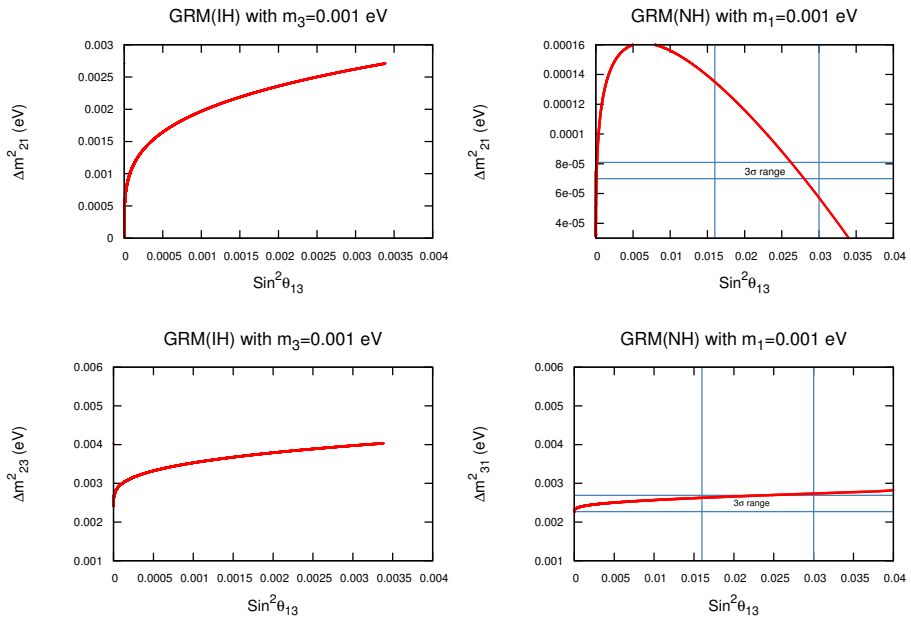

Figure 2.19: Δm^2_{21}, Δm^2_{23}, Δm^2_{31} with $\sin^2\theta_{13}$ for GRM with $m_1(m_3) = 0.001$ eV.

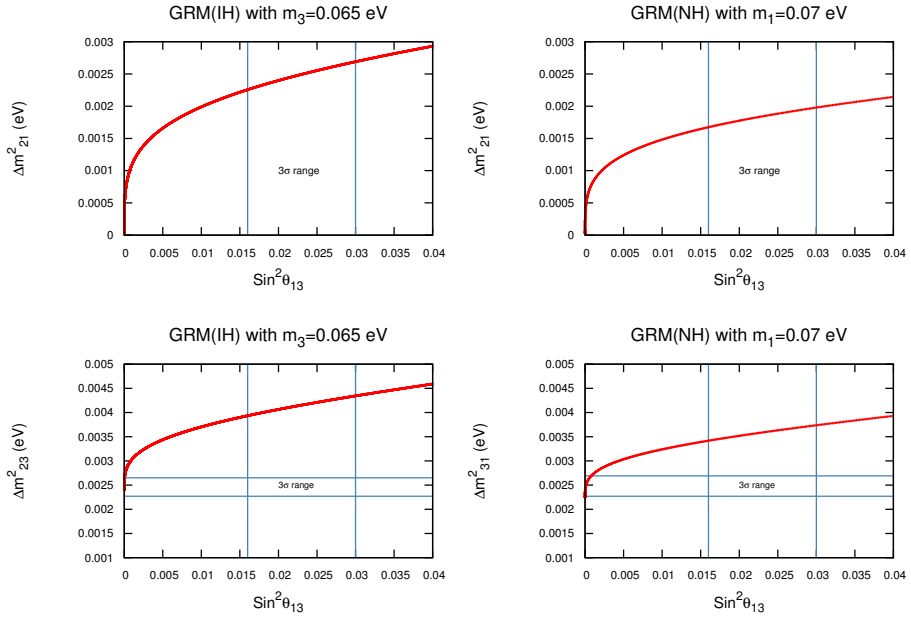

Figure 2.20: Δm^2_{21}, Δm^2_{23}, Δm^2_{31} with $\sin^2\theta_{13}$ for GRM with $m_1(m_3) = 0.07(0.065)$ eV.

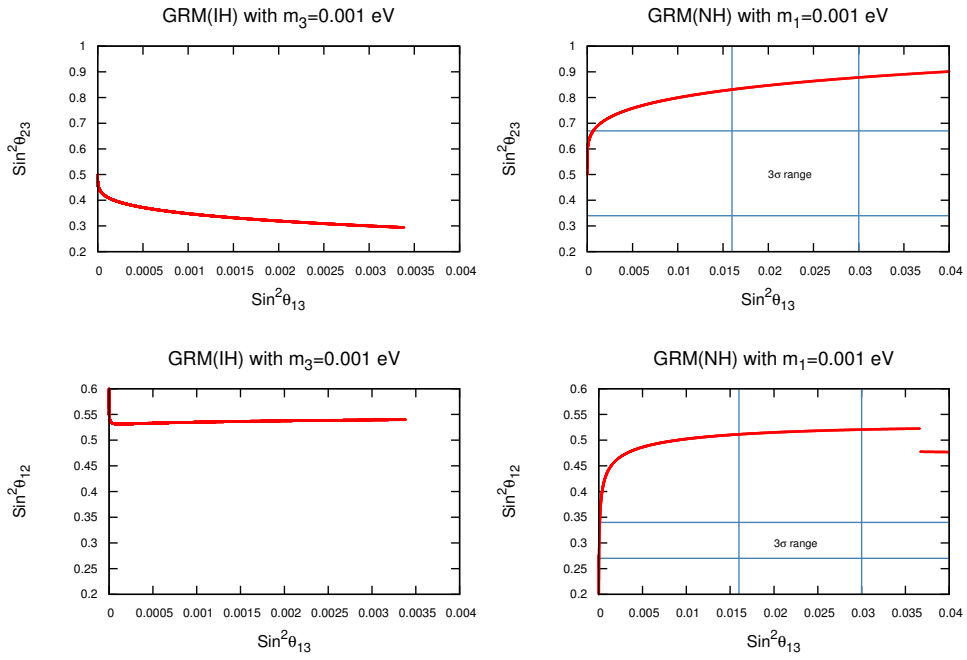

Figure 2.21: $\sin^2\theta_{23}$, $\sin^2\theta_{12}$ with $\sin^2\theta_{13}$ for GRM with $m_1(m_3) = 0.001$ eV.

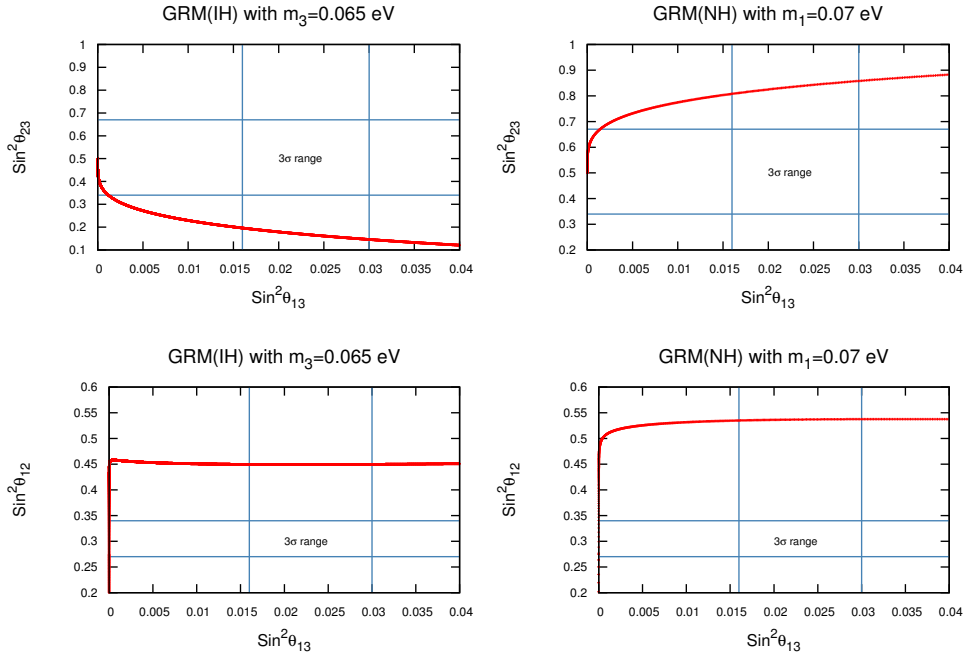

Figure 2.22: $\sin^2\theta_{23}$, $\sin^2\theta_{12}$ with $\sin^2\theta_{13}$ for GRM with $m_1(m_3) = 0.07(0.065)$ eV.

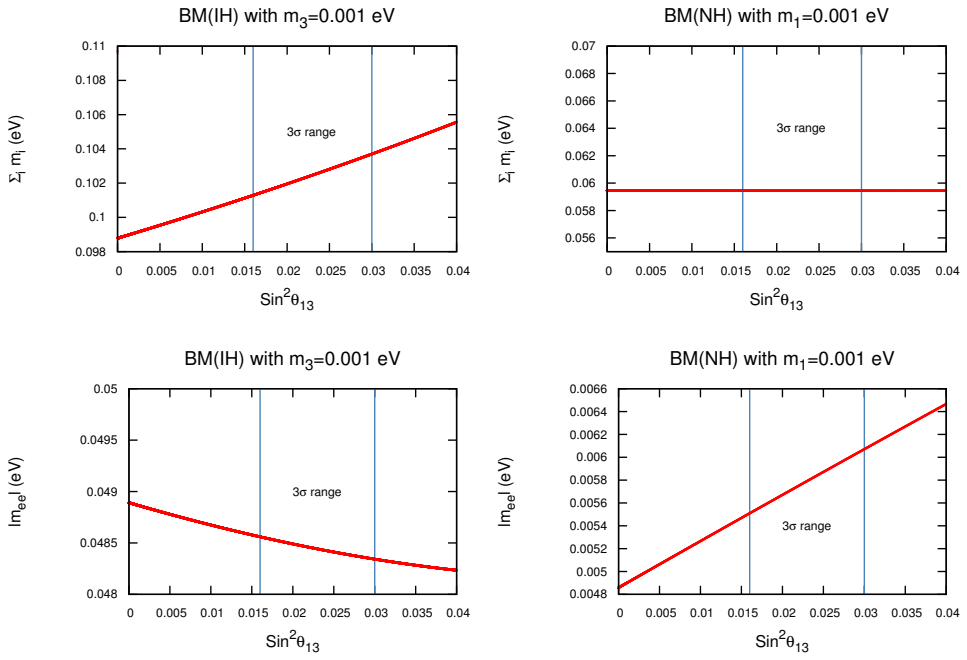

Figure 2.23: $\sum_i |m_i|$, $|m_{ee}|$ with $\sin^2\theta_{13}$ for BM with $m_1(m_3) = 0.001$ eV.

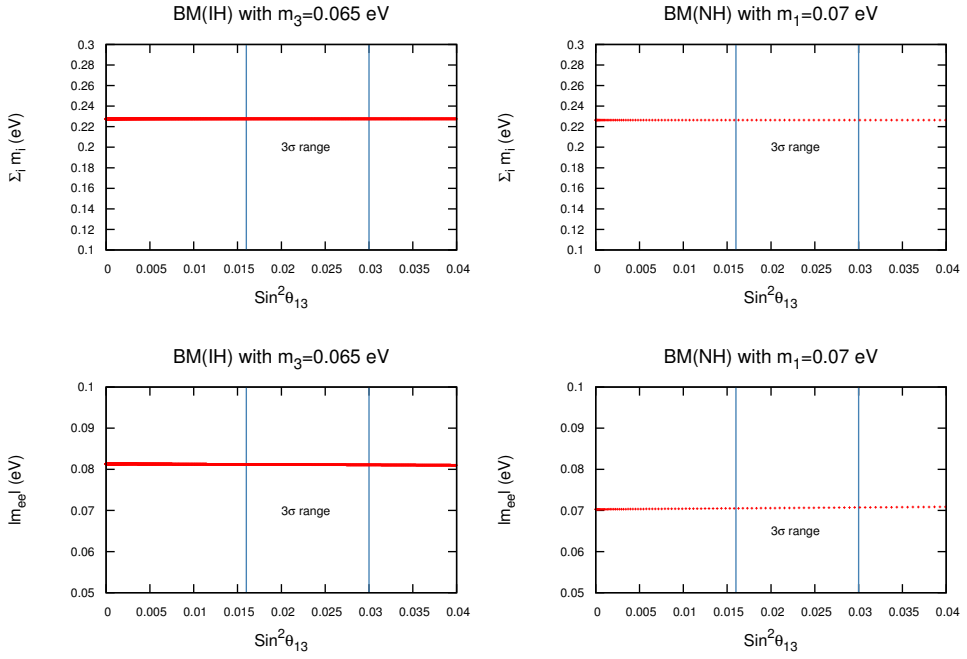

Figure 2.24: $\sum_i |m_i|$, $|m_{ee}|$ with $\sin^2\theta_{13}$ for BM with $m_1(m_3) = 0.07(0.065)$ eV.

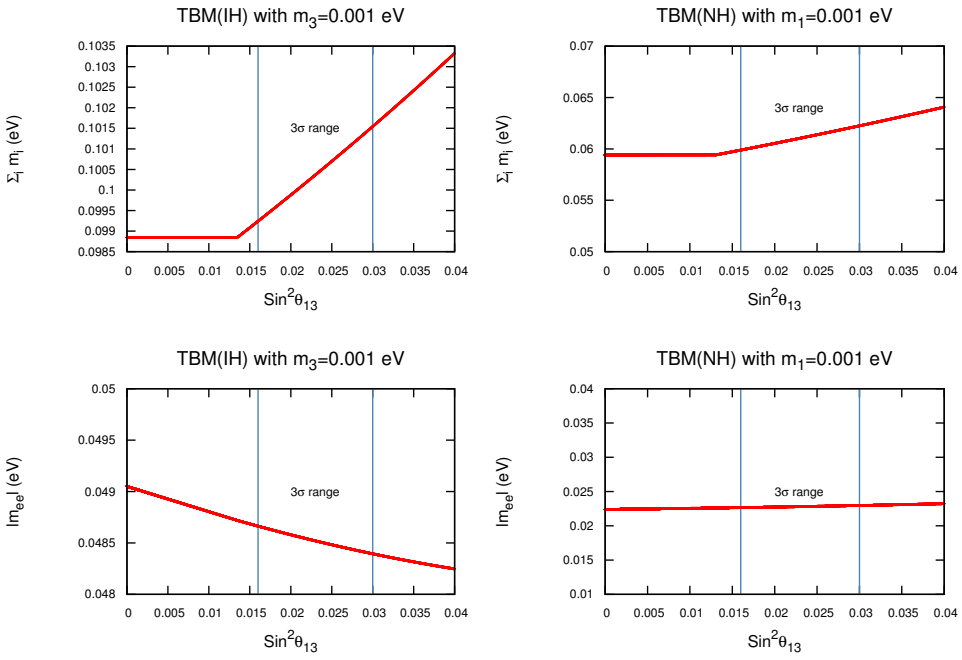

Figure 2.25: $\sum_i |m_i|$, $|m_{ee}|$ with $\sin^2\theta_{13}$ for TBM with $m_1(m_3) = 0.001$ eV.

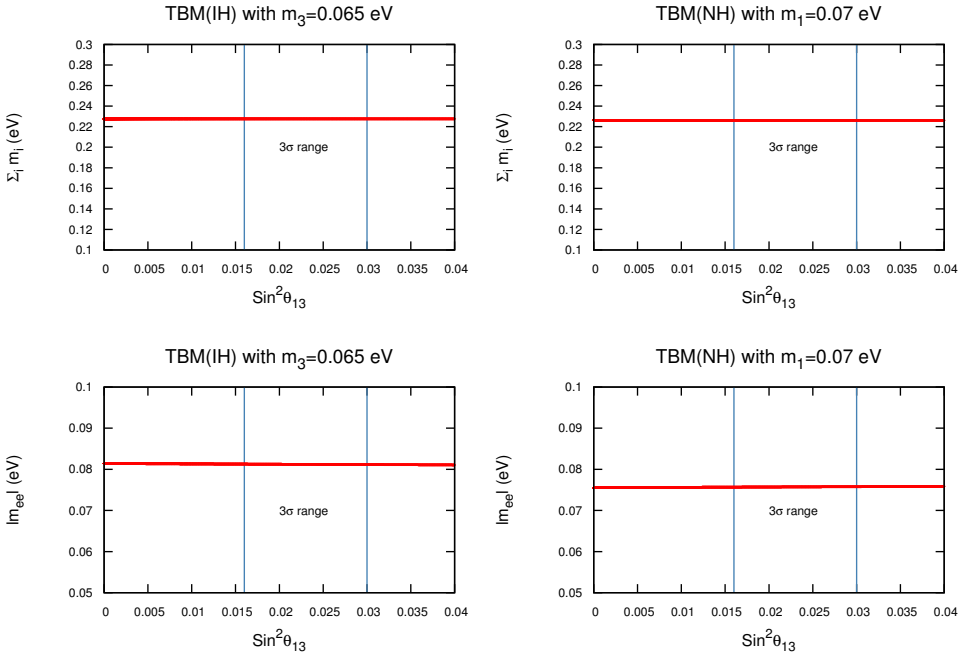

Figure 2.26: $\sum_i |m_i|$, $|m_{ee}|$ with $\sin^2\theta_{13}$ for TBM with $m_1(m_3) = 0.07(0.065)$ eV.

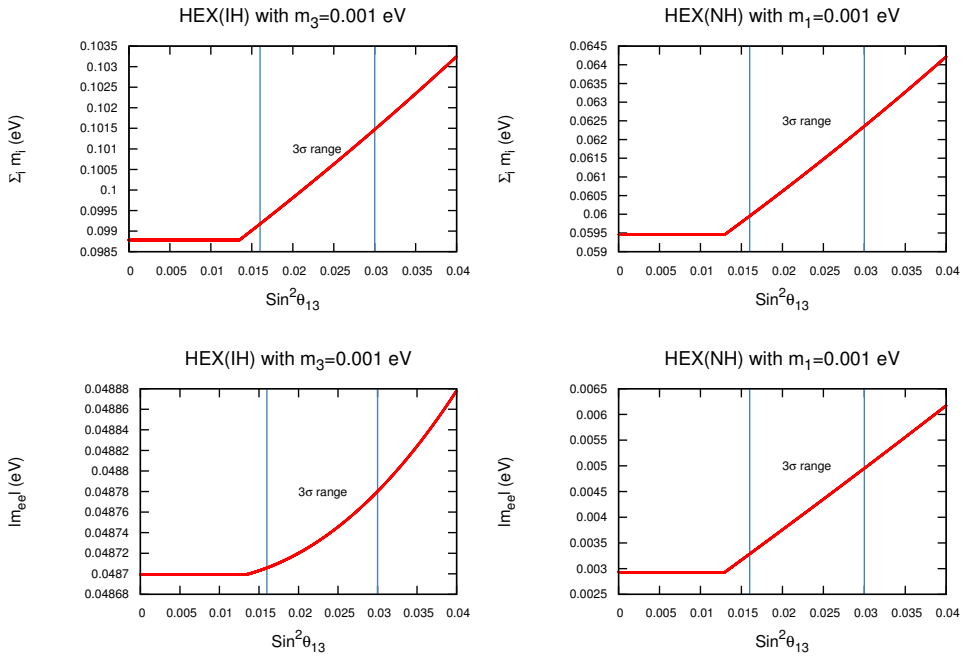

Figure 2.27: $\sum_i |m_i|$, $|m_{ee}|$ with $\sin^2\theta_{13}$ for HM with $m_1(m_3) = 0.001$ eV.

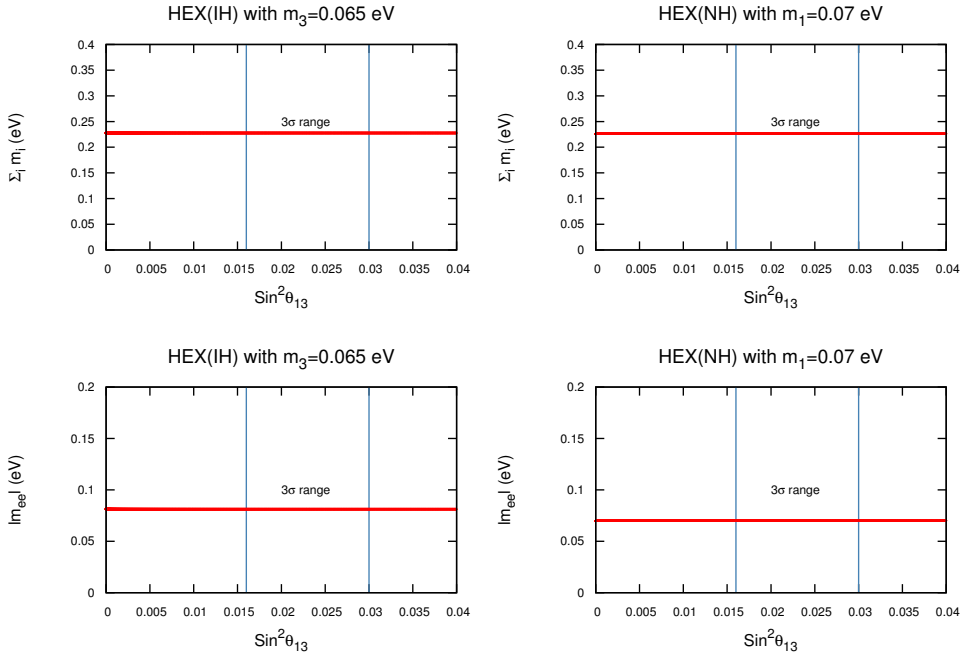

Figure 2.28: $\sum_i |m_i|$, $|m_{ee}|$ with $\sin^2\theta_{13}$ for HM with $m_1(m_3) = 0.07(0.065)$ eV.

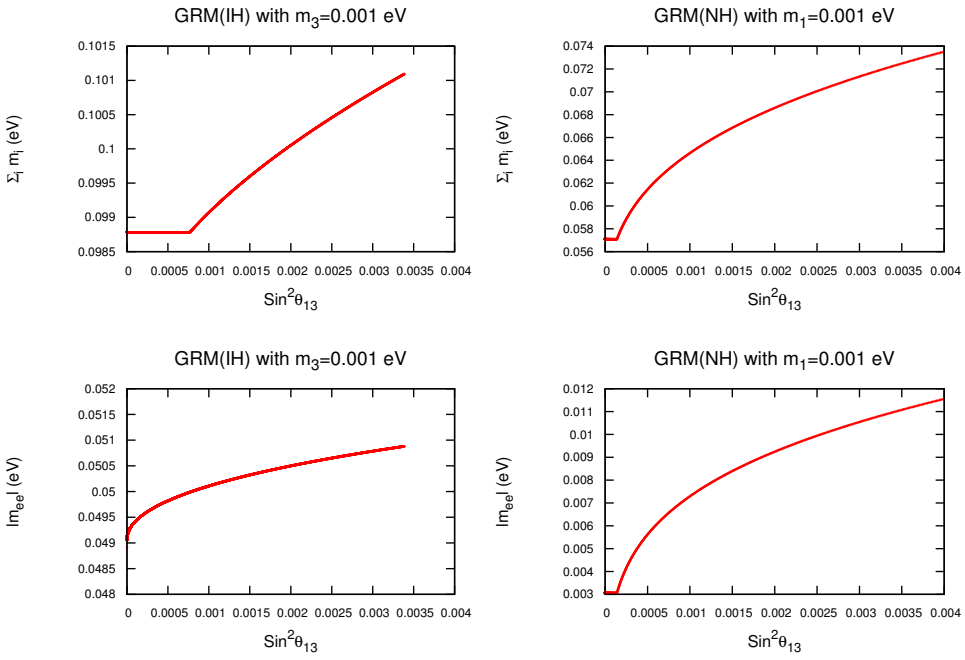

Figure 2.29: $\sum_i |m_i|$, $|m_{ee}|$ with $\sin^2\theta_{13}$ for GRM with $m_1(m_3) = 0.001$ eV.

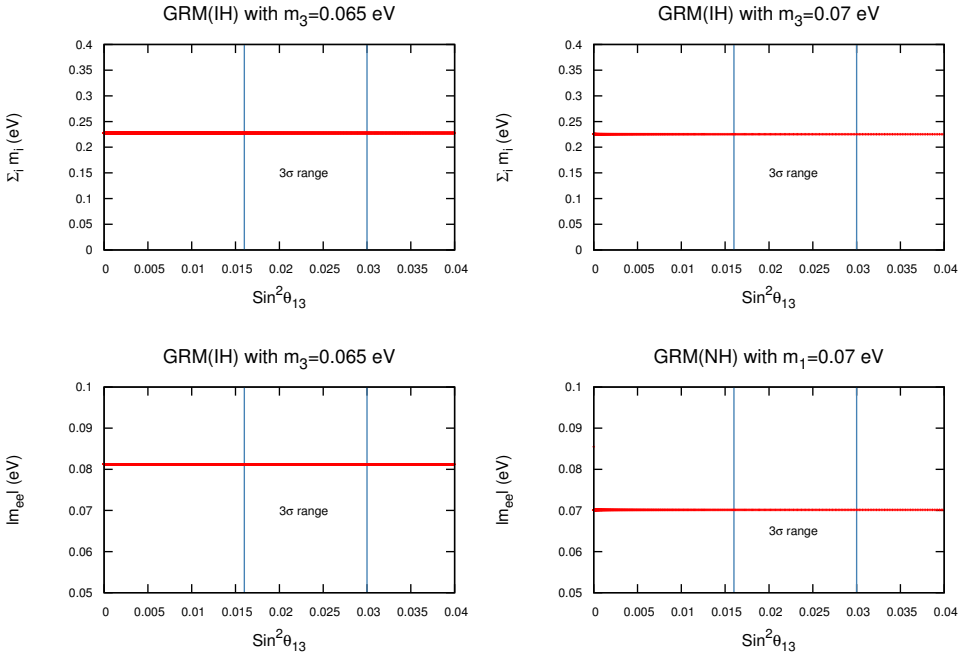

Figure 2.30: $\sum_i |m_i|$, $|m_{ee}|$ with $\sin^2\theta_{13}$ for GRM with $m_1(m_3) = 0.07(0.065)$ eV.

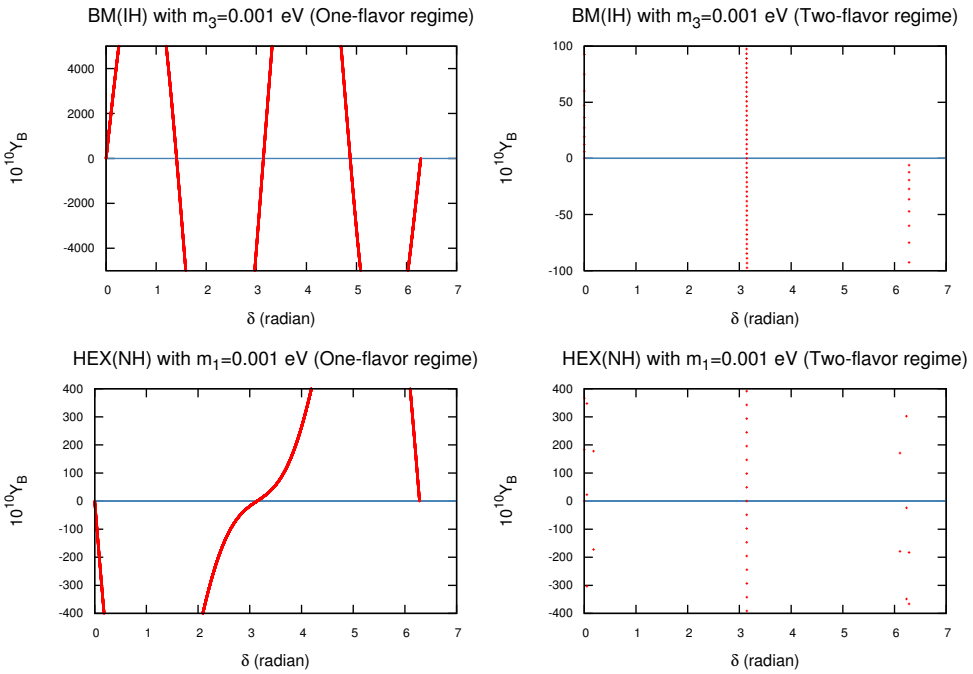

Figure 2.31: Variation of baryon asymmetry with δ for BM and HM

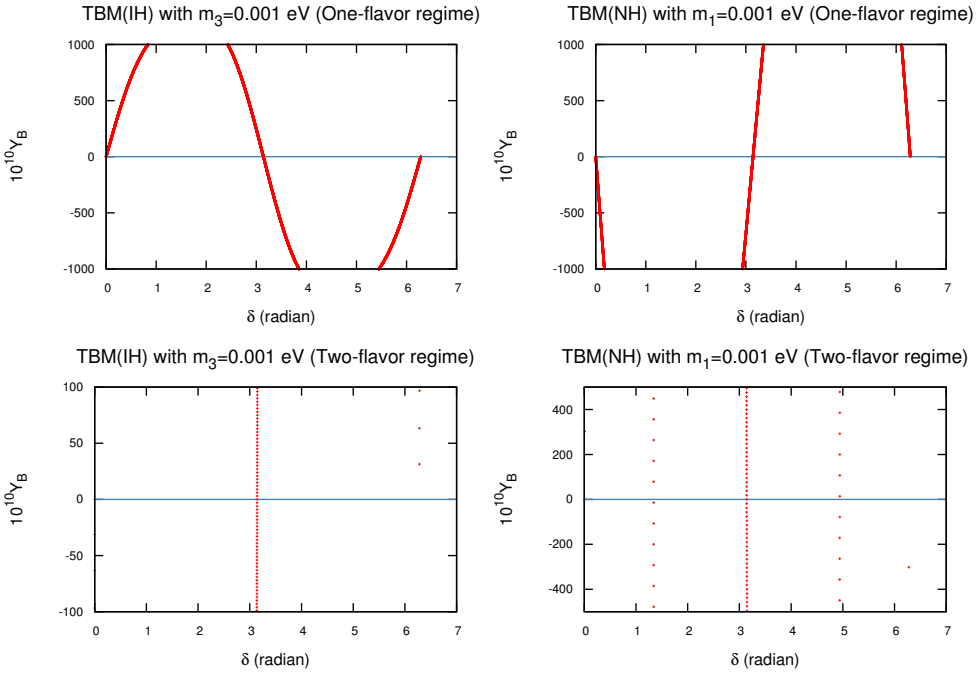

Figure 2.32: Variation of baryon asymmetry with δ for TBM

2.7 Results and Discussion

We have studied the possibility of generating non-zero θ_{13} by perturbing the $\mu - \tau$ symmetric neutrino mass matrix using type II seesaw. The leading order $\mu - \tau$ symmetric mass matrix originating from type I seesaw can be of four different types: bi-maximal, tri-bi-maximal, hexagonal and golden ratio mixing, which differ by the solar mixing angle they predict. All these four different types of mixing predict $\theta_{23} = 45^o$ and $\theta_{13} = 0$.

Model	Δm^2_{21}	$\frac{\Delta m^2_{23}}{\Delta m^2_{31}}$	θ_{13}	θ_{23}	θ_{12}	$\sum\|m_i\|$	Y_B (1 flav.)	Y_B (2 flav.)	Y_B (3 flav.)
BM(IH) (m_3=0.001)	✓	✓	✓	✓	✓	✓	✓	✓	×
BM(NH) (m_1=0.001)	✓	✓	✓	✓	×	✓	×	×	×
BM(IH) (m_3=0.065)	×	✓	✓	✓	×	✓	×	×	×
BM(NH) (m_1=0.07)	✓	✓	✓	✓	×	✓	×	×	×
TBM(IH) (m_3=0.001)	✓	✓	✓	✓	✓	✓	✓	✓	×
TBM(NH) (m_1=0.001)	✓	✓	✓	✓	✓	✓	✓	×	×
TBM(IH) (m_3=0.065)	×	✓	✓	✓	✓	✓	×	×	×
TBM(NH) (m_1=0.07)	×	✓	✓	✓	✓	✓	×	×	×
HEX(IH) (m_3=0.001)	✓	✓	✓	✓	×	✓	×	×	×
HEX(NH) (m_1=0.001)	✓	✓	✓	✓	✓	✓	✓	×	×
HEX(IH) (m_3=0.065)	×	✓	✓	✓	✓	✓	×	×	×
HEX(NH) (m_1=0.07)	×	✓	✓	✓	✓	✓	×	×	×
GRM(IH) (m_3=0.001)	×	×	×	×	×	✓	×	×	×
GRM(NH) (m_1=0.001)	✓	✓	✓	×	×	✓	×	×	×
GRM(IH) (m_3=0.065)	×	×	✓	×	×	✓	×	×	×
GRM(NH) (m_1=0.07)	×	×	✓	×	×	✓	×	×	×

Table 2.10: Summary of Results. The symbol ✓ (×) is used when the particular parameter in the column can (can not) be realized within a particular model denoted by the row.

We use a minimal $\mu - \tau$ symmetry breaking form of type II seesaw mass matrix to perturb the type I seesaw mass matrix and determine the strength of type II seesaw term in order to generate non-zero θ_{13} in the correct 3σ range. We find that except

the case of golden ratio mixing with inverted hierarchy and $m_3 = 0.001$ eV, all other cases under consideration give rise to correct values of θ_{13} as can be seen from figure 2.3, 2.4, 2.5 and 2.6. We then calculate other neutrino parameters as we vary the type II seesaw strength and show their variations as a function of $\sin^2\theta_{13}$. We find that bimaximal mixing with inverted hierarchy, tri-bimaximal mixing with both normal and inverted hierarchies and hexagonal mixing with normal hierarchy can give rise to correct values of neutrino parameters as well as baryon asymmetry. The variation of baryon asymmetry with respect to δ are shown in figure 2.31 and 2.32. It is seen that BM (IH) with $m_3 = 0.001$eV gives rise to correct baryon asymmetry in both 1- and 2-flavor regimes. Similarly, in case of HM (NH) with $m_1 = 0.001$eV, only 1-flavor regimes shows good results. For the TBM case, IH with $m_3 = 0.001$eV and NH with $m_1 = 0.001$eV produce exact baryogenesis in 1-flavor regime whereas TBM (IH) with $m_3 = 0.001$eV produces correct value of baryon asymmetry in 2-flavor regime. The golden ratio mixing is disfavored in our framework for both types of neutrino mass hierarchies.

We summarize our results for all the models under consideration in table 2.10. We also show the preferred values of Dirac CP phase δ for successful leptogenesis in table 2.9. More precise experimental data from neutrino oscillation and cosmology experiments should be able to falsify or verify some of the models discussed in this work.

Bibliography

[1] Fukuda, S., et al. Constraints on neutrino oscillations using 1258 days of Super-Kamiokande solar neutrino data, *Phys. Rev. Lett.*, **86**(25), 5656–5660, 2001.

[2] Ahmad, Q. R., et al. Direct evidence for neutrino flavor transformation from neutral-current interactions in the Sudbury Neutrino Observatory, *Phys. Rev. Lett.*, **89**(1), 011301, 2002.

[3] Ahmad, Q. R., et al. Measurement of day and night neutrino energy spectra at SNO and constraints on neutrino mixing parameters, *Phys. Rev. Lett.*, **89**(1), 011302, 2002.

[4] Bahcall, J. N., & Pena-Garay, C. Solar models and solar neutrino oscillations, *New Journal of Physics*, **6**(1), 63, 2004.

[5] Nakamura, K., et al. Review of particle physics, *J. Phys. G: Nucl. and Part. Phys.*, **37**(7A), 075021, 2010.

[6] Abe, K., et al. Indication of electron neutrino appearance from an accelerator-produced off-axis muon neutrino beam, *Phys. Rev. Lett.*, **107**(4), 041801, 2011.

[7] Abe, Y., et al. Indication of reactor ν_e disappearance in the Double Chooz experiment, *Phys. Rev. Lett.*, **108**(13), 131801, 2012.

[8] An, F. P., et al. Observation of electron-antineutrino disappearance at Daya Bay, *Phys. Rev. Lett.*, **108**(17), 171803, 2012.

[9] Ahn, J. K., et al. Observation of reactor electron antineutrinos disappearance in the RENO experiment, *Phys. Rev. Lett.*, **108**(19), 191802, 2012.

[10] Gonzalez-Garcia, M. C., et al. Global fit to three neutrino mixing: critical look at present precision, *JHEP*, **12**, 1–24, 2012.

[11] Fogli, G. L., et al. Global analysis of neutrino masses, mixings, and phases: Entering the era of leptonic C P violation searches, *Phys. Rev. D*, **86**(1), 013012, 2012.

[12] Minkowski, P. $\mu \to e\gamma$ at a rate of one out of 10^9 muon decays?, *Phys. Lett. B*, **67**(4), 421-428, 1977.

[13] Gell-Mann, M., Ramond, P., & Slansky, R. Print-80-0576 (CERN). T. Yanagida, *Prog. Theor. Phys.*, **64**, 1103, 1980.

[14] Mohapatra, R. N., & Senjanovic, G. Neutrino mass and spontaneous parity non-conservation, *Phys. Rev. Lett.*, **44**(14), 912–915, 1980.

[15] Schechter, J., & Valle, J.W.F. Neutrino masses in $SU(2) \times U(1)$ theories, *Phys. Rev. D*, **22**(9), 2227–2235, 1980.

[16] Mohapatra, R. N., and Senjanovic, G. Neutrino masses and mixings in gauge models with spontaneous parity violation, *Phys. Rev. D*, **23**(1), 165–180, 1981.

[17] Lazarides, G., Shafi, Q., & Wetterich, C. Proton lifetime and fermion masses in an SO (10) model, *Nucl. Phys. B*, **181**(2), 287–300, 1981.

[18] Wetterich, C. Neutrino masses and the scale of B-L violation, *Nucl. Phys. B*, **187**(2), 343–375, 1981.

[19] Brahmachari, B., & Mohapatra, R. N. Unified explanation of the solar and atmospheric neutrino puzzles in a supersymmetric SO (10) model, *Phys. Rev. D*, **58**(1), 015001, 1998.

[20] Mohapatra, R. N. Neutrino mass-an overview, *Nucl. Phys. B-Proceedings Supplements*, **138**, 257–266, 2005.

[21] Antusch, S., & King, S.F. Type II leptogenesis and the neutrino mass scale, *Phys. Lett. B*, **597**(2), 199–207, 2004.

[22] Foot, R., et al. See-saw neutrino masses induced by a triplet of leptons, *Z. Physics C*, **44**(3), 441–444, 1989.

[23] Vissani, F. A Study of the scenario with nearly degenerate Majorana neutrinos, arxiv:hep-ph/9708483, 1997.

[24] Barger, V., et al. Bi-maximal mixing of three neutrinos, *Phys. Lett. B*, **437**(1), 107–116, 1998.

[25] Baltz, A. J., Goldhaber, A.S., & Goldhaber, M. Solar Neutrino Puzzle: An Oscillation Solution with Maximal Neutrino Mixing, *Phys. Rev. Lett.*, **81**(26), 5730–5700, 1998.

[26] Harrison, P. F., Perkins, D. H. & Scott, W. G. Tri-bimaximal mixing and the neutrino oscillation data, *Phys. Lett. B*, **530**(1), 167–173, 2002.

[27] Harrison, P. F., & Scott, W.G. Symmetries and generalisations of tri-bimaximal neutrino mixing, *Phys. Lett. B*, **535**(1), 163–169, 2002.

[28] Xing, Z.Z. Nearly tri-bimaximal neutrino mixing and CP violation, *Phys. Lett. B*, **533**(1), 85–93, 2002.

[29] Harrison, P. F., & Scott, W.G. $\mu - \tau$ reflection symmetry in lepton mixing and neutrino oscillations, *Phys. Lett. B*, **547**(3), 219–228, 2002.

[30] Harrison, P. F., & Scott, W.G. Permutation symmetry, tri-bimaximal neutrino mixing and the S_3 group characters, *Phys. Lett. B*, **557**(1), 76–86, 2003.

[31] Harrison, P. F., & Scott, W.G. The simplest neutrino mass matrix, *Phys. Lett. B*, **594**(3), 324–332, 2004.

[32] Albright, C. H., Dueck, A., & Rodejohann, W. Possible alternatives to tri-bimaximal mixing, *EPJC*, **70**(4), 1099–1110, 2010.

[33] Datta, A., Ling, F., & Ramond, P. Correlated hierarchy, Dirac masses and large mixing angles, *Nucl. Phys. B*, **671**, 383–400, 2003.

[34] Kajiyama, Y., Raidal, M., & Strumia, A. Golden ratio prediction for solar neutrino mixing, *Phys. Rev. D*, **76**(11), 117301, 2007.

[35] Everett, L. L., & Stuart, A. J. Icosahedral (A_5) family symmetry and the golden ratio prediction for solar neutrino mixing, *Phys. Rev. D*, **79**(8), 085005, 2009.

[36] Feruglio, F., & Paris, A. The golden ratio prediction for the solar angle from a natural model with A_5 flavour symmetry, *JHEP*, **2011**(3), 1–30, 2011.

[37] Ding, G., Everett, L. L., & Stuart, A. J. Golden ratio neutrino mixing and A5 flavor symmetry, *Nucl. Phys. B*, **857**(3), 219–253, 2012.

[38] Cooper, I. K., King, S. F., & Stuart, A. J. A golden A_5 model of leptons with a minimal NLO correction, *Nucl. Phys. B*, **875**(3), 650–677, 2013 .

[39] Shimizu, Y., Tanimoto, M., & Watanabe, A. Breaking tri-bimaximal mixing and large $theta_{13}$, *Prog. Th. Phys.*, **126**(1), 81–90, 2011.

[40] King, S. F., & Luhn, C. Trimaximal neutrino mixing from vacuum alignment in A_4 and S_4 models, *JHEP*, **2011**(9), 1–25, 2011.

[41] Antusch, S., et al. Trimaximal mixing with predicted $theta_{13}$ from a new type of constrained sequential dominance, *Nucl. Phys. B*, 856(2), 328–341, 2012.

[42] King, S. F., & Luhn, C. A_4 models of tri-bimaximal-reactor mixing, *JHEP*, *2012*(3), 1–18, 2013.

[43] Ge, S., He, H., & Yin, F. Common origin of soft $\mu - \tau$ and CP breaking in neutrino seesaw and the origin of matter, *JCAP*, **2010**(05), 017, 2010.

[44] Ge, S., Dicus, D. A., & Repko, W. W. Z_2 symmetry prediction for the leptonic Dirac CP phase, *Phys. Lett. B*, **702**(4), 220–223, 2011.

[45] Chen, M., et al. Compatibility of θ_{13} and the type I seesaw model with A_4 symmetry, *JHEP*, **2013**(2), 1–22, 2013.

[46] Liao, J., Marfatia, D., & Whisnant, K. Perturbations to $\mu - \tau$ symmetry in neutrino mixing, *Phys. Rev. D*, **87**(1), 013003, 2013.

[47] He, H., & Yin, F. Common origin of $\mu - \tau$ and CP breaking in the neutrino seesaw, baryon asymmetry and hidden flavor symmetry, *Phys. Rev. D*, **84**(3), 033009, 2011.

[48] Altarelli, G., et al. Discrete flavour groups, θ_{13} and lepton flavour violation, *JHEP*, **2012**(8), 1–43, 2012.

[49] Ade, P. A. R., et al. Planck 2013 results. XVI, Cosmological parameters, *Astronomy & Astrophysics*, **571**, A16, 2014.

[50] Kuzmin, V. A., Rubakov, V. A., & Shaposhnikov, M. E. On anomalous electroweak baryon-number non-conservation in the early universe, *Phys. Lett. B*, **155**(1), 36–42, 1985.

[51] Fukugita, M., & Yanagida, T. Barygenesis without grand unification, *Phys. Lett. B*, **174**(1), 45–47, 1986.

[52] Ellis, J., & Nanopoulos, D. V. Leptogenesis in the light of Super-Kamiokande data and a realistic string model, *Phys. Lett. B*, **452**(1), 87–97, 1999.

[53] Lazarides, G., and Vlachos, N. D. Hierarchical neutrinos and supersymmetric inflation, *Phys. Lett. B*, **459**(4), 482–488, 1999.

[54] Berger, M. S., and Brahmachari, B. Leptogenesis and Yukawa textures, *Phys. Rev. D*, **60**(7), 073009, 1999.

[55] Berger, M. S. Abelian family symmetries and leptogenesis, *Physical Rev. D*, **62**(1), 013007, 2000.

[56] Buchmüller, W., & Plumacher, M. Neutrino masses and the baryon asymmetry, *Int. J. Mod. Phys. A*, **15**(32), 5047–5086, 2000.

[57] Kang, K., Kang, S. F., & Sarkar, U. Lepton flavor mixing and baryogenesis, *Phys. Lett. B*, **486**(3), 391–399, 2000.

[58] Goldberg, H. Leptogenesis and the small-angle MSW solution, *Phys. Lett. B*, **474**(3), 389–394, 2000.

[59] Jeannerot, R., Khalil, S., & Lazarides, G. Leptogenesis in smooth hybrid inflation, *Phys. Lett. B*, **506**(3), 344–350, 2001.

[60] Falcone, D., & Tramontano, F. "Leptogenesis and neutrino parameters, *Phys. Rev. D*, **63**(7), 073007, 2001.

[61] Falcone, D., & Tramontano, F. Leptogenesis with $SU(5)$-inspired mass matrices, *Phys. Lett. B*, **506**(1), 1–6, 2001.

[62] Nielsen, H. B., & Takanishi, Y. Baryogenesis via lepton number violation in anti-GUT model, *Phys. Lett. B*, **507**(1), 241–251, 2001.

[63] Nezri, E., and Orloff, J. Neutrino oscillations vs leptogenesis in $SO(10)$ models, *JHEP*, **2003**(04), 020, 2003.

[64] Joshipura, A. S., Paschos, E. A., & Rodejohann, W. Leptogenesis in left–right symmetric theories, *Nucl. Phys. B*, **611**(1), 227–238, 2001.

[65] Davidson, S., Nardi, E., & Nir, Y. Leptogenesis, *Phys. Rep.*, **466**(4), 105–177, 2008.

[66] Borah, D., & Das, M. K. Neutrino masses and leptogenesis in type I and type II seesaw models, *Phys. Rev. D*, **90**(1), 015006, 2014.

[67] Borah, D., Deviations from tri-bimaximal neutrino mixing using type II seesaw, *Nucl. Phys. B*, **876**(2), 575–586, 2013.

[68] Borah, D., Patra, S., & Pritimita, P. Sub-dominant type-II seesaw as an origin of non-zero θ_{13} in $SO(10)$ model with TeV scale Z' gauge boson, *Nucl. Phys. B*, **881**, 444–466, 2014.

[69] Borah, D., Type II seesaw origin of nonzero θ_{13}, $\delta_{\rm CP}$ and leptogenesis, *Int. J. Mod. Phys. A*, **29**(22), 1450108, 2014.

[70] Rodejohann, W. Type II seesaw mechanism, deviations from bimaximal neutrino mixing, and leptogenesis, *Phys. Rev. D*, **70**(7), 073010, 2004.

[71] Lindner, M., & Rodejohann, W. Large and almost maximal neutrino mixing within the type II see-saw mechanism, *JHEP*, **2007**(05), 089, 2007.

[72] Sierra, D. A., Varzielas, I., & Houet, E. Eigenvector-based approach to neutrino mixing, *Phys. Rev. D*, **87**(9), 093009, 2013.

[73] Das, M. K., Borah, D., & Mishra, R. Quasidegenerate neutrinos in type II seesaw models, *Phys. Rev. D*, **86**(9), 095006, 2012.

[74] Borah, D., & Das, M. K. Neutrino masses and mixings with non-zero θ_{13} in type I+ II seesaw models, *Nucl. Phys. B*, **870**(3), 461–476, 2013.

[75] Borah, D. Effects of Planck scale physics on neutrino mixing parameters in left-right symmetric models, *Phys. Rev. D*, **87**(9), 095009, 2013.

[76] Weinberg, S. Baryon and lepton-nonconserving processes, *Phys. Rev. Lett.*, **43**(21), 1566–1570, 1979.

[77] Ishimori, H., et al. Non-Abelian discrete symmetries in particle physics, *Prog. Theor. Phys. Suppl.*, **183**(1), 1–163, 2010.

[78] Grimus, W., & Ludl, P. Finite flavour groups of fermions, *J. Phys. A: Mathematical and Theoretical*, **45**(23), 233001, 2012.

[79] King, S. F., & Luhn, C. Neutrino Mass and Mixing with Discrete Symmetry, *Rept. Prog. Phys.*, **76**, 056201, 2013.

[80] Altarelli, G., & Feruglio, F. Tri-bimaximal neutrino mixing, $A4$ and the modular symmetry, *Nucl. Phys. B*, **741**(1), 215–235, 2006.

[81] Ma, E., & Wegman, D. Nonzero θ_{13} for neutrino mixing in the context of A_4 symmetry, *Phys. Rev. Lett.*, **107**(6), 061803, 2011.

[82] Gupta, S., Joshipura, A. S., & Patel, K. M. Minimal extension of tribimaximal mixing and generalized $Z_2 \times Z_2$ symmetries, *Phys. Rev. D*, **85**(3), 031903, 2012.

[83] Dev, S., Gautam, R. R., & Singh, L. Broken S_3 symmetry in the neutrino mass matrix and non-zero θ_{13}, *Phys. Lett. B*, **708**(3), 284–289, 2012.

[84] Gu, P., and He, H. Neutrino mass and baryon asymmetry from Dirac seesaw, *JCAP*, **2006**(12), 1–10, 2006.

[85] He, H. J., & Xu, X. J. Octahedral symmetry with geometrical breaking: New prediction for neutrino mixing angle θ_{13} and CP-violation, *Phys. Rev. D*, **86**(11), 111301, 2012.

[86] Branco, G. C., et al. Spontaneous leptonic CP violation and nonzero θ_{13}, *Phys. Rev. D*, **86**(7), 076008, 2012.

[87] Ma, E. Near tribimaximal neutrino mixing with $\Delta(27)$ symmetry, *Phys. Lett. B*, **660**(5), 505–507, 2008.

[88] Plentinger, F., Seidl, G., & Winter, W. Group space scan of flavor symmetries for nearly tribimaximal lepton mixing, *JHEP*, **2008**(04), 077, 2008.

[89] Haba, N., et al. Tribimaximal mixing from cascades, *Phys. Rev. D*, **78**(11), 113002(1)–113002(11), 2008.

[90] Ge, S.F., Dicus, D. A., & Repko, W. W. Residual symmetries for neutrino mixing with a large θ_{13} and nearly maximal δ_D, *Phys. Rev. D*, **108**(4), 041801, 2012.

[91] Ma, E., and Rajasekaran, G. Softly broken A_4 symmetry for nearly degenerate neutrino masses, *Phys. Rev. D*, **64**(11), 113012, 2001.

[92] Ma, E. A_4 symmetry and neutrinos with very different masses, *Phys. Rev. D*, **70**(3), 031901, 2004.

[93] Araki, T., & Li, Y. F. Q_6 flavor symmetry model for the extension of the minimal standard model by three right-handed sterile neutrinos, *Phys. Rev. D*, **85**(6), 065016, 2012.

[94] Xing, Z.Z. Implications of the Daya Bay observation of θ_{13} on the leptonic flavor mixing structure and CP violation, *Chin. Phys. C*, **36**(4), 281–297, 2012.

[95] Xing, Z. Z. A shift from democratic to tri-bimaximal neutrino mixing with relatively large θ_{13}, *Phys. Lett. B*, **696**(3), 232–236, 2011.

[96] Dev, P. S. B, et al. θ_{13} and proton lifetime in a minimal $SO(10) \times S_4$ model of flavor, *Phys. Rev. D*, **86**(3), 035002, 2012.

[97] Adhikary, B., et al. A_4 symmetry and prediction of U_{e3} in a modified Altarelli–Feruglio model, *Phys. Lett. B*, **638**(4), 345–349, 2006.

[98] Altarelli, G, & Feruglio, F. Discrete flavor symmetries and models of neutrino mixing, *Rev. Mod. Phys.*, **82**(3), 2701–2729, 2010.

[99] Parattu, K. M., & Wingerter, A. Tribimaximal mixing from small groups, *Phys. Rev. D*, **84**(1), 013011, 2011.

[100] Felipe, R. G., Serôdio, H., & Silva, J. P. Neutrino masses and mixing in A_4 models with three Higgs doublets, *Phys. Rev. D*, **88**(1), 015015, 2013.

[101] Kolb, E. W., & Turner, M. S. The Early Universe, *Frontiers in Physics*, **69**, 547, 1990.

[102] Pilaftsis, A. Heavy Majorana neutrinos and baryogenesis, *Int. J. Mod. Phys. A*, **14**(12), 1811–1857, 1999.

[103] Flanz, M., and Paschos, E. A. Further considerations on the CP asymmetry in heavy Majorana neutrino decays, *Phys. Rev. D*, **58**(11), 113009, 1998.

[104] Barbieri, R., et al. Baryogenesis through leptogenesis, *Nucl. Phys. B*, **575**(1), 61–77, 2000.

[105] Abada, A., et al. Flavour issues in leptogenesis, *JCAP*, **2006**(04), 1–22, 2006.

[106] Nardi, E., et al. The importance of flavor in leptogenesis, *JHEP*, **2006**(01), 164, 2006.

[107] Abada, Asmaa, et al. Flavour matters in leptogenesis, *JHEP*, **2006**(09), 010, 2006.

[108] Lazarides, G., & Shafi, Q. R symmetry in the minimal supersymmetric standard model and beyond with several consequences, *Phys. Rev. D*, **58**(7), 071702, 1998.

[109] Hambye, T., & Senjanovic, G. Consequences of triplet seesaw for leptogenesis, *Phys. Lett. B*, **582**(1), 73–81, 2004.

Chapter 3

Discriminating Majorana Neutrino Textures in the light of Baryon Asymmetry

This chapter deals with the study of different Majorana zero-textures allowed from neutrino oscillation data when the charged lepton mass matrix is assumed to take the diagonal form. Considering the two Majorana phases to be equal in case of one-zero textures, we calculate the lightest neutrino mass in terms of Dirac CP phase. Similarly, in case of two-zero texture we calculate all the three CP phases and the lightest mass by solving four real constrain equations and then adopting a type I seesaw framework, we end our study by evaluating baryogenesis through the process of leptogenesis.

3.1 Introduction

Origin of sub-eV scale neutrino masses and large leptonic mixing is one of the biggest unresolved mysteries in particle physics. Due to the absence of right handed neutrinos

in the standard model (SM), neutrinos remain massless at renormalizable level. Several beyond standard model (BSM) frameworks have been proposed to explain tiny neutrino masses observed by neutrino oscillation experiments more than a decade ago [1–4]. More recently, the experiments like T2K [5], Double Chooz [6], Daya-Bay [7] and RENO [8] have not only confirmed the earlier measurements but also discovered a small but non-zero reactor mixing angle. Two different sets of latest global fit values for 3σ range of neutrino oscillation parameters given in [9] and [10] are shown in table 3.1 and 3.2 respectively.

Parameters	Normal Hierarchy (NH)	Inverted Hierarchy (IH)
$\frac{\Delta m^2_{21}}{10^{-5}\text{eV}^2}$	$7.02 - 8.09$	$7.02 - 8.09$
$\frac{\lvert\Delta m^2_{31}\rvert}{10^{-3}\text{eV}^2}$	$2.317 - 2.607$	$2.307 - 2.590$
$\sin^2\theta_{12}$	$0.270 - 0.344$	$0.270 - 0.344$
$\sin^2\theta_{23}$	$0.382 - 0.643$	$0.389 - 0.644$
$\sin^2\theta_{13}$	$0.0186 - 0.0250$	$0.0188 - 0.0251$
δ_{CP}	$0 - 2\pi$	$0 - 2\pi$

Table 3.1: Global fit 3σ values of neutrino oscillation parameters [9]

Parameters	Normal Hierarchy (NH)	Inverted Hierarchy (IH)
$\frac{\Delta m^2_{21}}{10^{-5}\text{eV}^2}$	$7.11 - 8.18$	$7.11 - 8.18$
$\frac{\lvert\Delta m^2_{31}\rvert}{10^{-3}\text{eV}^2}$	$2.30 - 2.65$	$2.20 - 2.54$
$\sin^2\theta_{12}$	$0.278 - 0.375$	$0.278 - 0.375$
$\sin^2\theta_{23}$	$0.393 - 0.643$	$0.403 - 0.640$
$\sin^2\theta_{13}$	$0.0190 - 0.0262$	$0.0193 - 0.0265$
δ_{CP}	$0 - 2\pi$	$0 - 2\pi$

Table 3.2: Global fit 3σ values of neutrino oscillation parameters [10]

Although the 3σ range for the leptonic Dirac CP phase δ_{CP} is $0 - 2\pi$, there are two possible best fit values of it found in the literature: 306^o (NH), 254^o (IH) [9] and 254^o

(NH), 266^o (IH) [10]. If neutrinos are Majorana fermions whose masses are generated by conventional seesaw mechanism [11–15], then two Majorana phases also appear in the mixing matrix which do not affect neutrino oscillations and hence can not be measured by oscillation experiments. The Majorana phases can however, have interesting implications in lepton number violating process like neutrinoless double beta decay, origin of matter-antimatter asymmetry of the Universe etc. Apart from the mass squared differences and mixing angles, the sum of the absolute neutrino masses are also tightly constrained from cosmology $\sum_i |m_i| < 0.23$ eV [16].

One of the most popular BSM framework to understand the origin of tiny neutrino mass and large leptonic mixing is to identify the possible underlying symmetries. Symmetries can either relate two or more free parameters of the model or make them vanish, making the model more predictive. The widely studied $\mu - \tau$ symmetric neutrino mass matrix giving $\theta_{13} = 0$ is one such scenario where discrete flavor symmetries can relate two or more terms in the neutrino mass matrix. Non-zero θ_{13}, as required by latest oscillation data, can be generated by incorporating different possible corrections to leading order $\mu - \tau$ symmetric neutrino mass matrix, as discussed recently in many works including [17–21]. The other possible role symmetries can play is to impose texture zeros in the mass matrices. The symmetry realization of such texture zeros can be found in several earlier as well as recent works [22–28]. Recently, a systematic study of texture zeros in lepton mass matrices were done in [29]. In the simplest case, one can assume the charged lepton mass matrix to be diagonal and then consider the possible texture zeros in the symmetric Majorana neutrino mass matrix. It turns out that in this simplest case, only certain types of one-zero texture and two-zero textures in the Majorana neutrino mass matrix are consistent with neutrino data.

In this chapter, we consider all types of texture zeros allowed in the Majorana neutrino mass matrix (in the diagonal charged lepton basis) from neutrino oscillation

data and constrain them further from the requirement of producing successful baryon asymmetry through the mechanism of leptogenesis. Some earlier works related to the calculation of lepton asymmetry with texture zero Majorana neutrino mass matrix can be found in [30–34]. Leptogenesis is one of the most widely studied formalism which provides a dynamical origin of the observed baryon asymmetry in the Universe. The asymmetry is created in the leptonic sector first which later gets converted into baryon asymmetry through $B + L$ violating electroweak sphaleron transitions [35]. As pointed out first by Fukugita and Yanagida [36], the required lepton asymmetry can be generated by the out of equilibrium CP violating decay of heavy Majorana neutrinos which are present in several BSM frameworks which attempt to explain tiny SM neutrino masses. We consider the framework of type I seesaw mechanism [11–15] generating tiny SM neutrino masses where right handed neutrinos are present and discriminate between different texture zeros in the neutrino mass matrix from the requirement of producing the correct baryon asymmetry seen by Planck experiment [16]

$$Y_B = (8.58 \pm 0.22) \times 10^{-11} \tag{3.1.1}$$

Usually, the Majorana neutrino mass matrix can be constrained from the neutrino oscillation data on two mass squared differences and three mixing angles. But the most general neutrino mass matrix can still contain those neutrino parameters which are not yet determined experimentally: the lightest neutrino mass, leptonic Dirac CP phase and two Majorana CP phases. All these four free parameters can in general, affect the resulting lepton asymmetry calculated from the lightest right handed neutrino decay. Although it is difficult to make predictions with four free parameters, in case of texture zero Majorana mass matrix, it is possible to reduce the number of free parameters. As we show in details in this work, two of these free neutrino parameters can be determined in terms of the other two in one-zero texture case whereas all four free parameters can be numerically determined in case of two-zero

texture mass matrices. To simplify the calculation, we assume equality of Majorana phases in one-zero texture case and write down all the free parameters in the neutrino mass matrix in terms of Dirac CP phase. We then compute the baryon asymmetry as a function of Dirac CP phase. We not only constrain the Dirac CP phase from the requirement of producing the observed baryon asymmetry but also show that some of the texture zeros (allowed from neutrino oscillation data) are disfavored if leptogenesis through the lightest right handed neutrino decay is the only source of baryon asymmetry. Since all the neutrino parameters are fixed in two-zero texture mass matrices, we compute baryon asymmetry for different choices of diagonal Dirac neutrino mass matrices. Thus we not only discriminate between different two-zero texture mass matrices, but also constrain the diagonal form of Dirac neutrino mass matrices from the requirement of producing the observed baryon asymmetry.

It should be noted that we assume the Dirac neutrino mass matrix to be of diagonal type throughout our analysis. Also the charged lepton mass matrix is assumed to be diagonal so that the diagonalizing matrix of the light neutrino mass matrix is same as the leptonic mixing matrix. A more general discussion with non-diagonal Dirac neutrino as well as charged lepton mass matrices may give rise to a different set of conclusions from the ones obtained in this work.

This chapter is organized as follows. In section 3.2, we discuss all the possible texture zeros in the Majorana neutrino mass matrix with diagonal charged lepton basis. In section 3.3, we briefly outline the mechanism of leptogenesis through right handed neutrino decay. In section 3.4, we discuss the numerical analysis of all the texture zero models and finally conclude in section 3.5.

3.2 Majorana Texture Zeros

A symmetric 3×3 Majorana neutrino mass matrix M_ν can have six independent parameters. If k of them are vanishing then the total number of structurally different Majorana mass matrices with texture zeros is

$$^6C_k = \frac{6!}{k!(6-k)!} \tag{3.2.1}$$

A symmetric mass matrix with more than 3 texture zeros $k \geq 4$ can not be compatible with lepton masses and mixing. Similarly in the diagonal charged lepton basis, a symmetric Majorana neutrino mass matrix with 3 texture zeros is not compatible with neutrino oscillation data [37]. Therefore, we are left with either one-zero texture which can be of six different types and two-zero texture which can be of fifteen different types. Different possible Majorana neutrino mass matrices with one-zero texture and one vanishing eigenvalue was studied by the authors of [38] whereas one-zero texture in the light of recent neutrino oscillation data with non-zero θ_{13} was discussed in the work [39, 40]. Implications of one-zero texture for neutrinoless double beta decay can be found in [41]. Two-zero textures in the Majorana neutrino mass matrix have received lots of attention in several works in the last few years, some of which can be found in [42–53]. We briefly discuss these texture zero Majorana neutrino mass matrices in the following subsections 3.2.1 and 3.2.2 respectively.

3.2.1 One-zero texture

In case of one-zero texture, the Majorana neutrino mass matrix M_ν contains only one independent zero. There are six possible patterns of such one-zero texture which, following the notations of [40] can be written as

$$G_1 : \begin{pmatrix} 0 & \times & \times \\ \times & \times & \times \\ \times & \times & \times \end{pmatrix}, G_2 : \begin{pmatrix} \times & 0 & \times \\ 0 & \times & \times \\ \times & \times & \times \end{pmatrix}, G_3 : \begin{pmatrix} \times & \times & 0 \\ \times & \times & \times \\ 0 & \times & \times \end{pmatrix},$$

$$G_4 : \begin{pmatrix} \times & \times & \times \\ \times & 0 & \times \\ \times & \times & \times \end{pmatrix},$$

$$G_5 : \begin{pmatrix} \times & \times & \times \\ \times & \times & 0 \\ \times & 0 & \times \end{pmatrix}, G_6 : \begin{pmatrix} \times & \times & \times \\ \times & \times & \times \\ \times & \times & 0 \end{pmatrix} \tag{3.2.2}$$

Where the crosses "×" denote non-zero arbitrary elements of M_ν.

3.2.2 Two-zero texture

There are fifteen possible two-zero textures of the Majorana neutrino mass matrix M_ν . Using the notations of [50], these fifteen two-zero textures of M_ν can be classified into six categories given below:

$$A_1 : \begin{pmatrix} 0 & 0 & \times \\ 0 & \times & \times \\ \times & \times & \times \end{pmatrix}, A_2 : \begin{pmatrix} 0 & \times & 0 \\ \times & \times & \times \\ 0 & \times & \times \end{pmatrix}; \tag{3.2.3}$$

$$B_1 : \begin{pmatrix} \times & \times & 0 \\ \times & 0 & \times \\ 0 & \times & \times \end{pmatrix}, B_2 : \begin{pmatrix} \times & 0 & \times \\ 0 & \times & \times \\ \times & \times & 0 \end{pmatrix}, B_3 : \begin{pmatrix} \times & 0 & \times \\ 0 & 0 & \times \\ \times & \times & \times \end{pmatrix}, B_4 : \begin{pmatrix} \times & \times & 0 \\ \times & \times & \times \\ 0 & \times & 0 \end{pmatrix}; \tag{3.2.4}$$

$$C : \begin{pmatrix} \times & \times & \times \\ \times & 0 & \times \\ \times & \times & 0 \end{pmatrix}; \tag{3.2.5}$$

$$D_1 : \begin{pmatrix} \times & \times & \times \\ \times & 0 & 0 \\ \times & 0 & \times \end{pmatrix}, D_2 : \begin{pmatrix} \times & \times & \times \\ \times & \times & 0 \\ \times & 0 & 0 \end{pmatrix}; \tag{3.2.6}$$

$$E_1 : \begin{pmatrix} 0 & \times & \times \\ \times & 0 & \times \\ \times & \times & \times \end{pmatrix}, E_2 : \begin{pmatrix} 0 & \times & \times \\ \times & \times & \times \\ \times & \times & 0 \end{pmatrix}, E_3 : \begin{pmatrix} 0 & \times & \times \\ \times & \times & 0 \\ \times & 0 & \times \end{pmatrix}; \tag{3.2.7}$$

$$F_1 : \begin{pmatrix} \times & 0 & 0 \\ 0 & \times & \times \\ 0 & \times & \times \end{pmatrix}, F_2 : \begin{pmatrix} \times & 0 & \times \\ 0 & \times & 0 \\ \times & 0 & \times \end{pmatrix}, F_3 : \begin{pmatrix} \times & \times & 0 \\ \times & \times & 0 \\ 0 & 0 & \times \end{pmatrix}, \tag{3.2.8}$$

Where the crosses "×" imply non-zero arbitrary elements of M_ν. In the light of recent oscillation as well as cosmology data, only six different two-zero textures namely, $A_{1,2}$ and $B_{1,2,3,4}$ are favorable as discussed by the authors of [50,52]. We therefore, consider only these six possible two-zero textures for our analysis.

3.3 Leptogenesis

Leptogenesis is one of the most well motivated framework of producing baryon asymmetry of the Universe which creates an asymmetry in the leptonic sector first and then converts it into baryon asymmetry through $B+L$ violating electroweak sphaleron transitions. For a review of leptogenesis, please refer to [54]. Although the origin of leptonic mixing and baryon asymmetry could be entirely different, leptogenesis provides a minimal setup to understand the dynamical origin of both these problems in particle physics which remain unsolved till now. There are three basic requirements to produce baryon asymmetry in our Universe which most likely, was in a baryon symmetric state initially. As pointed out first by Sakharov [55], these three requirements are (i) Baryon number violation, (ii) C and CP violation and (iii) Departure

from equilibrium. Although the standard model satisfies the first two requirements and out of equilibrium conditions in principle, can be achieved in an expanding Universe like ours, it turns out that the amount of CP violation measured in the SM quark sector is too small to account for the entire baryon asymmetry of the Universe. Since there can be more sources of CP violating phases in the leptonic sector which are not yet from experimentally determined, leptogenesis provides an indirect way of constraining these unknown phases from the requirement of producing the observed baryon asymmetry.

In a model with type I seesaw mechanism at work, the CP violating out of equilibrium decay of the lightest right handed neutrino can give rise to the required lepton asymmetry. The neutrino mass matrix in type I seesaw mechanism can be written as

$$M_\nu = -m_{LR} M_{RR}^{-1} m_{LR}^T. \tag{3.3.1}$$

where m_{LR} is the Dirac neutrino mass matrix and M_{RR} is the right handed singlet neutrino mass matrix. We note that the Pontecorvo-Maki-Nakagawa-Sakata (PMNS) leptonic mixing matrix is related to the diagonalizing matrices of neutrino and charged lepton mass matrices U_ν, U_l respectively, as

$$U_{\text{PMNS}} = U_l^\dagger U_\nu \tag{3.3.2}$$

In the diagonal charged lepton basis, U_{PMNS} is same as the diagonalizing matrix U_ν of the neutrino mass matrix given by (3.3.1). The PMNS mixing matrix can be parametrized as

$$U_{\text{PMNS}} = \begin{pmatrix} c_{12}c_{13} & s_{12}c_{13} & s_{13}e^{-i\delta} \\ -s_{12}c_{23} - c_{12}s_{23}s_{13}e^{i\delta} & c_{12}c_{23} - s_{12}s_{23}s_{13}e^{i\delta} & s_{23}c_{13} \\ s_{12}s_{23} - c_{12}c_{23}s_{13}e^{i\delta} & -c_{12}s_{23} - s_{12}c_{23}s_{13}e^{i\delta} & c_{23}c_{13} \end{pmatrix} \text{diag}(1, e^{i\alpha}, e^{i(\beta+\delta)}) \tag{3.3.3}$$

where $c_{ij} = \cos\theta_{ij},\ s_{ij} = \sin\theta_{ij}$. δ is the Dirac CP phase and α, β are the Majorana phases.

In our work we are considering CP-violating out of equilibrium decay of heavy right handed neutrinos into Higgs and lepton within the framework type I seesaw mechanism. The lepton asymmetry from the decay of right handed neutrino into leptons and Higgs scalar is given by

$$\epsilon_{N_k} = \sum_i \frac{\Gamma(N_k \to L_i + H^*) - \Gamma(N_k \to \bar{L}_i + H)}{\Gamma(N_k \to L_i + H^*) + \Gamma(N_k \to \bar{L}_i + H)} \tag{3.3.4}$$

In a hierarchical pattern of three right handed neutrinos $M_{2,3} \gg M_1$, it is sufficient to consider the lepton asymmetry produced by the decay of the lightest right handed neutrino N_1. Following the notations of [56], the lepton asymmetry arising from the decay of N_1 in the presence of type I seesaw only can be written as

$$\begin{aligned} \epsilon_1^\alpha &= \frac{1}{8\pi v^2} \frac{1}{(m_{LR}^\dagger m_{LR})_{11}} \sum_{j=2,3} \mathrm{Im}[(m_{LR}^*)_{\alpha 1}(m_{LR}^\dagger m_{LR})_{1j}(m_{LR})_{\alpha j}] g(x_j) \\ &+ \frac{1}{8\pi v^2} \frac{1}{(m_{LR}^\dagger m_{LR})_{11}} \sum_{j=2,3} \mathrm{Im}[(m_{LR}^*)_{\alpha 1}(m_{LR}^\dagger m_{LR})_{j1}(m_{LR})_{\alpha j}] \frac{1}{1-x_j} \end{aligned} \tag{3.3.5}$$

where $v = 174$ GeV is the vev of the Higgs doublet responsible for breaking the electroweak symmetry,

$$g(x) = \sqrt{x}\left(1 + \frac{1}{1-x} - (1+x)\ln\frac{1+x}{x}\right)$$

and $x_j = M_j^2/M_1^2$. The second term in the expression for ϵ_1^α above vanishes when summed over all the flavors $\alpha = e, \mu, \tau$. The sum over flavors is given by

$$\epsilon_1 = \frac{1}{8\pi v^2} \frac{1}{(m_{LR}^\dagger m_{LR})_{11}} \sum_{j=2,3} \mathrm{Im}[(m_{LR}^\dagger m_{LR})_{1j}^2] g(x_j) \tag{3.3.6}$$

The corresponding baryon asymmetry is related to the lepton asymmetry as

$$Y_B = c\kappa \frac{\epsilon_1}{g_*} \tag{3.3.7}$$

through electroweak sphaleron processes [35]. Here, c is a measure of the fraction of lepton asymmetry being converted into baryon asymmetry and is approximately

equal to -0.55. κ is the dilution factor due to wash-out processes which erase the produced asymmetry and can be parametrized as [57–59]

$$\begin{aligned} -\kappa &\simeq \sqrt{0.1K}\exp[-4/(3(0.1K)^{0.25})], \text{ for } K \geq 10^6 \\ &\simeq \frac{0.3}{K(\ln K)^{0.6}}, \text{ for } 10 \leq K \leq 10^6 \\ &\simeq \frac{1}{2\sqrt{K^2+9}}, \text{ for } 0 \leq K \leq 10. \end{aligned} \tag{3.3.8}$$

where K is given as

$$K = \frac{\Gamma_1}{H(T=M_1)} = \frac{(m_{LR}^{\dagger} m_{LR})_{11} M_1}{8\pi v^2} \frac{M_{Pl}}{1.66\sqrt{g_*} M_1^2}$$

Here Γ_1 is the decay width of N_1 and $H(T = M_1)$ is the Hubble constant at temperature $T = M_1$. The factor g_* is the effective number of relativistic degrees of freedom at $T = M_1$ and is approximately 110.

It should be noted that the lepton asymmetry given by equation (3.3.6) has been obtained by summing over all the lepton flavors $\alpha = e, \mu, \tau$. A non-zero lepton asymmetry can however, be obtained only when the right handed neutrino decay is out of equilibrium. Otherwise both the forward and the backward processes will happen at the same rate resulting in a vanishing asymmetry. Departure from equilibrium can be estimated by comparing the interaction rate with the expansion rate of the Universe, parametrized by the Hubble parameter. At very high temperatures ($T \geq 10^{12}$GeV) all charged lepton flavors are out of equilibrium and hence all of them behave similarly resulting in the one flavor regime mentioned above. However at temperatures $T < 10^{12}$ GeV ($T < 10^9$GeV), interactions involving tau (muon) Yukawa couplings enter equilibrium and flavor effects become important in the calculation of lepton asymmetry [60–64]. The temperature regimes $10^9 < T/\text{GeV} < 10^{12}$ and $T/\text{GeV} < 10^9$ correspond to two and three flavor regimes of leptogenesis respectively. The final baryon asymmetry in the two and three flavor regimes can be written as

$$Y_B^{2flavor} = \frac{-12}{37g^*}[\epsilon_2 \eta \left(\frac{417}{589}\tilde{m_2}\right) + \epsilon_1^{\tau} \eta \left(\frac{390}{589}\tilde{m_\tau}\right)]$$

$$Y_B^{3flavor} = \frac{-12}{37g^*}[\epsilon_1^e \eta\left(\frac{151}{179}\tilde{m_e}\right) + \epsilon_1^\mu \eta\left(\frac{344}{537}\tilde{m_\mu}\right) + \epsilon_1^\tau \eta\left(\frac{344}{537}\tilde{m_\tau}\right)]$$

where $\epsilon_2 = \epsilon_1^e + \epsilon_1^\mu, \tilde{m_2} = \tilde{m_e} + \tilde{m_\mu}, \tilde{m_\alpha} = \frac{(m_{LR}^*)_{\alpha 1}(m_{LR})_{\alpha 1}}{M_1}$. The function η is given by

$$\eta(\tilde{m_\alpha}) = \left[\left(\frac{\tilde{m_\alpha}}{8.25 \times 10^{-3}\text{eV}}\right)^{-1} + \left(\frac{0.2 \times 10^{-3}\text{eV}}{\tilde{m_\alpha}}\right)^{-1.16}\right]^{-1}$$

For the calculation of baryon asymmetry, we first calculate the right handed neutrino mass spectrum by diagonalizing the right handed singlet neutrino mass matrix M_{RR} as

$$U_R^* M_{RR} U_R^\dagger = \text{diag}(M_1, M_2, M_3) \tag{3.3.9}$$

In this diagonal M_{RR} basis, according to the type I seesaw formula, the Dirac neutrino mass matrix also changes to

$$m_{LR} = m_{LR}^0 U_R \tag{3.3.10}$$

where m_{LR}^0 is the Dirac neutrino mass matrix given. If the Dirac neutrino mass matrix is assumed to be diagonal, it can be parametrized by

$$m_{LR}^d = \begin{pmatrix} \lambda^m & 0 & 0 \\ 0 & \lambda^n & 0 \\ 0 & 0 & 1 \end{pmatrix} m_f \tag{3.3.11}$$

where $\lambda = 0.22$ is the standard Wolfenstein parameter and (m, n) are positive integers. We choose the integers (m, n) in such a way which keeps the lightest right handed neutrino mass in the appropriate flavor regime.

3.4 Numerical Analysis

Using the parametric form of PMNS matrix shown in (3.3.3), the Majorana neutrino mass matrix M_ν can be found as

$$M_\nu = U_{\text{PMNS}} M_\nu^{\text{diag}} U_{\text{PMNS}}^T \tag{3.4.1}$$

where

$$M_\nu^{\rm diag} = \begin{pmatrix} m_1 & 0 & 0 \\ 0 & m_2 & 0 \\ 0 & 0 & m_3 \end{pmatrix}, \tag{3.4.2}$$

where m_1, m_2 and m_3 are the three neutrino mass eigenvalues. As mentioned earlier, here we assume that the diagonalizing matrix of the neutrino mass matrix M_ν is same as the PMNS mixing matrix due to the chosen charged lepton mass matrix in the diagonal form.

For the case of normal hierarchy (NH), the three neutrino mass eigenvalues can be written as $m_{\rm diag} = {\rm diag}(m_1, \sqrt{m_1^2 + \Delta m_{21}^2}, \sqrt{m_1^2 + \Delta m_{31}^2})$, while for the case of inverted hierarchy (IH), it can be written as $m_{\rm diag} = {\rm diag}(\sqrt{m_3^2 + \Delta m_{23}^2 - \Delta m_{21}^2}, \sqrt{m_3^2 + \Delta m_{23}^2}, m_3)$. For illustrative purposes, we consider two different order of magnitude values for the lightest neutrino mass m_1 for NH and m_3 for IH. In the first case, we assume $m_{\rm lightest}$ as large as possible so that the sum of the absolute neutrino masses lie just below the cosmological upper bound and it turns out to be 0.07 eV and 0.065 eV for NH and IH respectively. This gives rise to a quasi-degenerate type of neutrino mass spectrum. Secondly. we choose the lightest mass eigenvalue to be 10^{-6} eV for both NH and IH cases so that we have a hierarchical pattern of neutrino masses. The PMNS mixing matrix is evaluated by taking the best fit values of the neutrino mixing angles given in Table 3.1. After using the best fit values of two mass squared differences and three mixing angles, the most general neutrino mass matrix given by (3.4.1) contain four parameters: the lightest neutrino mass, Dirac CP phase and two Majorana phases. Comparing the most general neutrino mass matrix to the texture zero mass matrices, we can either relate two or more terms in the mass matrix or equate them to zero. Depending upon the number of constraints for a specific texture zero mass matrix, we can either write down some free parameters in the most general neutrino mass matrix in terms of the others or we can find the

exact numerical values of the free parameters. We briefly discuss the procedure we adopt for numerical analysis involving different types of Majorana texture zero mass matrices in the following subsections 3.4.1 and 3.4.2.

3.4.1 Parametrization of One-zero Texture

In the case of one-zero texture mass matrices discussed in subsection 3.2.1, there is only one independent zero and hence we have only one complex equation as constraint resulting in two real equations relating $m_1(m_3), \delta, \alpha, \beta$. To simplify the analysis, we assume equality of two Majorana phases $\alpha = \beta$. Using the constraints, we write down the Majorana phases $\alpha = \beta$ as well as lightest neutrino mass in terms of Dirac CP phase δ.

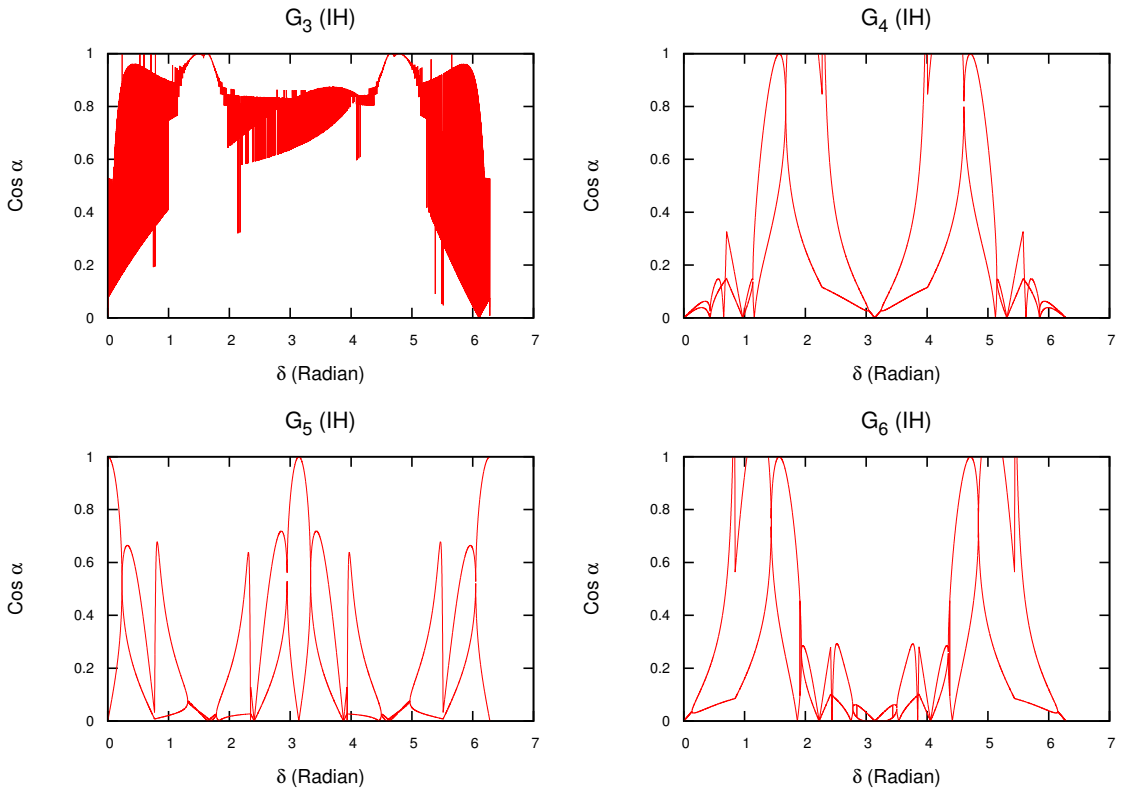

Figure 3.1: Variation of $\cos\alpha$ with δ for one-zero texture with inverted hierarchy.

However, for a specific type of one-zero texture mass matrix denoted by G_1, the zero appears in the $(1,1)$ term and in the most general neutrino mass matrix (3.4.1), the $(1,1)$ term does not depend upon the Dirac CP phase. Therefore, in this case the Majorana phase is independent of the Dirac phase, but depends upon the value of lightest neutrino mass. The lightest neutrino mass for normal hierarchy is found to be 0.0062 eV, whereas for inverted hierarchy, we do not get any real solution for lightest neutrino mass, satisfying the constraint. For one-zero texture G_2 also, we do not get any real solution for lightest neutrino mass in the case of inverted hierarchy. For $G_{3,4,5,6}$ with inverted hierarchy, the variation of Majorana CP phase with Dirac CP phase is shown in figure 3.1. Similarly, the dependence of lightest neutrino mass on Dirac CP phase is shown in the first panel of figures 3.2 and 3.3 respectively. For normal hierarchy, we do not get any real solution for lightest neutrino mass for the one-zero textures $G_{4,5,6}$. For $G_{2,3}$ the dependence of Majorana CP phase with Dirac CP phase is shown in figure 3.4. For G_1, the lightest neutrino mass is exactly determined whereas for $G_{2,3}$ its dependence on δ can be seen in figure 3.6.

3.4.2 Parametrization of Two-zero Texture

In two-zero texture mass matrices discussed in subsection 3.2.2, the Majorana neutrino mass matrix contains two independent zeros. Therefore, we have two complex and hence four real constraint equations to relate the four independent parameters. We numerically solve these four equations to find lightest neutrino mass, Dirac CP phase δ and Majorana CP phases α, β. A set of such solutions are shown in table 3.3 and 3.4.

Patterns	m_3 (eV)	δ	α	β
$A1$	0.00019	0.0059	2.99	0.99
$A2$	0.00038	0.34	2.99	0.87
$B1$	0.049	1.57	3.10	3.11
$B2$	0.0048	1.62	0.93	3.88
$B3$	0.00055	0.055	4.99	6.098
$B4$	0.0052	0.37	2.00	0.73

Table 3.3: Values of m_3, δ, α and β for two-zero texture with inverted hierarchy.

Patterns	m_1 (eV)	δ	α	β
$A1$	0.005	4.36	1.73	4.21
$A2$	0.0069	0.039	1.57	1.55
$B1$	0.068	1.59	0.041	3.14
$B2$	0.022	0.84	2.72	3.31
$B3$	0.07	1.55	3.11	0.0017
$B4$	0.07	4.79	3.15	6.19

Table 3.4: Values of m_1, δ, α and β for two-zero texture with normal hierarchy.

3.4.3 Calculation of Baryon Asymmetry

To calculate the baryon asymmetry in the appropriate flavor regime, we choose the diagonal Dirac neutrino mass matrix in such a way that the lightest right handed singlet neutrino mass lies in the same flavor regime. Similar to the discussion in earlier works [19–21], we choose $m_f = 82.43$ GeV in the Dirac neutrino mass matrix given by (3.3.11). We also choose $(m, n) = (1, 1), (3, 1)$ and $(5, 3)$ to keep the lightest right handed neutrino mass in one, two and three flavor regimes respectively. The resulting baryon asymmetry as a function of Dirac CP phase for different patterns of one-zero texture in the Majorana neutrino mass matrix are shown in figures 3.2-3.6.

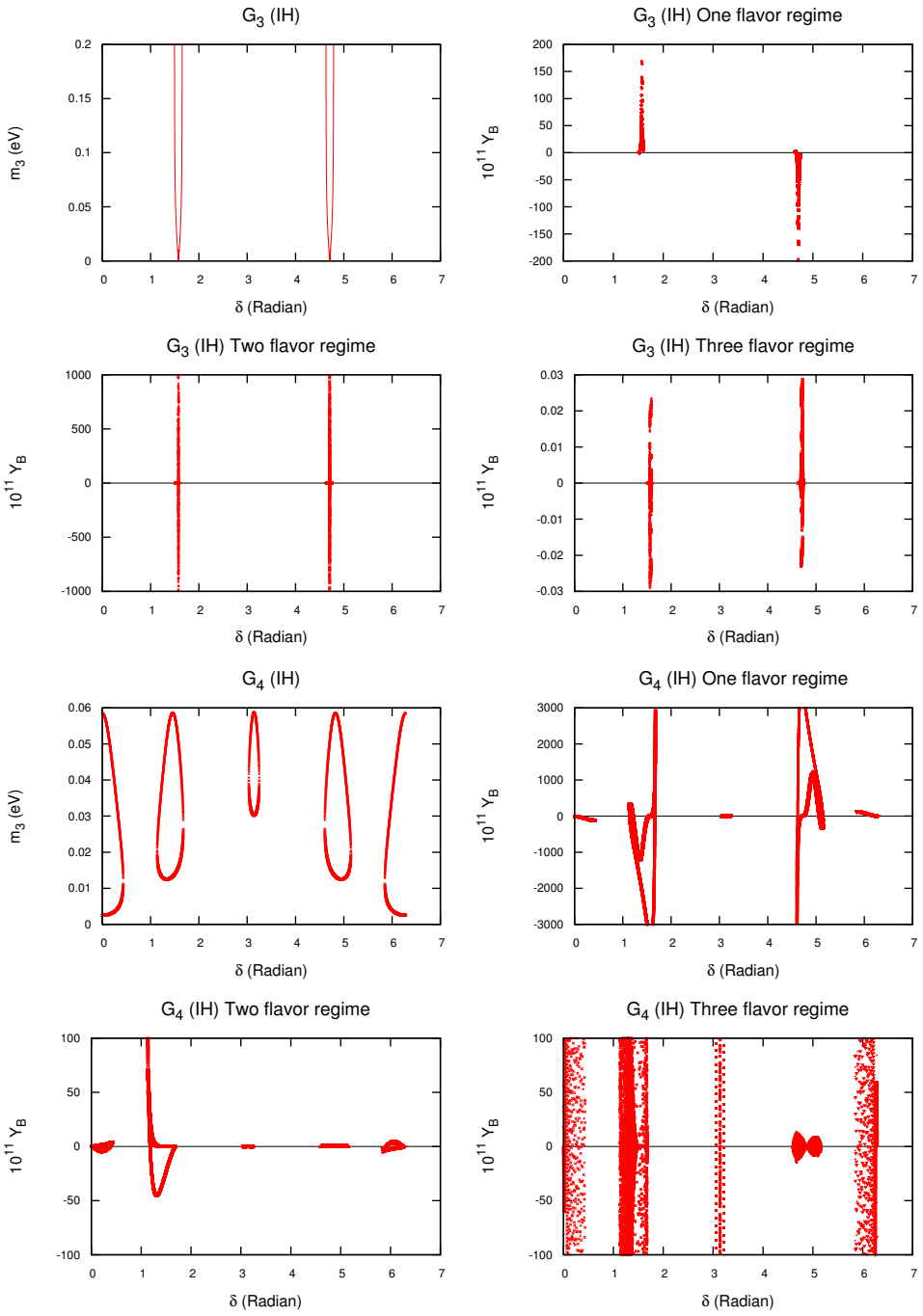

Figure 3.2: Variation of lightest neutrino mass m_3 and baryon asymmetry with Dirac CP phase δ for one-zero textures G_3 and G_4 with inverted hierarchy.

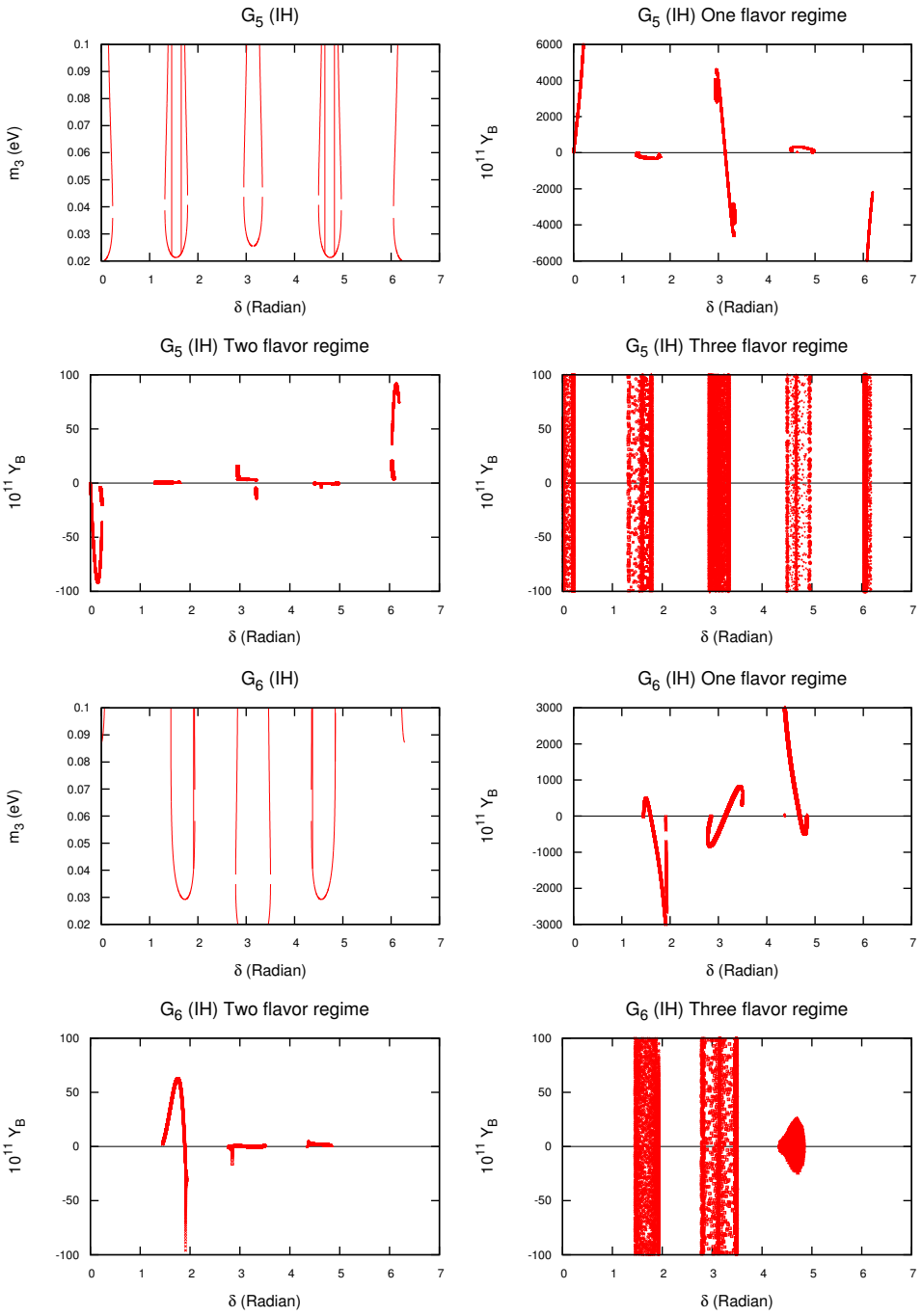

Figure 3.3: Variation of lightest neutrino mass m_3 and baryon asymmetry with Dirac CP phase δ for one-zero textures G_5 and G_6 with inverted hierarchy.

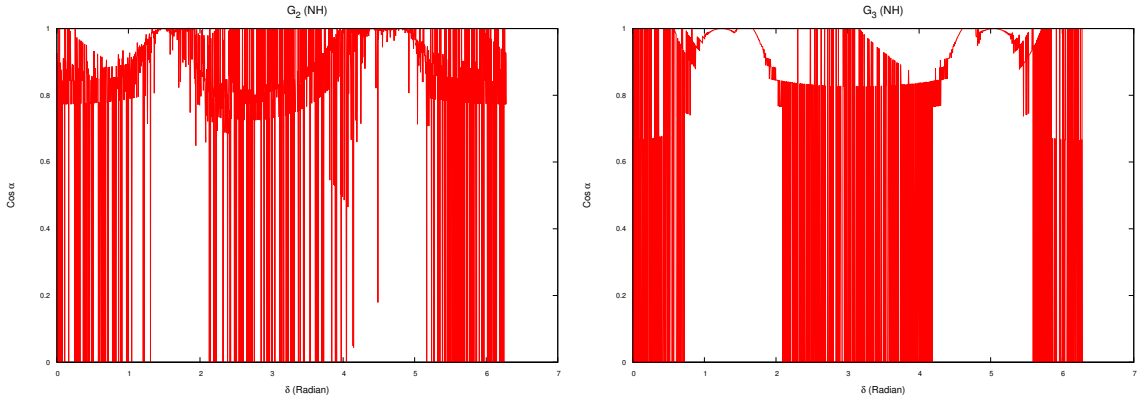

Figure 3.4: Variation of $\cos\alpha$ with δ for one-zero texture with normal hierarchy.

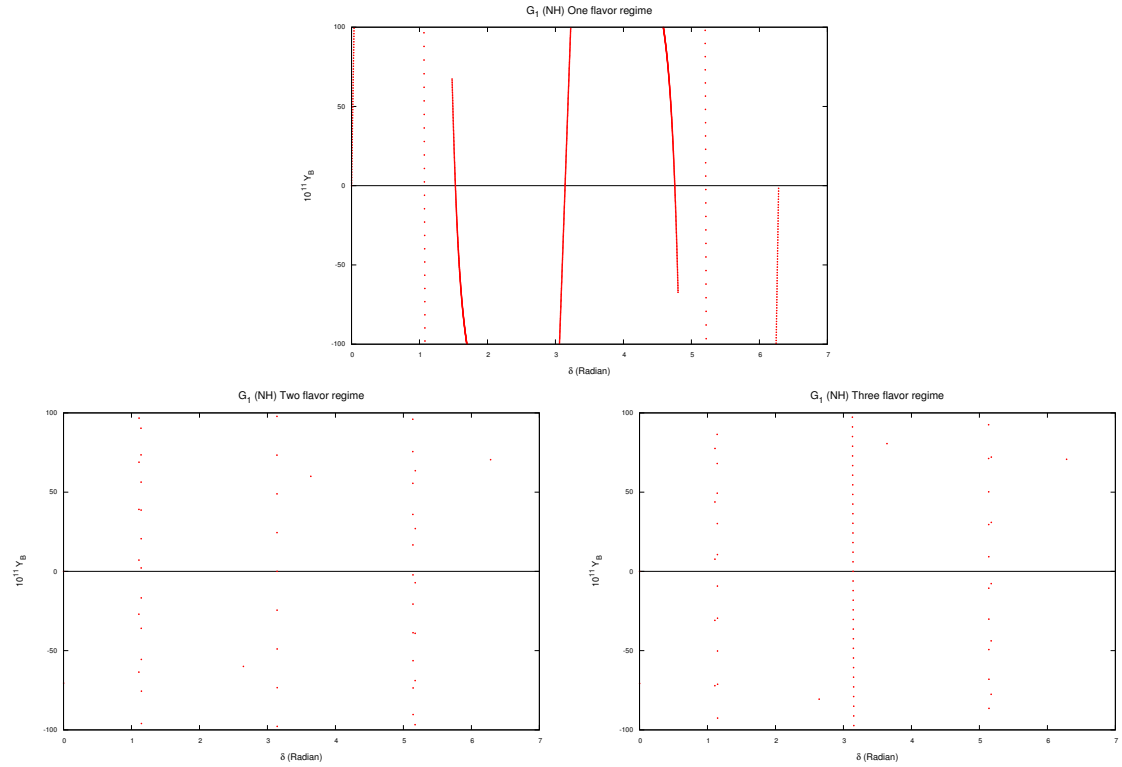

Figure 3.5: Variation of baryon asymmetry with Dirac CP phase δ for one-zero texture G_1 with normal hierarchy.

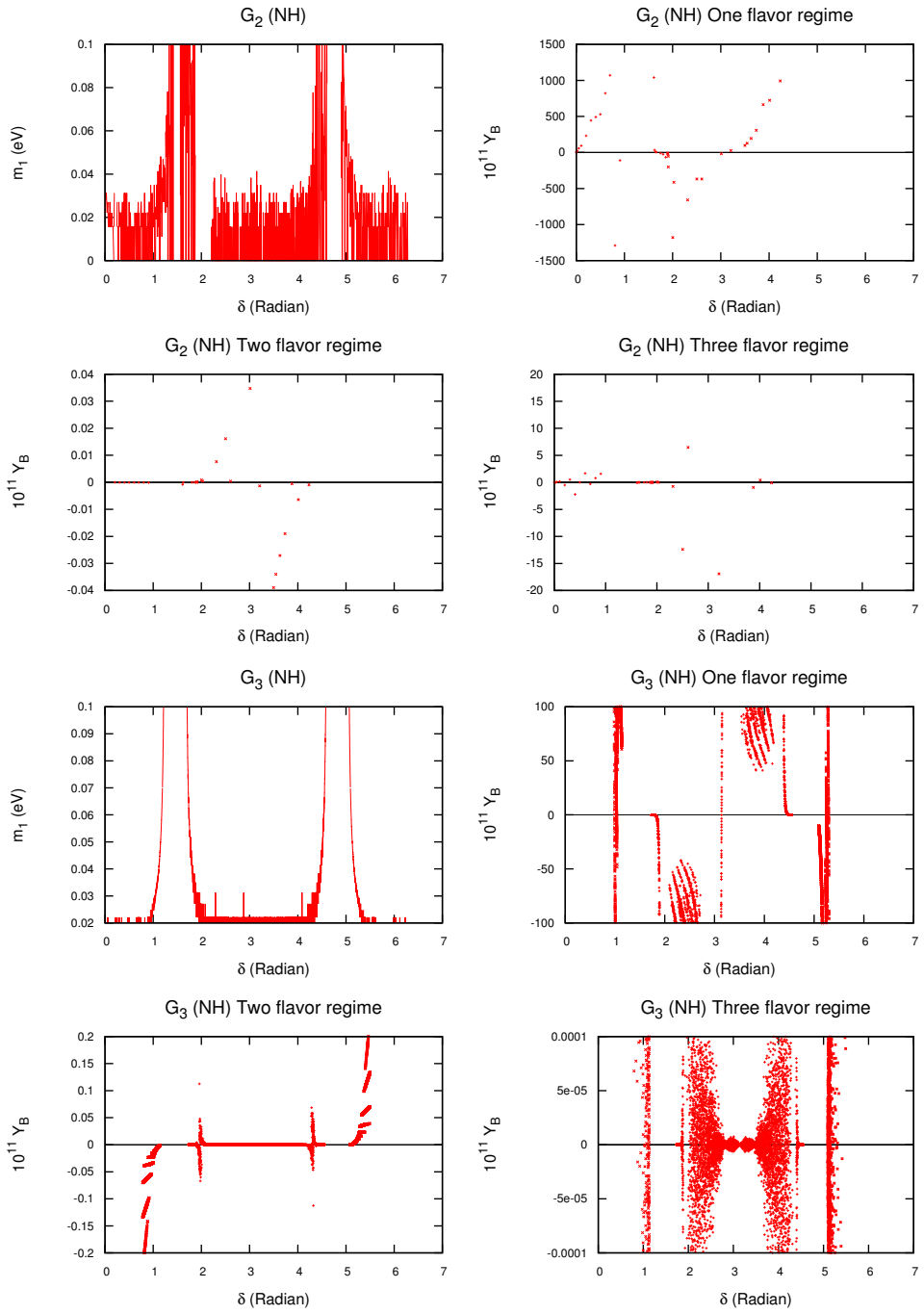

Figure 3.6: Variation of lightest neutrino mass m_1 and baryon asymmetry with Dirac CP phase δ for one-zero textures G_2 and G_3 with normal hierarchy.

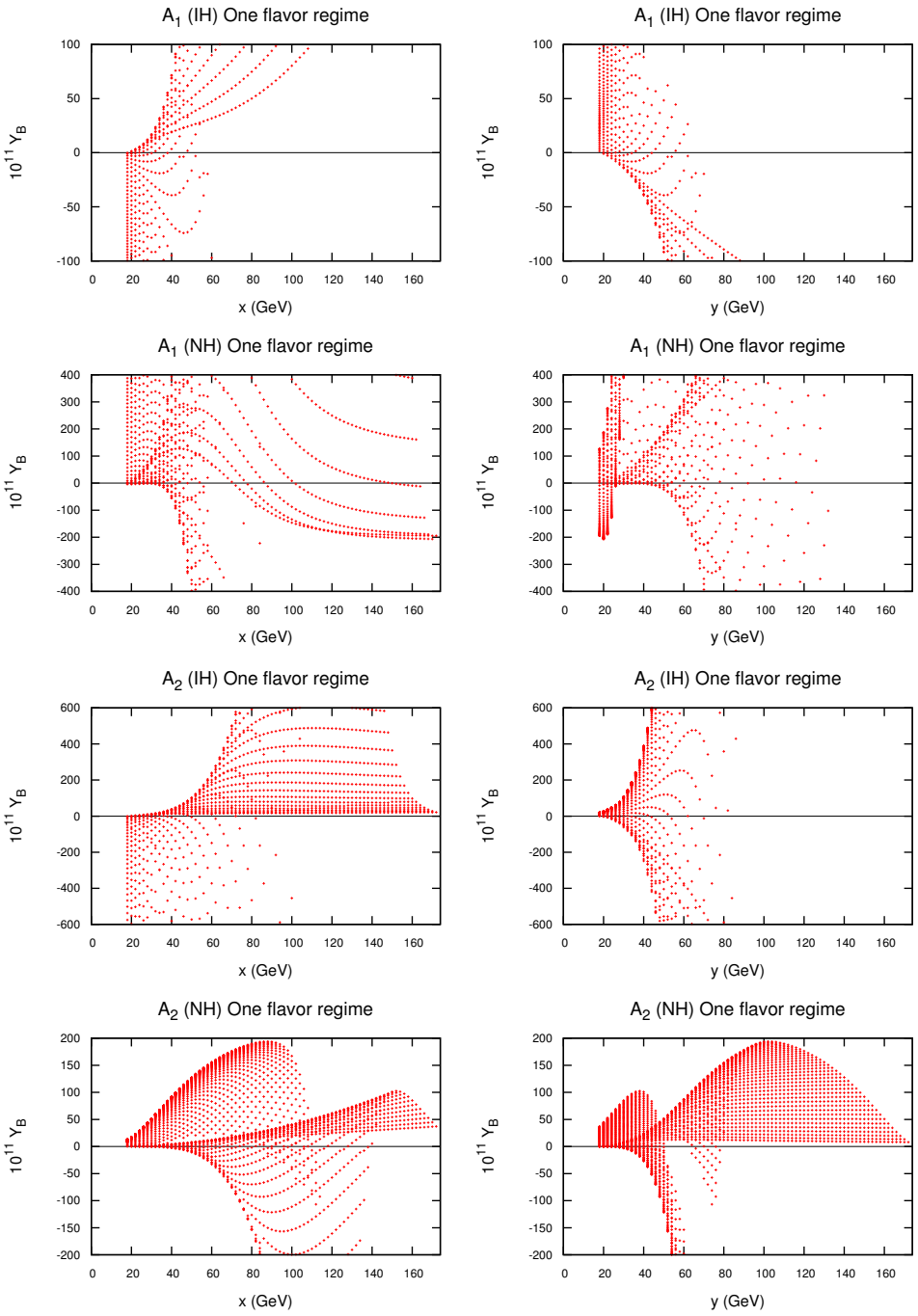

Figure 3.7: Variation of baryon asymmetry in one flavor regime with Dirac neutrino masses for two-zero textures A_1 and A_2.

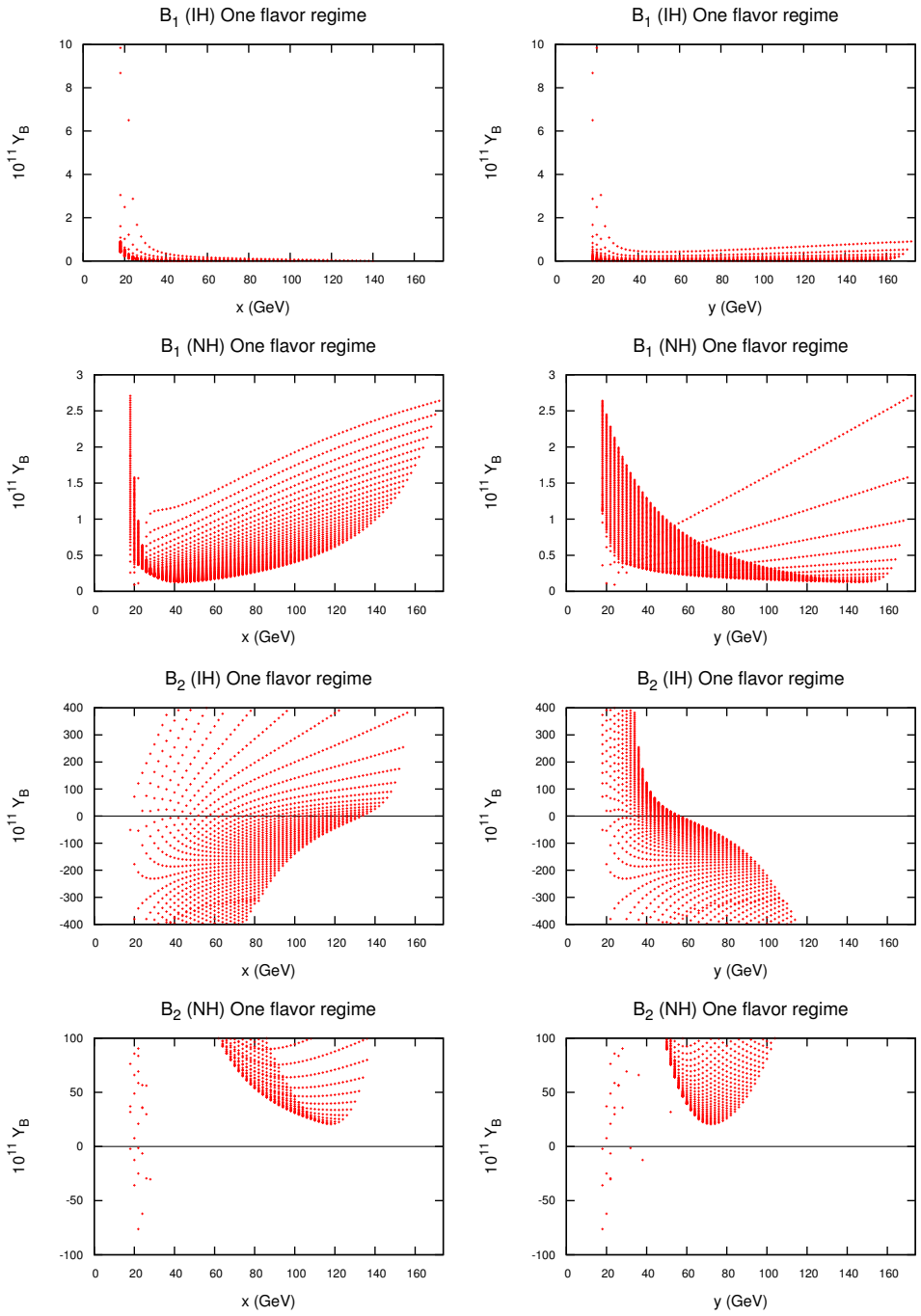

Figure 3.8: Variation of baryon asymmetry in one flavor regime with Dirac neutrino masses for two-zero textures B_1 and B_2.

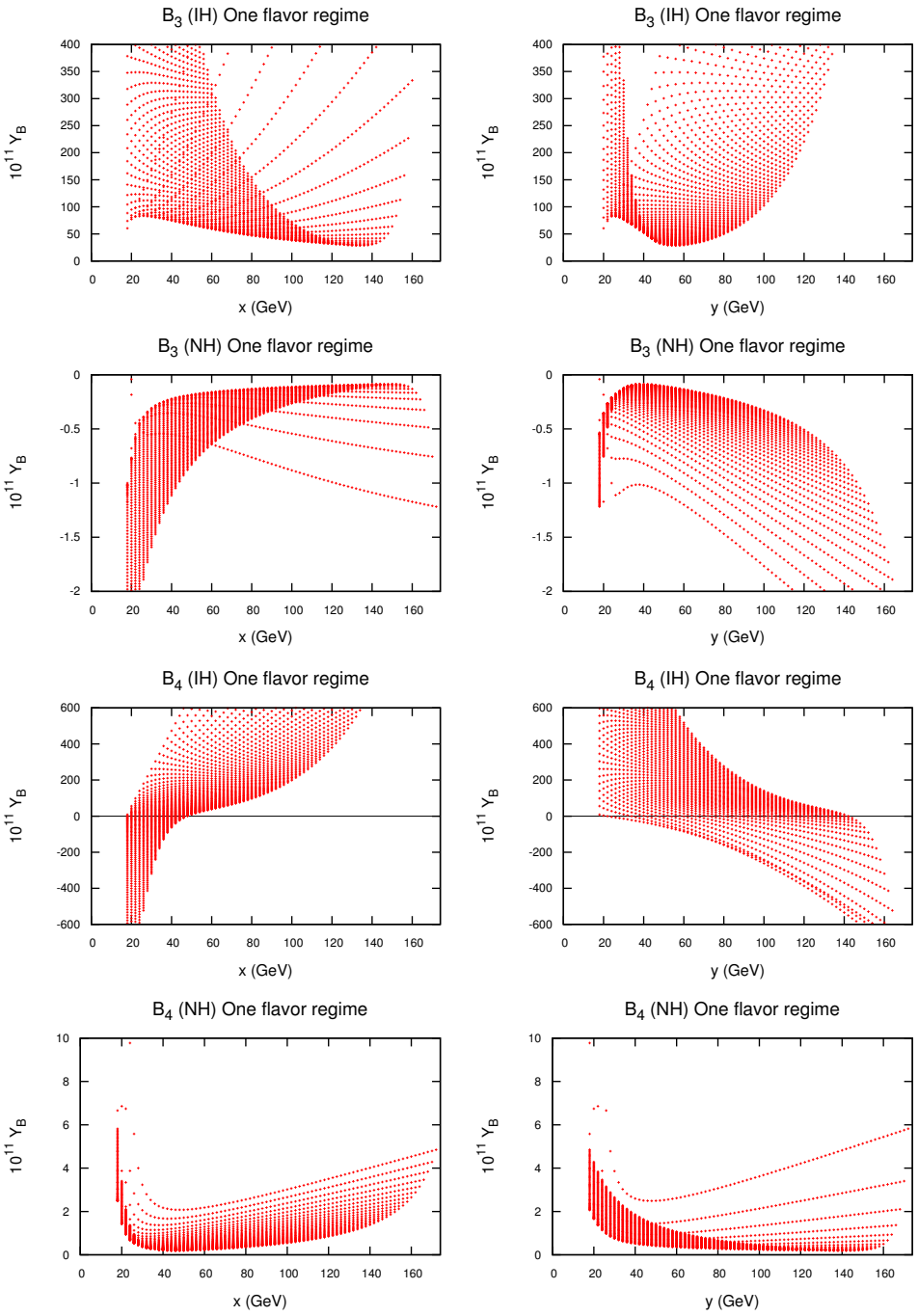

Figure 3.9: Variation of baryon asymmetry in one flavor regime with Dirac neutrino masses for two-zero textures B_3 and B_4.

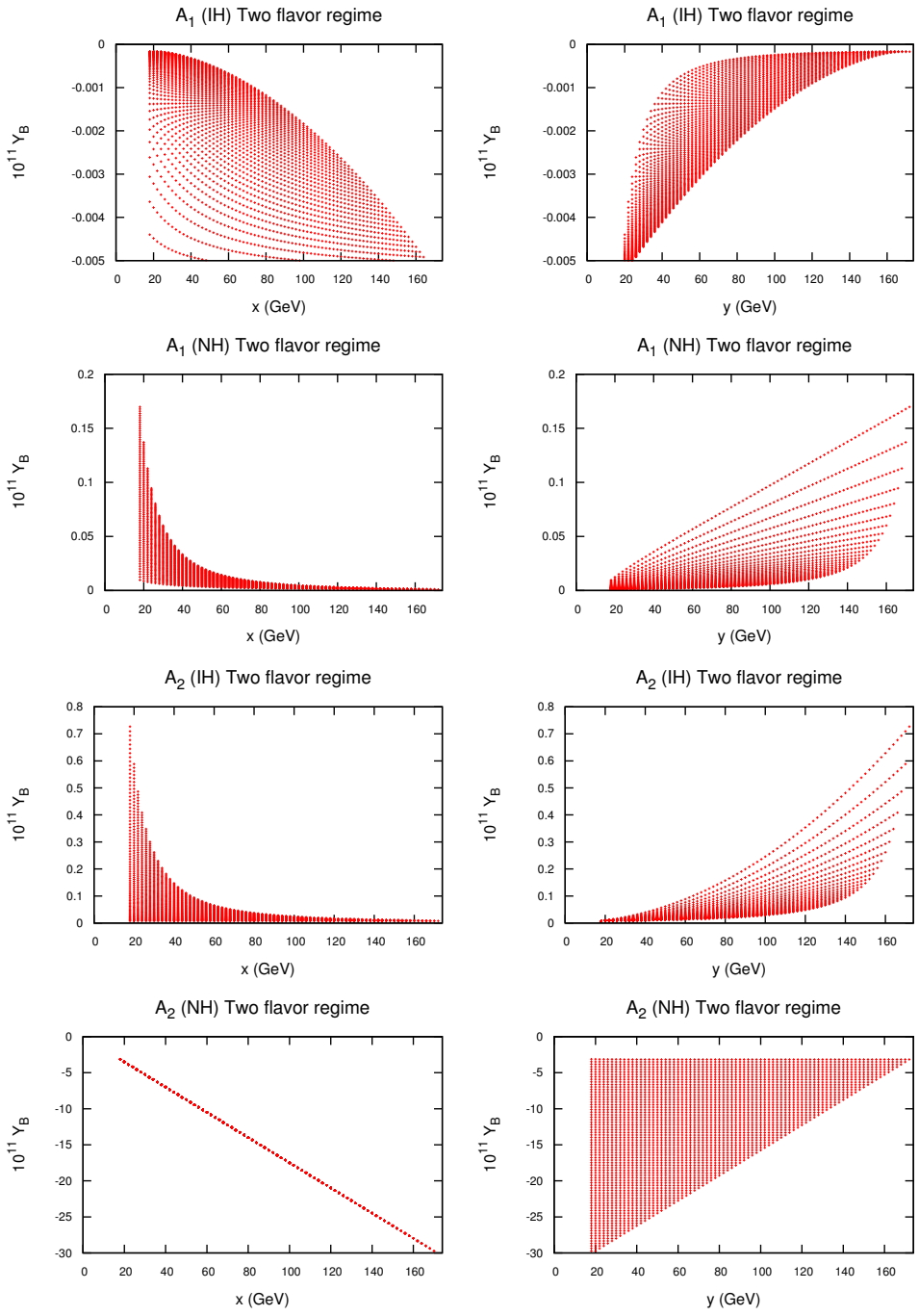

Figure 3.10: Variation of baryon asymmetry in two flavor regime with Dirac neutrino masses for two-zero texture A_1 and A_2.

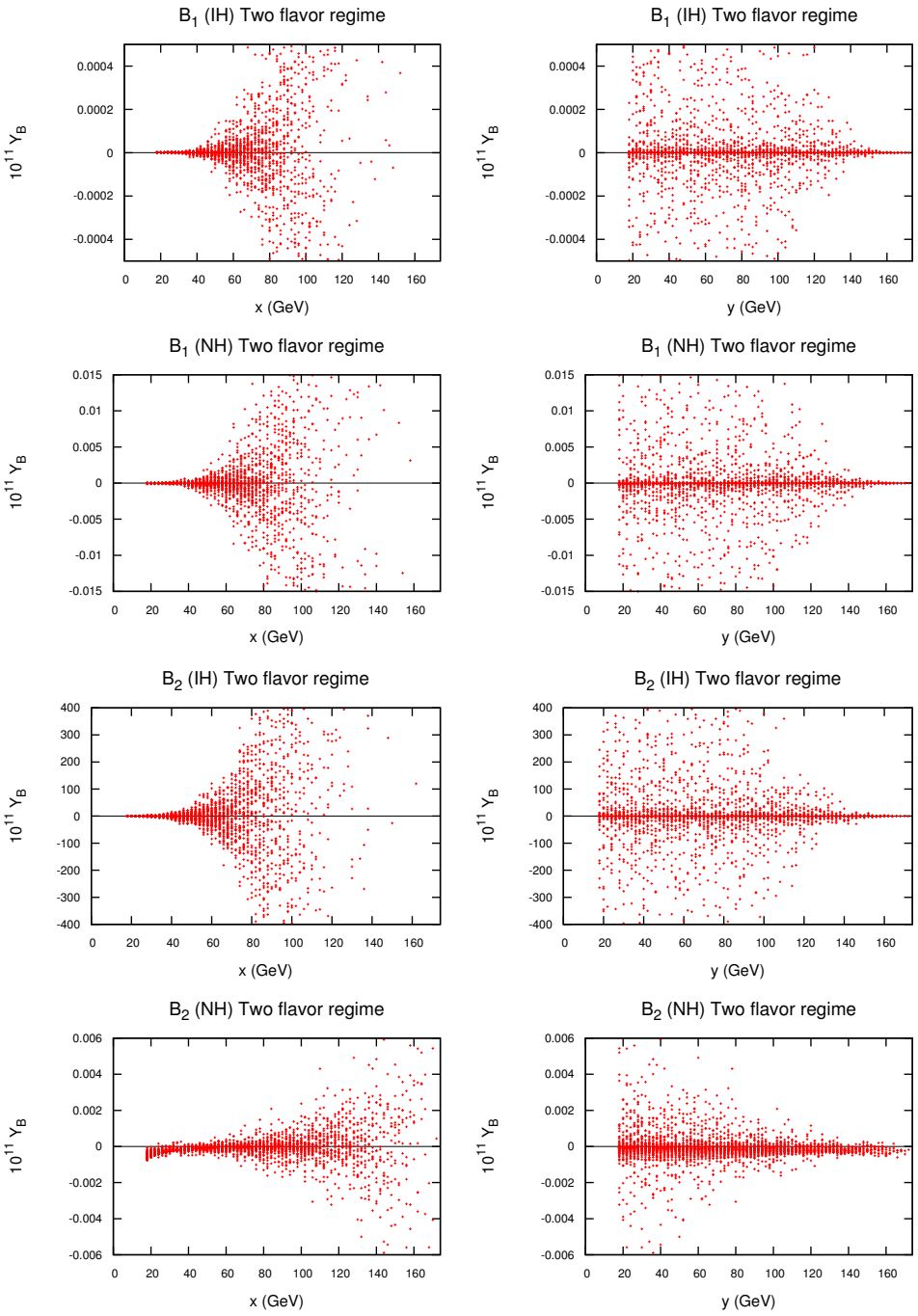

Figure 3.11: Variation of baryon asymmetry in two flavor regime with Dirac neutrino masses for two-zero texture B_1 and B_2.

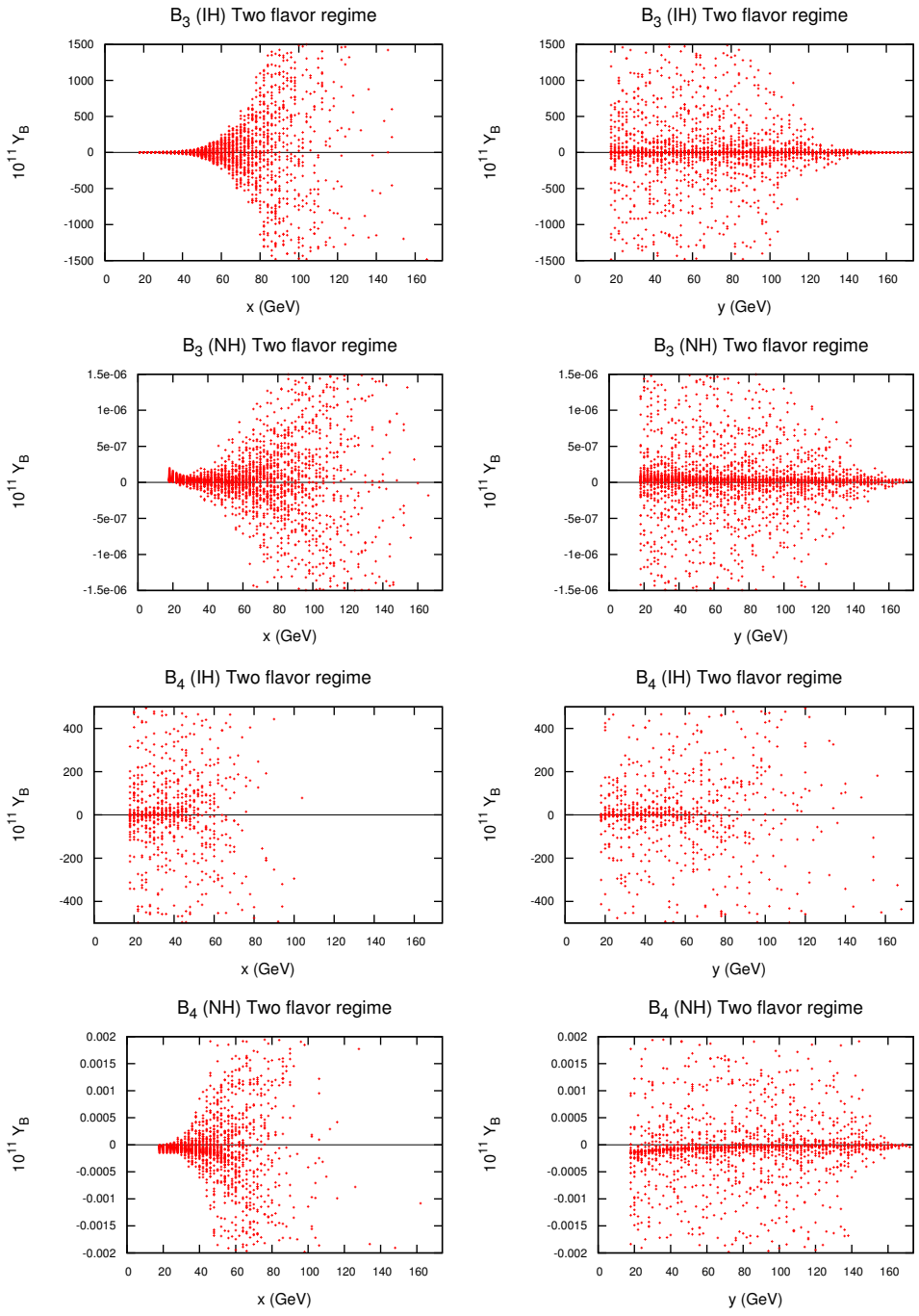

Figure 3.12: Variation of baryon asymmetry in two flavor regime with Dirac neutrino masses for two-zero texture B_3 and B_4.

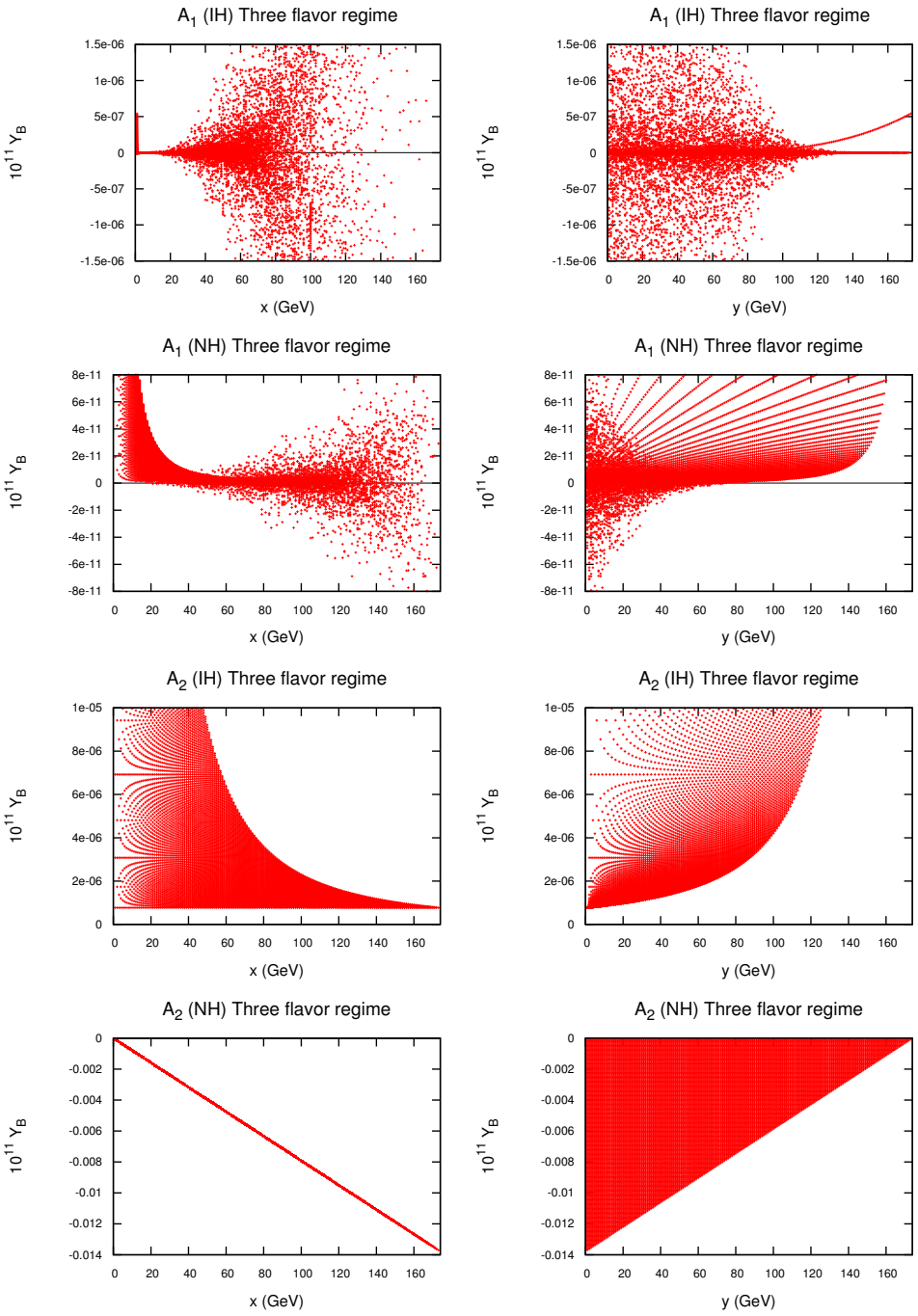

Figure 3.13: Variation of baryon asymmetry in three flavor regime with Dirac neutrino masses for two-zero texture A_1 and A_2.

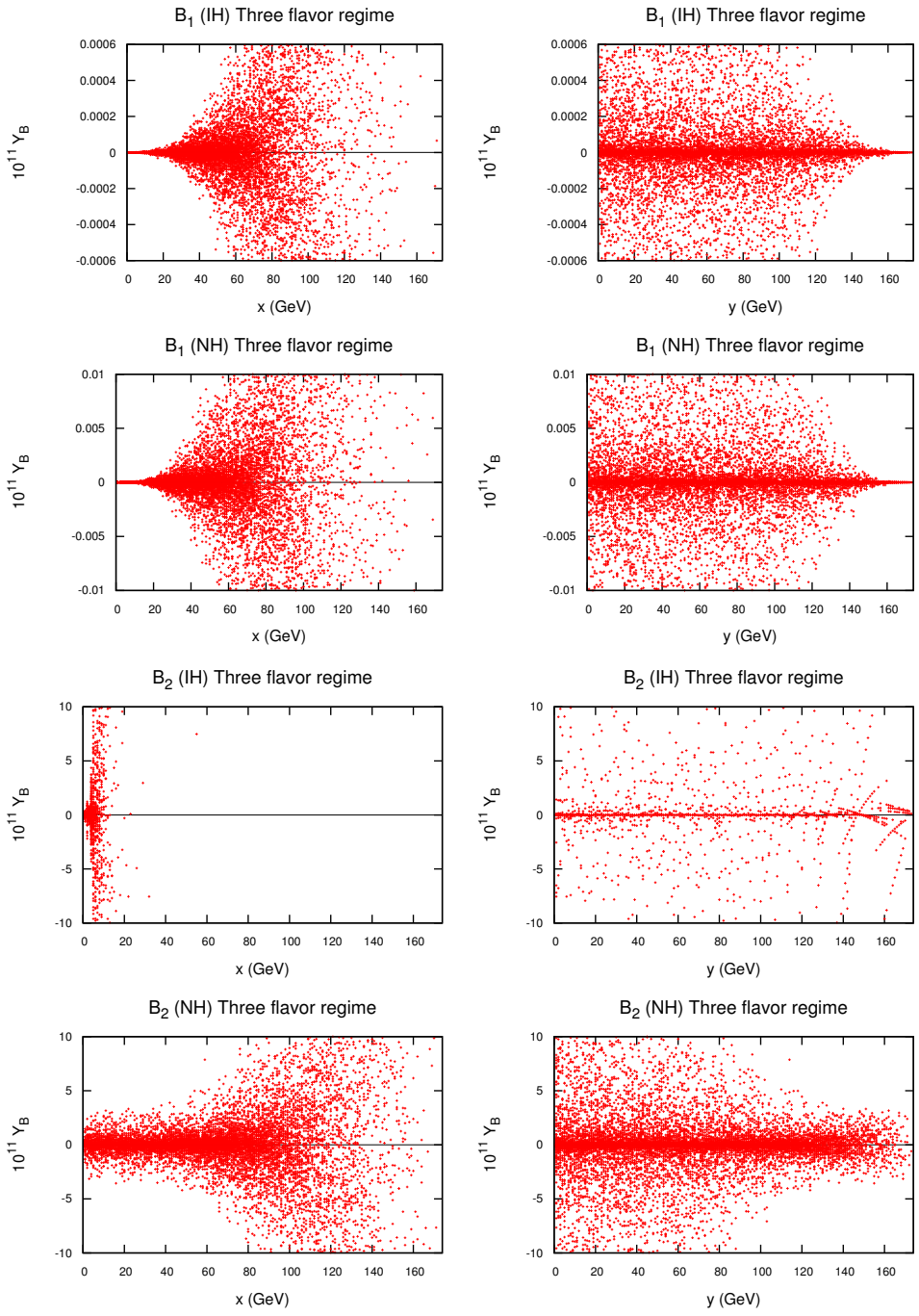

Figure 3.14: Variation of baryon asymmetry in three flavor regime with Dirac neutrino masses for two-zero texture B_1 and B_2.

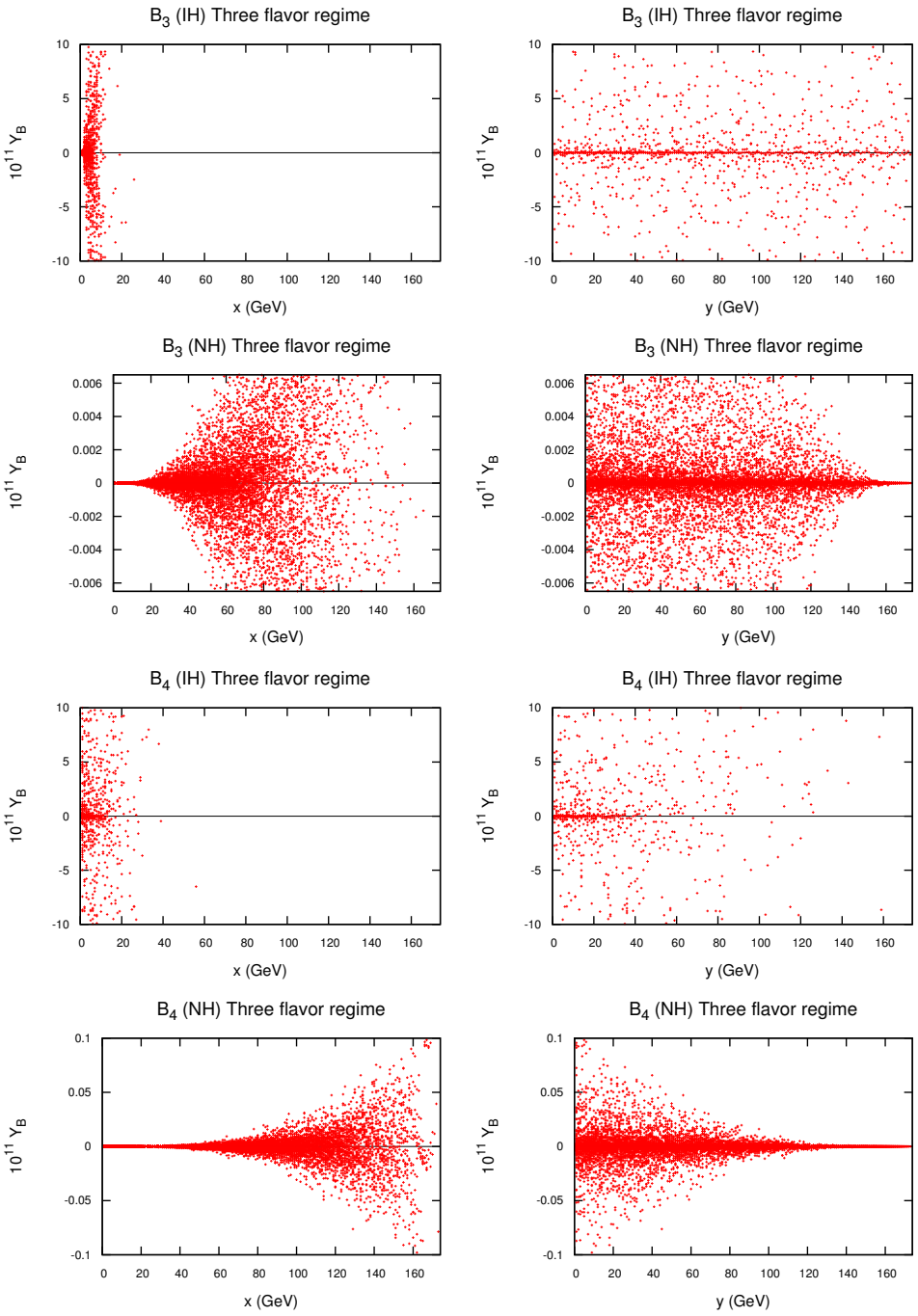

Figure 3.15: Variation of baryon asymmetry in three flavor regime with Dirac neutrino masses for two-zero texture B_3 and B_4.

In case of two-zero texture mass matrices, since all the neutrino parameters are fixed, we compute the baryon asymmetry by varying the Dirac neutrino mass matrix. We choose the Dirac neutrino mass matrix to be of the form

$$m_{LR}^{d} = \begin{pmatrix} m_{11} & 0 & 0 \\ 0 & m_{22} & 0 \\ 0 & 0 & m_{33} \end{pmatrix} \tag{3.4.3}$$

We fix m_{11} such that the lightest right handed neutrino mass falls in the appropriate flavor regime, and vary $m_{22} = x, m_{33} = y \geq x$ and calculate baryon asymmetry. The resulting baryon asymmetry as a function of $m_{22} = x, m_{33} = y \geq x$ are shown in figures from figure 3.7 to figure 3.15.

3.5 Results and Conclusion

Assuming the charged lepton mass matrix to be diagonal, we have studied all possible texture zeros in the Majorana neutrino mass matrix that are allowed by latest neutrino oscillation data as well as the Planck bound on the sum of absolute neutrino masses and constrain them further from the requirement of producing correct baryon asymmetry of the Universe through the mechanism of leptogenesis. The allowed Majorana texture zeros broadly fall into two categories: one-zero texture and two-zero texture. There are six different one-zero textures all of which are allowed by latest oscillation and cosmology data and hence we consider all of them in our analysis. Out of fifteen possible two-zero textures, only six are compatible with oscillation data and the Planck bound, as pointed out by [50, 52].

We have first derived the most general Majorana neutrino mass matrix in terms of the neutrino best fit values as well as the free parameters: lightest neutrino mass, Dirac CP phase and two Majorana phases. Comparing this mass matrix to a specific type of texture zero mass matrix we arrive at one or two complex constraints relating

some or all of the free parameters. Since in case of one-zero texture we have only one complex and hence two real constraints but four free parameters, we assume the equality between two Majorana phases so that we can write them as a function of Dirac CP phase. In case of two-zero textures, we have two complex and hence four real constraints that allow us to find all the four free parameters numerically. We get several solutions for $(m_{\text{lightest}}, \delta, \alpha, \beta)$ all of which give m_{lightest} of the same order of magnitude but different possible values of phases. We list one such set of solutions for each two-zero texture in table 3.3 and 3.4. Since all the free neutrino parameters are numerically determined in this case, any future measurement of Dirac CP phase in neutrino experiments will verify or falsify some of these sets of solutions.

Patterns	One flavor	Two flavor	Three flavor
G_1	$\times$	$\times$	$\times$
G_2	$\times$	$\times$	$\times$
G_3	✓	✓	$\times$
G_4	✓	✓	✓
G_5	✓	$\times$	✓
G_6	✓	✓	✓

Table 3.5: Summary of results for one-zero texture with inverted hierarchy. The symbol ✓ ($\times$) is used when the baryon asymmetry Y_B is in (not in) range.

The summary of our baryon asymmetry results in one-zero texture models is given in table 3.5 and 3.6. It can be seen from these tables that in the one-flavor regime, all one-zero textures can give rise to correct baryon asymmetry depending upon the hierarchy of light neutrino masses. However, in two flavor regime, only G_1 with NH and $G_{3,4,6}$ with IH can give rise to correct baryon asymmetry. In the three flavor regime, G_1 with NH and $G_{4,5,6}$ with IH can give rise to correct baryon asymmetry.

Patterns	One flavor	Two flavor	Three flavor
G_1	✓	✓	✓
G_2	✓	×	×
G_3	✓	×	×
G_4	×	×	×
G_5	×	×	×
G_6	×	×	×

Table 3.6: Summary of results for one-zero texture with normal hierarchy. The symbol ✓ (×) is used when the baryon asymmetry Y_B is in (not in) range.

Patterns	One flavor IH (NH)	Two flavor IH (NH)	Three flavor IH (NH)
A_1	✓(✓)	×(×)	×(×)
A_2	✓(✓)	×(×)	×(×)
B_1	✓(×)	×(×)	×(×)
B_2	✓(✓)	✓(×)	✓(✓)
B_3	×(×)	✓(×)	✓(×)
B_4	✓(×)	✓(×)	✓(×)

Table 3.7: Summary of results for two-zero texture with inverted and normal hierarchy. The symbol ✓ (×) is used when the baryon asymmetry Y_B is in (not in) range.

The summary of results in two-zero texture models are shown in table 3.7. In one flavor regime, all the two-zero texture mass matrices except B_3 can give rise to correct Y_B, depending on the neutrino mass hierarchy. For two flavor regime, only $B_{2,3,4}$ with IH can give rise to the observed baryon asymmetry. Similarly, in three flavor regime B_2 with both IH, NH and $B_{3,4}$ with only IH can produce correct Y_B. Thus if $M_1 < 10^{12}$ GeV, then all the allowed two-zero textures except $B_{2,3,4}$ are disfavored in the light of baryon asymmetry. For the two-zero texture mass matrices

that give correct baryon asymmetry, we also constrain the entries in the diagonal Dirac neutrino mass matrices as can be seen from figures 3.7 to 3.15.

In all the tables mentioned above, the symbol ✓ (×) is used when the baryon asymmetry Y_B for a particular case in (not in) the range given by the Planck experiment. As we mention above, here we have tried to discriminate between all possible Majorana neutrino textures by demanding the observed baryon asymmetry to arise from leptogenesis through the CP violating decay of the lightest right handed neutrino. We have not only constrained the number of texture zero mass matrices, but also constrained the parameters of the neutrino mass matrix which are yet undetermined in experiments. We should however, note that although a certain number of texture zero mass matrices with a particular light neutrino mass hierarchy do not give rise to correct baryon asymmetry, this does not rule out that particular texture as there could be some other source of baryon asymmetry in the Universe. Also, we have arrived at our conclusions by doing the calculations for diagonal Dirac neutrino and charged lepton mass matrices and hence are subject to change if more general forms of these mass matrices are considered. We leave such a general discussion to future studies. Our analysis in this work only provide a guideline for future works related to model building in neutrino physics attempting to understand the dynamical origin of neutrino mass and mixing.

Bibliography

[1] Fukuda, S., et al. Constraints on neutrino oscillations using 1258 days of Super-Kamiokande solar neutrino data, *Phys. Rev. Lett.*, **86**(25), 5656–5660, 2001.

[2] Ahmad, Q. R., et al. Direct evidence for neutrino flavor transformation from neutral-current interactions in the Sudbury Neutrino Observatory, *Phys. Rev. Lett.*, **89**(1), 011301, 2002.

[3] Ahmad, Q. R., et al. Measurement of day and night neutrino energy spectra at SNO and constraints on neutrino mixing parameters, *Phys. Rev. Lett.*, **89**(1), 011302, 2002.

[4] Bahcall, J. N., & Pena-Garay, C. Solar models and solar neutrino oscillations, *New Journal of Physics*, **6**(1), 63, 2004.

[5] Abe, K., et al. Indication of electron neutrino appearance from an accelerator-produced off-axis muon neutrino beam, *Phys. Rev. Lett.*, **107**(4), 041801, 2011.

[6] Abe, Y., et al. Indication of reactor ν_e disappearance in the Double Chooz experiment, *Phys. Rev. Lett.*, **108**(13), 131801, 2012.

[7] An, F. P., et al. Observation of electron-antineutrino disappearance at Daya Bay, *Phys. Rev. Lett.*, **108**(17), 171803, 2012.

[8] Ahn, J. K., et al. Observation of reactor electron antineutrinos disappearance in the RENO experiment, *Phys. Rev. Lett.*, **108**(19), 191802, 2012.

[9] Gonzalez-Garcia, M. C., Maltoni, M., & Schwetz, T. Updated fit to three neutrino mixing: status of leptonic CP violation, *JHEP*, **2014**(11), 1–28, 2014.

[10] Forero, D. V., Tortola, M. and Valle, J. W. F. Neutrino oscillations refitted, *Phys. Rev. D*, **90**(9), 093006, 2014.

[11] Minkowski, P. $\mu \to e\gamma$ at a rate of one out of 10^9 muon decays?, *Phys. Lett. B*, **67**(4), 421-428, 1977.

[12] Gell-Mann, M., Ramond, P., & Slansky, R. Print-80-0576 (CERN). T. Yanagida, *Prog. Theor. Phys.*, **64**, 1103, 1980.

[13] Yanagida, T. Horizontal symmetry and masses of neutrinos, *Progress of Theoretical Physics*, **64**(3), 1103-1105, 1980.

[14] Mohapatra, R. N., & Senjanovic, G. Neutrino mass and spontaneous parity nonconservation, *Phys. Rev. Lett.*, **44**(14), 912–915, 1980.

[15] Schechter, J., & Valle, J.W.F. Neutrino masses in $SU(2) \times U(1)$ theories, *Phys. Rev. D*, **22**(9), 2227–2235, 1980.

[16] Ade, P. A. R., et al. Planck 2013 results. XVI, Cosmological parameters, *Astronomy & Astrophysics*, **571**, A16, 2014.

[17] Borah, D. Deviations from tri-bimaximal neutrino mixing using type II seesaw, *Nucl. Phys. B*, **876**(2), 575–586, 2013.

[18] Borah, D., Patra, S., & Pritimita, P. Sub-dominant type-II seesaw as an origin of non-zero θ_{13} in $SO(10)$ model with TeV scale Z' gauge boson, *Nucl. Phys. B*, **881**, 444–466, 2014.

[19] Borah, D., Type II seesaw origin of nonzero θ_{13}, $\delta_{\rm CP}$ and leptogenesis, *Int. J. Mod. Phys. A*, **29**(22), 1450108, 2014.

[20] Borah, M., et al. Perturbations to the $\mu - \tau$ symmetry, leptogenesis, and lepton flavor violation with the type II seesaw mechanism, *Phys. Rev. D*, **90**(9), 095020, 2014.

[21] Kalita, R., & Borah, D. Connecting leptonic CP violation, lightest neutrino mass and baryon asymmetry through type II seesaw, *Int. J. Mod. Phys. A*, **30**(09), 1550045, 2015.

[22] Berger, M. S., & Siyeon, K. Discrete flavor symmetries and mass matrix textures, *Phys. Rev. D*, **64**(5), 053006, 2001.

[23] Low, C. I. Generating extremal neutrino mixing angles with Higgs family symmetries, *Phys. Rev. D*, **70**(7), 073013, 2004.

[24] Low, C. I. Abelian family symmetries and the simplest models that give $\theta_{13} = 0$ in the neutrino mixing matrix, *Phys. Rev. D*, **71**(7), 073007, 2005.

[25] Grimus, W., et al. Symmetry realization of texture zeros, *EPJC*, **36**(2), 227–232, 2004.

[26] Dighe, A., & Sahu, N. Texture zeroes and discrete flavor symmetries in light and heavy Majorana neutrino mass matrices: a bottom-up approach, arXiv:0812.0695, 2008.

[27] Dev, S., Gupta, S., & Gautam, R. R. Zero textures of the neutrino mass matrix from cyclic family symmetry, *Phys. Lett. B*, **701**(5), 605–608, 2011.

[28] Felipe, R. G., & Serodio, H. Abelian realization of phenomenological two-zero neutrino textures, *Nucl. Phys. B*, **886**, 75–92, 2014.

[29] Ludl, P. O., & Grimus, W. A complete survey of texture zeros in the lepton mass matrices, *JHEP*, **2014**(7), 1-30, 2014.

[30] Kaneko, S., & Tanimoto, M. Neutrino mass matrix with two zeros and leptogenesis, *Phys. Lett. B*, **551**(1), 127–136, 2003.

[31] Kaneko, S., Katsumata, M., & Tanimoto, M. Leptogenesis in neutrino textures with two zeros, *JHEP*, **2003**(07), 025, 2003.

[32] Dev, S., & Verma, S. Leptogenesis in a Hybrid Texture Neutrino Mass Model, *Mod. Phys. Lett. A*, **25**(33), 2837–2848, 2010.

[33] Bando, M., et al. Symmetric mass matrix with two zeros in SUSY $SO(10)$ GUT, lepton flavor violations and leptogenesis, *Prog. Th. Phys.*, **112**(3), 533–567, 2004.

[34] Nguyen, T. P. Texture zeros of neutrino mass matrix with seesaw mechanism and leptogenesis, *Mod. Phys. Lett. A*, **29**(08), 1450038–1450053, 2014.

[35] Kuzmin, V. A., Rubakov, V. A., & Shaposhnikov, M. E. On anomalous electroweak baryon-number non-conservation in the early universe, *Phys. Lett. B*, **155**(1), 36–42, 1985.

[36] Fukugita, M., & Yanagida, T. Barygenesis without grand unification, *Phys. Lett. B*, **174**(1), 45–47, 1986.

[37] Xing, Z. Z. Texture zeros and CP-violating phases in the neutrino mass matrix, *Proceedings of the Fifth International Workshop*, **11**, 2004.

[38] Xing, Z. Z. Implications of generalized Frampton-Glashow-Yanagida ansaetze on neutrino masses and lepton flavor mixing, *Phys. Rev. D*, **69**(1), 013006, 2004.

[39] Lashin, E. I., & Chamoun, N. One-zero textures of Majorana neutrino mass matrix and current experimental tests, *Phys. Rev. D*, **85**(11), 113011, 2012.

[40] Deepthi, K. N., Gollu, S., & Mohanta, R. Neutrino mixing matrices with relatively large θ_{13} and with texture one-zero, *EPJC*, **72**(2), 1–8, 2012.

[41] Merle, A., & Rodejohann, W. "Elements of the neutrino mass matrix: Allowed ranges and implications of texture zeros, *Phys. Rev. D*, **73**(7), 073012, 2006.

[42] Frampton, P. H., Glashow, S. L., & Marfatia, D. Zeroes of the neutrino mass matrix, *Phys. Lett. B*, **536**(1), 79–82, 2002.

[43] Xing, Z. Z. Texture zeros and Majorana phases of the neutrino mass matrix, *Phys. Lett. B*, **530**(1), 159–166, 2002.

[44] Xing, Z. Z. A full determination of the neutrino mass spectrum from two-zero textures of the neutrino mass matrix, *Phys. Lett. B*, **539**(1), 85–90, 2002.

[45] Kageyama, A., et al. See-saw realization of the texture zeros in the neutrino mass matrix, *Phys. Lett. B*, **538**(1), 96–106, 2002.

[46] Grimus, W., & Lavoura, L. On a model with two zeros in the neutrino mass matrix, *J. Phys. G: Nucl. and Part. Phys.*, **31**(7), 693, 2005.

[47] Dev, S., et al. Phenomenology of two-texture zero neutrino mass matrices, *Phys. Rev. D*, **76**(1), 013002, 2007.

[48] Ludl, P. O., Morisi, S., & Peinado, E. The reactor mixing angle and CP violation with two texture zeros in the light of T2K, *Nucl. Phys. B*, **857**(3), 411–423, 2012.

[49] Kumar, S. Implications of a class of neutrino mass matrices with texture zeros for nonzero θ_{13}, *Phys. Rev. D*, **84**(7), 077301, 2011.

[50] Fritzsch, H., Xing, Z.Z., & Zhou, S. Two-zero textures of the Majorana neutrino mass matrix and current experimental tests, *JHEP*, **2011**(9), 1–43, 2011.

[51] Blankenburg, G., & Meloni, D. Fine-tuning and naturalness issues in the two-zero neutrino mass textures, *Nucl. Phys. B*, **867**(3), 749–762, 2013.

[52] Meloni, D., Meroni, A., & Peinado, E. Two-zero Majorana textures in the light of the Planck results, *Phys. Rev. D*, **89**(5), 053009, 2014.

[53] Dev, S., et al. Near maximal atmospheric neutrino mixing in neutrino mass models with two texture zeros, *Phys. Rev. D*, **90**(1), 013021, 2014.

[54] Davidson, S., Nardi, E., & Nir, Y. Leptogenesis, *Phys. Rep.*, **466**(4), 105–177, 2008.

[55] Sakharov, A. D. Violation of CP invariance, C asymmetry, and baryon asymmetry of the universe, *Sov. Phys. Usp.*, **34**(5), 392–393, 1991.

[56] Joshipura, A. S., Paschos, E. A., & Rodejohann, W. Leptogenesis in left–right symmetric theories,*Nucl. Phys. B*, **611**(1), 227–238, 2001.

[57] Kolb, E. W., & Turner, M. S. The early universe, *Front. Phys.*, **69**(1), 1990.

[58] Flanz, M., and Paschos, E. A. Further considerations on the CP asymmetry in heavy Majorana neutrino decays, *Phys. Rev. D*, **58**(11), 113009, 1998.

[59] Pilaftsis, A. Heavy Majorana neutrinos and baryogenesis, *Int. J. Mod. Phys. A*, **14**(12), 1811–1857, 1999.

[60] Barbieri, R., et al. Baryogenesis through leptogenesis, *Nucl. Phys. B*, **575**(1), 61–77, 2000.

[61] Abada, A., et al. Flavour issues in leptogenesis, *JCAP*, **2006**(04), 1–22, 2006.

[62] Abada, A., et al. Flavour matters in leptogenesis, *JHEP*, **2006**(09), 010, 2006.

[63] Nardi, E., et al. The importance of flavor in leptogenesis, *JHEP*, **2006**(01), 164, 2006.

[64] Dev, P. S B., et al. Flavour covariant transport equations: an application to resonant leptogenesis, *Nucl. Phys. B*, **886**, 569–664, 2014.

Chapter 4

Stability of Neutrino Masses and Mixing with non-zero θ_{13} using RGE

In this chapter, we use renormalisation group equations to study their effects on neutrino masses and mixings. For this purpose, we consider a $\mu - \tau$ symmetric TBM type mass matrix at high scale. Keeping the three neutrino mass eigenvalues as input parameters at high scale, we compute them at low scale using the RGE's. We also calculate the absolute neutrino mass and the effective neutrino mass considering both inverted and normal hierarchies.

4.1 Introduction

Exploration of the origin of neutrino masses and mixing has been one of the major goals of particle physics community for the last few decades. The results of recent neutrino oscillation experiments have provided a clear evidence favoring the existence of tiny but non-zero neutrino masses [1–5]. Recent neutrino oscillation experiments

like T2K [6], Double ChooZ [7], Daya-Bay [8] and RENO [9] have not only confirmed the earlier predictions for neutrino parameters, but also provided strong evidence for a non-zero value of the reactor mixing angle θ_{13}. The latest global fit values for 3σ range of neutrino oscillation parameters [10] are as follows:

$$\Delta m^2_{21} = (7.00 - 8.09) \times 10^{-5}\ \text{eV}^2$$

$$\Delta m^2_{31}\ (\text{NH}) = (2.27 - 2.69) \times 10^{-3}\ \text{eV}^2$$

$$\Delta m^2_{23}\ (\text{IH}) = (2.24 - 2.65) \times 10^{-3}\ \text{eV}^2$$

$$\sin^2\theta_{12} = 0.27 - 0.34$$

$$\sin^2\theta_{23} = 0.34 - 0.67$$

$$\sin^2\theta_{13} = 0.016 - 0.030 \tag{4.1.1}$$

where NH and IH refers to normal and inverted hierarchy respectively. Another global fit study [11] reports the 3σ values as

$$\Delta m^2_{21} = (6.99 - 8.18) \times 10^{-5}\ \text{eV}^2$$

$$\Delta m^2_{31}\ (\text{NH}) = (2.19 - 2.62) \times 10^{-3}\ \text{eV}^2$$

$$\Delta m^2_{23}\ (\text{IH}) = (2.17 - 2.61) \times 10^{-3}\ \text{eV}^2$$

$$\sin^2\theta_{12} = 0.259 - 0.359$$

$$\sin^2\theta_{23} = 0.331 - 0.637$$

$$\sin^2\theta_{13} = 0.017 - 0.031 \tag{4.1.2}$$

The observation of non-zero θ_{13} which is evident from the above global fit data can have non- trivial impact on neutrino mass hierarchy as studied in recent papers [12,13]. Non-zero θ_{13} can also shed light on the Dirac CP violating phase in the leptonic sector which would have remained unknown if θ_{13} were exactly zero. The detailed analysis

of this non-zero θ_{13} have been demonstrated both from theoretical [14–18], as well as phenomenological [19–24] point of view, prior to and after the confirmation of this important result announced in 2012. It should be noted that prior to the discovery of non-zero θ_{13}, the neutrino oscillation data were compatible with the so called TBM form of the neutrino mixing matrix [25–30] given by

$$U_{TBM} == \begin{pmatrix} \sqrt{\frac{2}{3}} & \frac{1}{\sqrt{3}} & 0 \\ -\frac{1}{\sqrt{6}} & \frac{1}{\sqrt{3}} & \frac{1}{\sqrt{2}} \\ \frac{1}{\sqrt{6}} & -\frac{1}{\sqrt{3}} & \frac{1}{\sqrt{2}} \end{pmatrix}, \tag{4.1.3}$$

which predicts $\sin^2\theta_{12} = \frac{1}{3}$, $\sin^2\theta_{23} = \frac{1}{2}$ and $\sin^2\theta_{13} = 0$. However, since the latest data have ruled out $\sin^2\theta_{13} = 0$, there arises the need to go beyond the TBM framework. In view of the importance of the non-zero reactor mixing and hence, CP violation in neutrino sector, the present work demonstrates how a specific μ-τ symmetric mass matrix (giving rise to TBM type mixing) at high energy scale can produce non-zero θ_{13} along with the desired values of other neutrino parameters $\Delta m^2_{21}, \Delta m^2_{23}, \theta_{23}, \theta_{12}$ at low energy scale through renormalization group evolution (RGE). We also outline how the $\mu - \tau$ symmetric neutrino mass matrix with TBM type mixing can be realized at high energy scale within the framework of MSSM with an additional A_4 flavor symmetry at high energy scale. After taking the RGE effects into account, we observe that the output at TeV scale is very much sensitive to the choice of neutrino mass ordering at high scale as well as the value of $\tan\beta = \frac{v_u}{v_d}$, the ratio of vev's of two MSSM Higgs doublets $H_{u,d}$. We point out that this model allows only a very mild hierarchy of both inverted and normal type at high energy scale. We scan the neutrino mass eigenvalues at high energy and constrain them to be large $|m_{1,2,3}| = 0.08 - 0.12$ eV in order to produce correct neutrino parameters at low energy. We consider two such input values for mass eigenvalues, one with inverted hierarchy and the other with normal hierarchy and show the predictions for neutrino parameters at low energy scale. We also show the evolution of effective neutrino mass $m_{ee} = |\sum_i U^2_{ei} m_i|$ (where U is the neutrino

mixing matrix) that could be interesting from neutrino-less double beta decay point of view. Finally we consider the cosmological upper bound on the sum of absolute neutrino masses ($\sum_i |m_i| < 0.23$ eV) reported by the Planck collaboration [31] to check if the output at low energy satisfy this or not.

This chapter is organized as follows. In section 4.2, we discuss briefly the A_4 model at high energy scale. In section 4.3 we outline the RGE's of mass eigenvalues and mixing parameters. In section 4.4 we discuss our numerical results, and finally conclude in section 4.5.

4.2 A_4 model for neutrino mass

Type I seesaw framework is the simplest mechanism for generating tiny neutrino masses and mixing. In this seesaw mechanism neutrino mass matrix can be written as

$$m_{LL} = -m_{LR} M_R^{-1} m_{LR}^T. \tag{4.2.1}$$

Within this framework of seesaw mechanism neutrino mass has been extensively studied by discrete flavor groups by many authors [32–55] available in the literature. Among the different discrete groups the model by the finite group of even permutation, A_4 also can explain the $\mu - \tau$ symmetric mass matrix obtained from this type I seesaw mechanism. This group has 12 elements having 4 irreducible representations, with dimensions n_i, such that $\sum_i n_i^2 = 12$. The characters of 4 representations are shown in table 4.1. The complex number ω is the cube root of unity. In the present work we outline a neutrino mass model with A_4 symmetry given in the ref. [56, 57]. This flavor symmetry is also accompanied by an additional Z_3 symmetry in order to achieve the desired leptonic mixing. In this model, the three families of left-handed lepton doublets $l = (l_e, l_\mu, l_\tau)$ transform as triplets, while the electroweak singlets e^c, μ^c, τ^c and the electroweak Higgs doublets $H_{u,d}$ transform as singlets under the

A_4 symmetry. In order to break the flavor symmetry spontaneously, two A_4 triplet scalars $\phi_l = (\phi_{l1}, \phi_{l2}, \phi_{l3}), \phi_\nu = (\phi_{\nu 1}, \phi_{\nu 2}, \phi_{\nu 3})$ and three scalars $\zeta_1, \zeta_2, \zeta_3$ transforming as $\mathbf{1}, \mathbf{1}', \mathbf{1}''$ under A_4 are introduced. The Z_3 charges for $l, H_{u,d}, \phi_l, \phi_\nu, \zeta_{1,2,3}$ are $\omega, 1, 1, \omega, \omega$ respectively.

Class	$\chi^{(1)}$	$\chi^{(2)}$	$\chi^{(3)}$	$\chi^{(4)}$
C_1	1	1	1	3
C_2	1	ω	ω^2	0
C_3	1	ω^2	ω	0
C_4	1	1	1	-1

Table 4.1: Character table of A_4

Under the electroweak gauge symmetry as well as the flavor symmetry mentioned above, the superpotential for the neutrino sector can be written as

$$W_\nu = (y_{\nu\phi}\phi_\nu + y_{\nu\zeta 1}\zeta_1 + y_{\nu\zeta 2}\zeta_2 + y_{\nu\zeta 3}\zeta_3)\frac{llH_uH_u}{\Lambda^2} \tag{4.2.2}$$

where Λ is the cutoff scale and y's are dimensionless couplings. Decomposing the first term (which is in a $\mathbf{3} \times \mathbf{3} \times \mathbf{3}$ form of A_4) into A_4 singlets, we get

$$ll\phi_\nu = (2l_el_e - l_\mu l_\tau - l_\tau l_\mu)\phi_{\nu 1} + (2l_\mu l_\mu - l_e l_\tau - l_\tau l_e)\phi_{\nu 2} + (2l_\tau l_\tau - l_e l_\mu - l_\mu l_e)\phi_{\nu 3}$$

Similarly, the decomposition of the last three terms into A_4 singlet gives

$$ll\zeta_1 = (l_el_e + l_\mu l_\tau + l_\tau l_\mu)\zeta_1$$

$$ll\zeta_2 = (l_\mu l_\mu + l_e l_\tau + l_\tau l_e)\zeta_2$$

$$ll\zeta_3 = (l_\tau l_\tau + l_e l_\mu + l_\mu l_e)\zeta_3$$

Assuming the vacuum alignments of the scalars as $\langle\phi_\nu\rangle = \alpha_\nu\Lambda(1,1,1), \langle\zeta_1\rangle = \alpha_\zeta\Lambda$, $\langle\zeta_{2,3}\rangle = 0$, the neutrino mass matrix can be written as

$$m_{LL} = \frac{v_u^2}{\Lambda}\begin{pmatrix} a+2d/3 & -d/3 & -d/3 \\ -d/3 & 2d/3 & a-d/3 \\ -d/3 & a-d/3 & 2d/3 \end{pmatrix}, \tag{4.2.3}$$

where $d = y_{\nu\phi}\alpha_\nu, a = y_{\nu\zeta 1}\alpha_\zeta$ and v_u is the vev of H_u. The above mass matrix has eigenvalues $m_1 = \frac{v_u^2}{\Lambda}(a+d)$, $m_2 = \frac{v_u^2}{\Lambda}a$ and $m_3 = \frac{v_u^2}{\Lambda}(-a+d)$. Without adopting any un-natural fine tuning condition to relate the mass eigenvalues further, we wish to keep all the three neutrino mass eigenvalues as free parameters in the A_4 symmetric theory at high energy and determine the most general parameter space at high energy scale which can reproduce the correct neutrino oscillation data at low energy through renormalization group evolution (RGE).

Such a parameterization of the neutrino mass matrix however, does not disturb the generic features of the model for example, the $\mu-\tau$ symmetric nature of m_{LL}, TBM type mixing as well the diagonal nature of the charged lepton mass matrix, which at leading order (LO) is given by [56–58]

$$m_l = v_d\alpha_l\begin{pmatrix} y_e & 0 & 0 \\ 0 & y_\mu & 0 \\ 0 & 0 & y_\tau \end{pmatrix} \tag{4.2.4}$$

Here v_d is the vev of H_d; y_e, y_μ, y_τ and α_l are dimensionless couplings. These matrices in the leptonic sector given by (4.2.3) and (4.2.4) are used in the next section for numerical analysis.

4.3 RGE for neutrino masses and mixing

The left-handed Majorana neutrino mass matrix m_{LL} which is generally obtained from seesaw mechanism at high scale M_R, is usually expressed in terms of $K(t)$, the

coefficient of the dimension five neutrino mass operator [59–62] in a scale-dependent manner [63, 64],

$$m_{LL}(t) = v_u^2 K(t), \tag{4.3.1}$$

where $t = \ln(\mu/1GeV)$ and the vev is $v_u = v_0 \sin\beta$ with $v_0 = 174$ GeV in MSSM. The neutrino mass eigenvalues m_i and the Pontecorvo-Maki-Nakagawa-Sakata (PMNS) mixing matrix U_{PMNS} [65, 66] are then extracted through the diagonalization of $m_{LL}(t)$ at every point in the energy scale t using the equations (4.3.1),

$$m_{LL}^{\rm diag} = {\rm diag}(m_1, m_2, m_3) = V_{\nu L}^T m_{LL} V_{\nu L}, \tag{4.3.2}$$

and $U_{PMNS} = V_{\nu L}$ in the basis where the charged lepton mass matrix is diagonal. The PMNS mixing matrix,

$$U_{PMNS} = \begin{pmatrix} U_{e1} & U_{e2} & U_{e3} \\ U_{\mu 1} & U_{\mu 2} & U_{\mu 3} \\ U_{\tau 1} & U_{\tau 2} & U_{\tau 3} \end{pmatrix}, \tag{4.3.3}$$

is usually parameterized in terms of the product of three rotations $R(\theta_{23})$, $R(\theta_{13})$ and $R(\theta_{12})$, (neglecting CP violating phases) by

$$U_{PMNS} = U_l^\dagger U_\nu = \begin{pmatrix} c_{13}c_{12} & c_{13}s_{12} & s_{13} \\ -c_{23}s_{12} - c_{12}s_{13}s_{23} & c_{12}c_{23} - s_{12}s_{13}s_{23} & c_{13}s_{23} \\ s_{12}s_{23} - c_{12}s_{13}c_{23} & -c_{12}s_{23} - c_{23}s_{13}s_{12} & c_{13}c_{23} \end{pmatrix}, \tag{4.3.4}$$

where U_l is unity in the basis where charge lepton mass matrix is diagonal, $s_{ij} = \sin\theta_{ij}$ and $c_{ij} = \cos\theta_{ij}$ respectively.

The RGE's for v_u and the eigenvalues of coefficient $K(t)$ in equation (4.3.1), defined in the basis where the charged lepton mass matrix is diagonal, can be expressed as [67, 69]

$$\frac{d}{dt}\ln v_u = \frac{1}{16\pi^2}[\frac{3}{20}g_1^2 + \frac{3}{4}g_2^2 - 3h_t^2] \tag{4.3.5}$$

$$\frac{d}{dt}\ln K = -\frac{1}{16\pi^2}[\frac{6}{5}g_1^2 + 6g_2^2 - 6h_t^2 - \delta_{i3}h_\tau^2 - \delta_{3j}h_\tau^2] \tag{4.3.6}$$

Neglecting h_μ^2 and h_e^2 compared to h_τ^2, and taking scale-independent vev as in equation (4.3.1), we have the complete RGE's for three neutrino mass eigenvalues,

$$\frac{d}{dt}m_i = \frac{1}{16\pi^2}[(-\frac{6}{5}g_1^2 - 6g_2^2 + 6h_t^2) + 2h_\tau^2 U_{\tau i}^2]m_i. \tag{4.3.7}$$

The above equations together with the evolution equations for mixing angles (4.3.16-4.3.17), are used for the numerical analysis in our work.

The approximate analytical solution of equation (4.3.7) can be obtained by taking static mixing angle $U_{\tau i}^2$ in the integration range as [68]

$$m_i(t_0) = m_i(t_R)exp(\frac{6}{5}I_{g1} + 6I_{g2} - 6I_t)exp(-2U_{\tau i}^2 I_\tau) \tag{4.3.8}$$

The integrals in the above expression are usually defined as [63, 64, 68]

$$I_{gi}(t_0) = \frac{1}{16\pi^2}\int_{t_0}^{t_R} g_i^2(t)dt \tag{4.3.9}$$

and

$$I_f(t_0) = \frac{1}{16\pi^2}\int_{t_0}^{t_R} h_f^2(t)dt \tag{4.3.10}$$

where $i = 1, 2, 3$ and $f = t, b, \tau$ respectively. For a two-fold degenerate neutrino masses that is, $m_{LL}^{diag} = \text{diag}(m, m, m') = U_{PMNS}^T m_{LL} U_{PMNS}$, the equation (4.3.8) is further simplified to the following expressions

$$m_1(t_0) \approx m(t_R)(1 + 2\delta_\tau(c_{12}s_{13}c_{23} - s_{12}s_{23})^2) + O(\delta_\tau^2) \tag{4.3.11}$$

$$m_2(t_0) \approx m(t_R)(1 + 2\delta_\tau(c_{23}s_{13}s_{12} + c_{12}s_{23})^2) + O(\delta_\tau^2) \tag{4.3.12}$$

$$m_3(t_0) \approx m'(t_R)(1 + 2\delta_\tau(c_{13}c_{23})^2) + O(\delta_\tau^2). \tag{4.3.13}$$

While deriving the above expressions, the following approximations are used

$$\exp(-2|U_{\tau i}|^2 I_\tau) \simeq 1 - 2|U_{\tau i}|^2 I_\tau = 1 + 2|U_{\tau i}|^2\delta_\tau$$

$$-\delta_\tau = I_\tau \simeq \frac{1}{\cos^2\beta}(m_\tau/4\pi v)^2 \ln(M_R/m_t)$$

The sign of the quantity δ_τ in MSSM depends on the neutrino mixing matrix parameters and the approximation on δ_τ taken here is valid only if t_0 is associated with the top quark mass. From equations (4.3.11) and (4.3.12), the low energy solar neutrino mass scale is then obtained as

$$\triangle m_{21}^2(t_0) = m_2^2 - m_1^2 \approx 4\delta_\tau m^2(\cos 2\theta_{12}(s_{23}^2 - s_{13}^2 c_{23}^2) + s_{13}\sin 2\theta_{12}\sin 2\theta_{23}) + O(\delta_\tau^2) \tag{4.3.14}$$

4.3.1 Evolution equations for mixing angles

The corresponding evolution equations for the PMNS matrix elements U_{fi} are given by [67]

$$\frac{dU_{fi}}{dt} = -\frac{1}{16\pi^2}\sum_{k\neq i}\frac{m_k + m_i}{m_k - m_i}U_{fk}(U^T H_e^2 U)_{ki}, \tag{4.3.15}$$

where $f = e, \mu, \tau$ and $i, k = 1, 2, 3$ respectively. Here H_e is the Yukawa coupling matrices of the charged leptons in the diagonal basis and

$$(U^T H_e^2 U)_{ki} = h_\tau^2(U_{k\tau}^T U_{\tau i}) + h_\mu^2(U_{k\mu}^T U_{\mu i}) + h_e^2(U_{ke}^T U_{ei})$$

Neglecting h_μ^2 and h_e^2 as before and denoting $A_{ki} = \frac{m_k + m_i}{m_k - m_i}$, equation (4.3.15) simplifies to [67]

$$\frac{ds_{12}}{dt} = \frac{1}{16\pi^2}h_\tau^2 c_{12}[c_{23}s_{13}s_{12}U_{\tau 1}A_{31} - c_{23}s_{13}c_{12}U_{\tau 2}A_{32} + U_{\tau 1}U_{\tau 2}A_{21}], \tag{4.3.16}$$

$$\frac{ds_{13}}{dt} = \frac{1}{16\pi^2}h_\tau^2 c_{23}c_{13}^2[c_{12}U_{\tau 1}A_{31} + s_{12}U_{\tau 2}A_{32}], \tag{4.3.17}$$

$$\frac{ds_{23}}{dt} = \frac{1}{16\pi^2}h_\tau^2 c_{23}^2[-s_{12}U_{\tau 1}A_{31} + c_{12}U_{\tau 2}A_{32}]. \tag{4.3.18}$$

These equations are valid for a generic MSSM with the minimal field content and are independent of the flavor symmetry structure at high energy scale.

4.4 Numerical analysis and results

For the analysis of the RGE's, equations (4.3.7),(4.3.16)-(4.3.18) for neutrino masses and mixing angles, here we follow two consecutive steps (i) bottom-up running [68] in the first place, and then (ii) top-down running [63, 64] in the next. In the first step (i), the running of the RGE's for the third family Yukawa couplings (h_t, h_b, h_τ) and three gauge couplings (g_1, g_2, g_3) in MSSM , are carried out from top-quark mass scale $(t_0 = \ln m_t)$ at low energy end to high energy scale M_R [68, 69]. In the present analysis we consider the high scale value as the unification scale $M_R = 1.6 \times 10^{16}$ GeV, with different $\tan\beta$ input values to check the stability of the model at low energy scale. For simplicity of the calculation, the SUSY breaking scale is taken at the top-quark mass scale $t_0 = \ln m_t$ [63, 64, 68]. We adopt the standard procedure to get the values of gauge couplings at top-quark mass scale from the experimental CERN-LEP measurements at M_Z, using one-loop RGE's, assuming the existence of a one-light Higgs doublet and five quark flavors below m_t scale [68,69]. Using CERN-LEP data, $M_Z = 91.187GeV$,$\alpha_s(M_Z) = 0.118 \pm 0.004$, $\alpha_1^{-1}(M_Z) = 127.9 \pm 0.1$, $sin^2\theta_W(M_Z) = 0.2316 \pm 0.0003$, and SM relations,

$$\frac{1}{\alpha_1(M_Z)} = \frac{3}{5}\frac{(1 - sin^2\theta_W(M_Z))}{\alpha(M_Z)}, \frac{1}{\alpha_2(M_Z)} = \frac{sin^2\theta_W(M_Z)}{\alpha(M_Z)} \quad , g_i^2 = 4\pi\alpha_i, \qquad (4.4.1)$$

we calculate the gauge couplings at M_Z scale, $\alpha_1(M_Z) = 0.0169586$, $\alpha_2(M_Z) = 0.0337591$, $\alpha_3(M_Z) = 0.118$. As already mentioned, we consider the existence of one light Higgs doublet $(n_H = 1)$ and five quark flavors $(n_F = 5)$ in the scale $M_Z - m_t$. Using one-loop RGE's of gauge couplings, we get $g_1(m_t) = 0.463751$, $g_2(m_t) = 0.6513289$ and $g_3(m_t) = 1.1891996$. Similarly, the Yukawa couplings are also evaluated at top-quark mass scale for input values of $m_t(m_t) = 174$ GeV, $m_b(m_t) = 4.25$ GeV, $m_\tau(m_t) = 1.785$ GeV and the QED-QCD rescaling factors $\eta_b = 1.55$, $\eta_\tau = 1.015$ in the standard fashion [69],

$$h_t(m_t) = \frac{m_t(m_t)\sqrt{1+tan^2\beta}}{174tan\beta},$$
$$h_b(m_t) = \frac{m_b(m_t)\sqrt{1+tan^2\beta}}{174},$$
$$h_\tau(m_t) = \frac{m_\tau(m_t)\sqrt{1+tan^2\beta}}{174}. \tag{4.4.2}$$

where $m_b(m_t) = \frac{m_b(m_b)}{\eta_b}$, $m_\tau(m_t) = \frac{m_\tau(m_\tau)}{\eta_\tau}$. The one-loop RGE's for top quark, bottom quark and τ-lepton Yukawa couplings in the MSSM in the range of mass scales $m_t \leq \mu \leq M_R$ are given by

$$\frac{d}{dt}h_t = \frac{h_t}{16\pi^2}(6h_t^2 + h_b^2 - \sum_{i=1}^{3} c_i g_i^2), \tag{4.4.3}$$

$$\frac{d}{dt}h_b = \frac{h_b}{16\pi^2}(6h_b^2 + h_\tau^2 + - \sum_{i=1}^{3} c_i^{'} g_i^2), \tag{4.4.4}$$

$$\frac{d}{dt}h_\tau = \frac{h_\tau}{16\pi^2}(4h_\tau^2 + 3h_b^2 - \sum_{i=1}^{3} c_i^{''} g_i^2), \tag{4.4.5}$$

where

$$c_i = \begin{pmatrix} \frac{13}{15} \\ 3 \\ \frac{16}{3} \end{pmatrix}, c_i^{'} = \begin{pmatrix} \frac{7}{15} \\ 3 \\ \frac{16}{3} \end{pmatrix}, c_i^{''} = \begin{pmatrix} \frac{9}{5} \\ 3 \\ 0 \end{pmatrix}. \tag{4.4.6}$$

The two-loop RGE's for the gauge couplings are similarly expressed in the range of mass scales $m_t \leq \mu \leq M_R$ as

$$\frac{d}{dt}g_i = \frac{g_i}{16\pi^2}[b_i g_i^2 + \frac{1}{16\pi^2}(\sum_{j=1}^{3} b_{ij} g_i^2 g_j^2) - \sum_{j=t,b,\tau}^{3} a_{ij} g_i^2 h_j^2)], \tag{4.4.7}$$

where

$$b_i = \begin{pmatrix} 6.6 \\ 1 \\ -3 \end{pmatrix}, b_{ij} = \begin{pmatrix} 7.9 & 5.4 & 17 \\ 1.8 & 25 & 24 \\ 2.2 & 9 & 14 \end{pmatrix}, a_{ij} = \begin{pmatrix} 5.2 & 2.8 & 3.6 \\ 6 & 6 & 2 \\ 4 & 4 & 0 \end{pmatrix}. \tag{4.4.8}$$

Values of h_t, h_b, h_τ, g_1, g_2, g_3 evaluated for $\tan\beta = 55$ at high scale $M_R = 1.6 \times 10^{16}$ from equation (4.4.3)-(4.4.5) and (4.4.7) are

$$h_t(M_R) = 0.142685458, h_b(M_R) = 0.378832042$$
$$h_\tau(M_R) = 0.380135357, g_1(M_R) = 0.381783873$$
$$g_2(M_R) = 0.377376229, g_3(M_R) = 0.374307543$$

In the second step (ii), the running of three neutrino masses (m_1, m_2, m_3) and mixing angles (s_{12}, s_{23}, s_{13}) are carried out together with the running of Yukawa and gauge couplings, from high scale $t_R(= lnM_R)$ to low scale t_o. In this case, we use the input values of Yukawa and gauge couplings evaluated earlier at scale t_R from the first stage running of RGE's in case (i). In principle, one can evaluate neutrino masses and mixing angles at every point of the energy scale. It can be noted that in the present problem, the running of other SUSY parameters such as M_0, $M_{1/2}$, μ, are not required and hence, it is not necessary to supply their input values.

We are now interested in studying radiative generation θ_{13} for the case when $m_{1,2,3} \neq 0$ and $s_{13} = 0$ at high energy scale. Such studies can give the possible origin of the reactor angle in a broken A_4 model. During the running of mass eigenvalues and mixing angles from high to low scale, the non-zero input value of mass eigenvalues $m_{1,2,3}$ will induce radiatively a non-zero values of s_{13}. Similar approach was followed in [70,71] considering $m_3 = 0$. The authors in [70,71] used inverted hierarchy neutrino mass pattern $(m, -m, 0)$ at high scale. Such a specific structure of mass eigenvalues however, require fine tuning conditions in the flavor symmetry model at high energy. Instead of assuming a specific relation between mass eigenvalues at high energy scale, here we attempt to find out the most general mass eigenvalues at high energy which can give rise to the correct neutrino data at low energy scale. The only assumption in our work is the opposite CP phases i.e. $(m_1, -m_2, m_3)$. In another work [72],

authors have shown the radiative generation of $\triangle m^2_{21}$ considering the non-zero θ_{13} at high scale and tanβ values lower than 50. They have also shown that Δm^2_{21} can run from zero at high energy to the observed value at the low energy scale, only if θ_{13} is relatively large and the Dirac CP-violating phase is close to π. The running effects can be observed only when θ_{13} is non-zero at high-energy scale as per their analysis. In the present work, θ_{13} is assumed to be zero at high scale consistent with a TBM type mixing within A_4 symmetric model. We also examine the running behavior of neutrino parameters in a neutrino mass model obeying special kind of μ-τ symmetry at high scale, which was not studied in the earlier work mentioned above.

Input Values		Output Values for different tanβ					
–	–	tanβ=15	tanβ=25	tanβ=40	tanβ=45	tanβ=50	tanβ=55
m_1 (eV)	0.0924619	0.0924619	0.0925375	0.0933433	0.0945343	0.0978126	0.1086331
m_2 (eV)	-0.0938539	-0.0938539	-0.0939295	-0.0947101	-0.0958434	-0.0989746	-0.1089959
m_3 (eV)	0.0853599	0.0853599	0.0854102	0.0860902	0.0870723	0.0897417	0.0979824
sinθ_{23}	0.707107	0.7070999	0.7066970	0.7030523	0.6975724	0.6831660	0.6398494
sinθ_{13}	0.00	0.0000655	0.0006287	0.0081088	0.0188213	0.0467352	0.1265871
sinθ_{12}	0.57735	0.57735	0.57735	0.57735	0.5774592	0.5779958	0.5820936

Table 4.2: Input and output values with different tanβ values for Inverted Hierarchy

For a complete numerical analysis, first we parameterize the neutrino mass matrix to have a TBM type structure with eigenvalues in the form $(m_1, -m_2, m_3)$. Since the mixing angles at high energy scale are fixed (TBM type), we only need to provide three input values namely, m_1, m_2, m_3. Using these values at the high energy scale, neutrino parameters are computed at low energy scale by simultaneously solving the RGE's discussed above. We first allow moderate as well as large hierarchies between the lightest and the heaviest mass eigenvalues (with the lighter being at least two orders of magnitudes smaller) of both normal and inverted type and find that the

output values of θ_{13} do not lie in the experimentally allowed range for all values of $\tan\beta = 15, 25, 40, 45, 50, 55$ used in our analysis.

Input Values		Output Values for different tanβ					
–	–	tanβ=15	tanβ=25	tanβ=40	tanβ=45	tanβ=50	tanβ=55
m_1 (eV)	0.0992596	0.0992596	0.0993352	0.1001914	0.1014757	0.1049422	0.1159424
m_2 (eV)	-0.1000997	-0.1000996	-0.1001752	-0.1010062	-0.1022256	-0.1055608	-0.1162467
m_3 (eV)	0.1085996	0.1085996	0.1086751	0.1095313	0.1107905	0.1142319	0.1253917
sinθ_{23}	0.707107	0.7070999	0.7073014	0.7107263	0.7159094	0.7305902	0.7876961
sinθ_{13}	0.00	0.0000582	0.0005604	0.0073647	0.0176199	0.0474922	0.1684841
sinθ_{12}	0.57735	0.57735	0.57735	0.57735	0.5774410	0.5780104	0.5857702

Table 4.3: Input and output values with different tanβ values for Normal Hierarchy

We then consider very mild hierarchical pattern of mass eigenvalues keeping them in the same order of magnitude range. We vary the neutrino mass eigenvalues at high energy scale in the range $0.01 - 0.12$ eV and generate the neutrino parameters at low energy. We restrict the neutrino parameters $\theta_{13}, \theta_{12}, \theta_{23}$ and Δm^2_{21} at low energy to be within the allowed 3σ range and show the variation of $\Delta m^2_{23}(\text{IH}), \Delta m^2_{31}(\text{NH})$ at low energy with respect to the input mass eigenvalues at high energy. We show the results in figure 4.1, 4.2, 4.3, 4.4, 4.5 and 4.6 for a specific value of tan$\beta = 55$. It can be seen from these figures that the correct value of neutrino parameters at low energy can be obtained only for large values of mass eigenvalues at high energy scale $|m_{1,2,3}| = 0.08 - 0.12$ eV. We then choose two specific sets of mass eigenvalues at high energy scale corresponding to inverted hierarchy and normal hierarchy respectively and show the evolution of several neutrino observables including oscillation parameters, effective neutrino mass $m_{ee} = |\sum_i U^2_{ei} m_i|$, sum of absolute neutrino masses $\sum_i |m_i|$ in figure 4.7, 4.8, 4.9, 4.10, 4.11, 4.12, 4.13, 4.14, 4.15, 4.16, 4.17, 4.18, 4.19, 4.20. It can be seen from figure 4.7 and 4.14 that the correct value of θ_{13} can be obtained at low

energy only for very high values of $\tan\beta = 55$. The other neutrino parameters also show a preference for higher $\tan\beta$ values. The output values of neutrino parameters at low energy are given in table 4.2 and 4.3 for both sets of input parameters. The large deviation of θ_{13} at low energy from its value at high energy ($\theta_{13} = 0$ for TBM at high energy) whereas smaller deviation of other two mixing angles can be understood from the RGE equations for mixing angles (4.3.16), (4.3.17), (4.3.18). Using the input values given in table 4.2 and 4.3, the slope of $\sin\theta_{13}$ can be calculated to be $\frac{h_\tau^2}{16\pi^2}(-5.88)$ and $\frac{h_\tau^2}{16\pi^2}(5.23)$ for inverted and normal hierarchies respectively. On the other hand, the slope of $\sin\theta_{23}$ at high energy scale is found to be $\frac{h_\tau^2}{16\pi^2}(2.95)$ and $\frac{h_\tau^2}{16\pi^2}(-2.63)$ for inverted and normal hierarchies respectively. Thus, the lower value of slope for $\sin\theta_{23}$ results in smaller deviation from TBM values compared to that of $\sin\theta_{13}$. We also note from figure 4.12, 4.19 that the sum of the absolute neutrino masses at low energy is 0.315 eV and 0.3555 eV for inverted and normal hierarchy respectively. This lies outside the limit set by the Planck experiment $\Sigma|m_i| < 0.23$ eV [31]. However, there still remains a little room for the sum of absolute mass to lie beyond this limit depending on the cosmological model, as suggested by several recent studies [73–75]. Ongoing as well as future cosmology experiments should be able to rule out or confirm such a scenario.

It is interesting to note that, our analysis shows a preference for very mild hierarchy of either inverted or normal type at high energy scale which also produces a very mild hierarchy at low energy. This can have interesting consequences in the ongoing neutrino oscillation as well as neutrino-less double beta decay experiments. Also, the large $\tan\beta$ region of MSSM (which gives better results in our model) will undergo serious scrutiny at the collider experiments making our model falsifiable both from neutrino as well as collider experiments. We note that the present analysis will be more accurate if the two loop contributions [76–78] RGE's are taken into account.

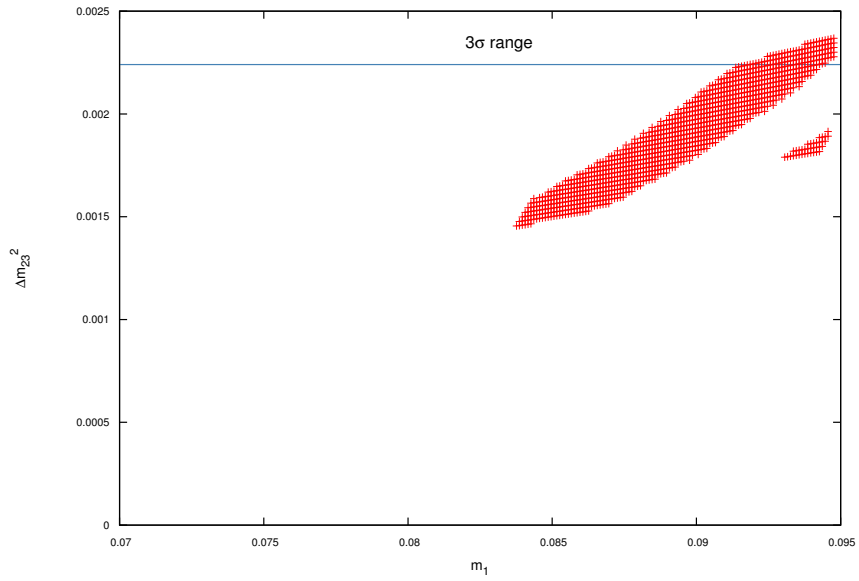

Figure 4.1: Scatter plot of Δm^2_{23} at low energy versus initial value of m_1 at high energy for IH keeping all other neutrino parameters at low energy within 3σ range

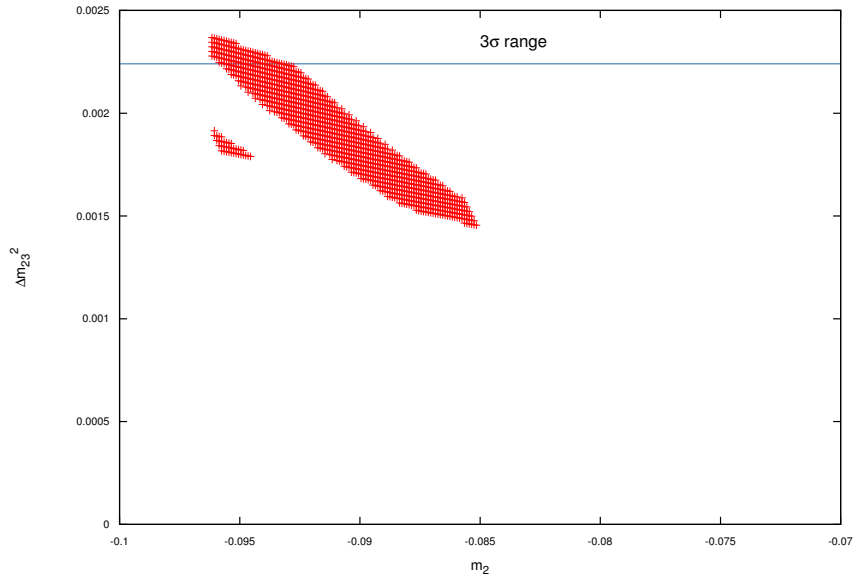

Figure 4.2: Scatter plot of Δm^2_{23} at low energy versus initial value of m_2 at high energy for IH keeping all other neutrino parameters at low energy within 3σ range

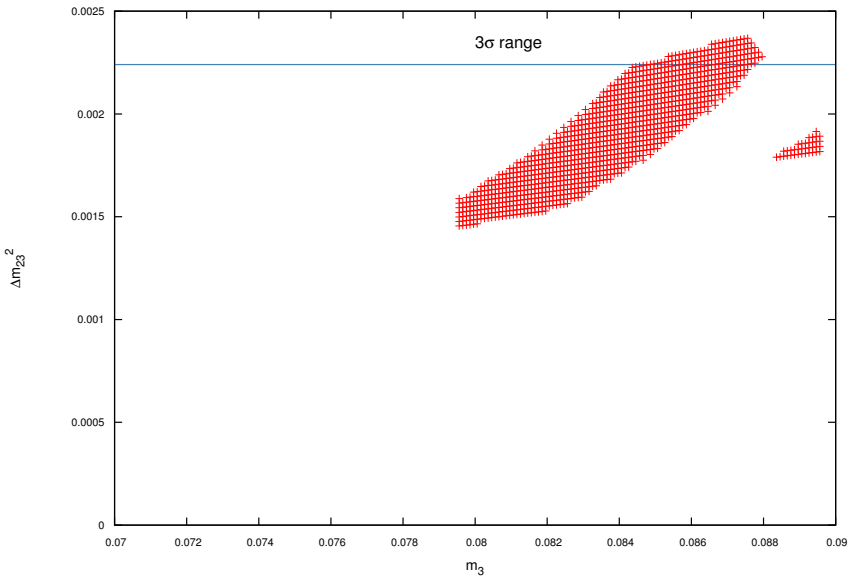

Figure 4.3: Scatter plot of Δm^2_{23} at low energy versus initial value of m_3 at high energy for IH keeping all other neutrino parameters at low energy within 3σ range

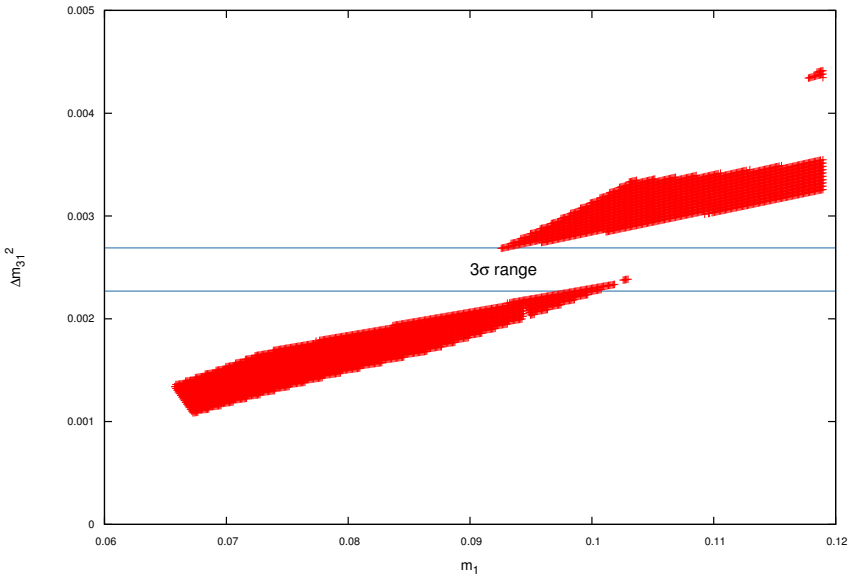

Figure 4.4: Scatter plot of Δm^2_{31} at low energy versus initial value of m_1 at high energy for NH keeping all other neutrino parameters at low energy within 3σ range

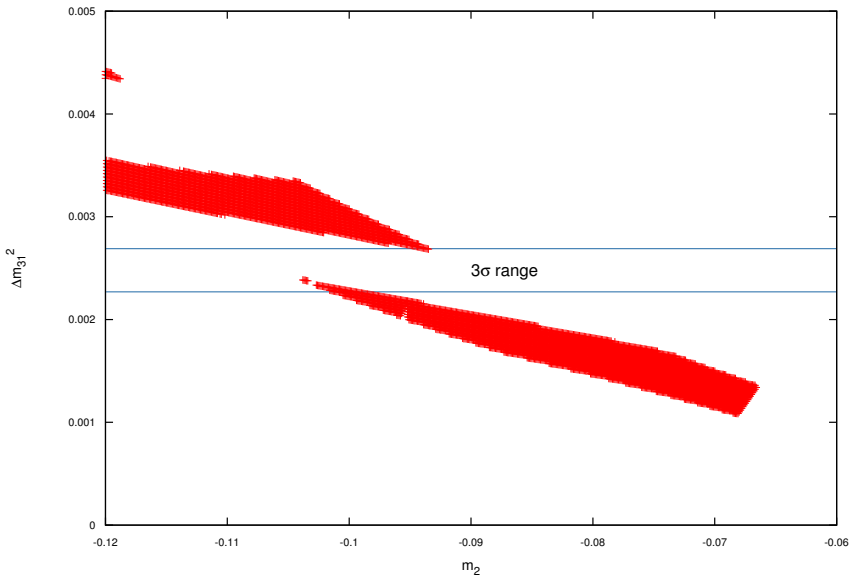

Figure 4.5: Scatter plot of Δm^2_{31} at low energy versus initial value of m_2 at high energy for NH keeping all other neutrino parameters at low energy within 3σ range

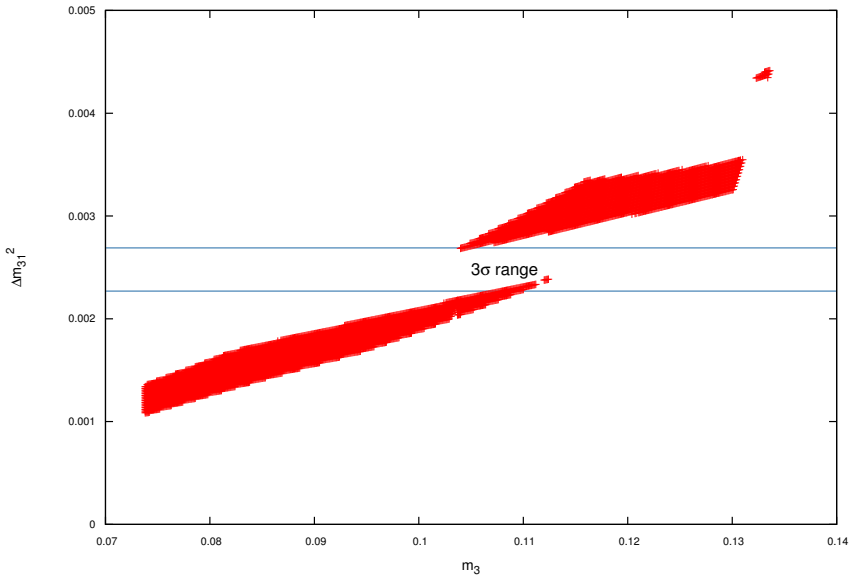

Figure 4.6: Scatter plot of Δm^2_{31} at low energy versus initial value of m_3 at high energy for NH keeping all other neutrino parameters at low energy within 3σ range

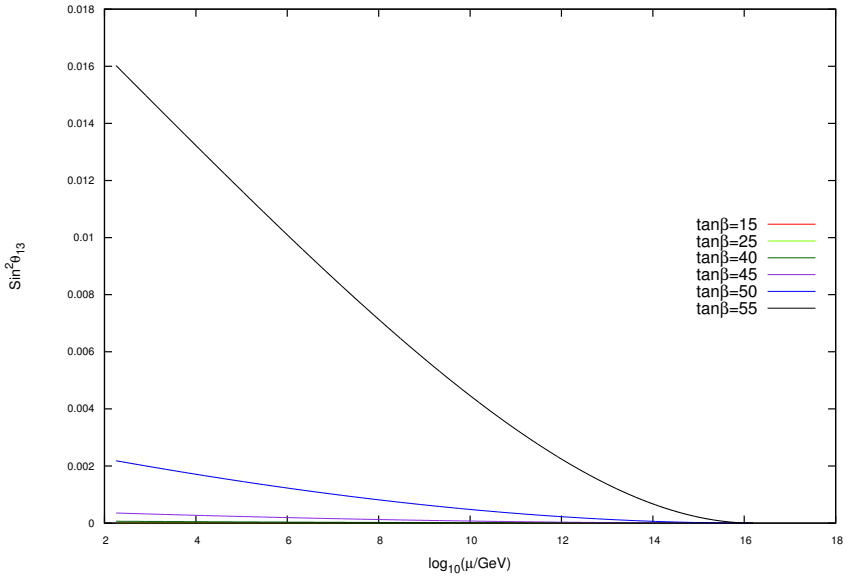

Figure 4.7: Radiative generation of $\sin^2\theta_{13}$ for tanβ=15, 25, 40, 45, 50, 55 for IH using input values given in Table 4.2

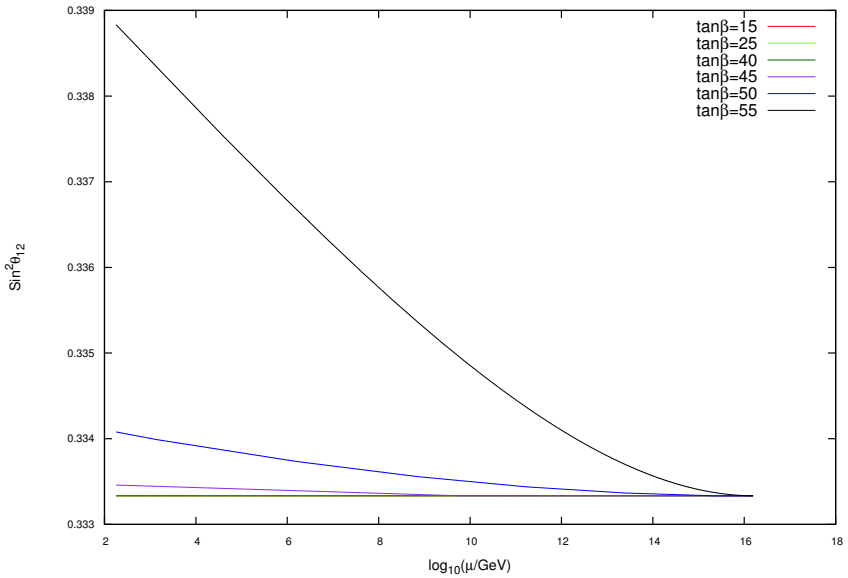

Figure 4.8: Evolution of $\sin^2\theta_{12}$ for tanβ=15, 25, 40, 45, 50, 55 for IH using input values given in Table 4.2

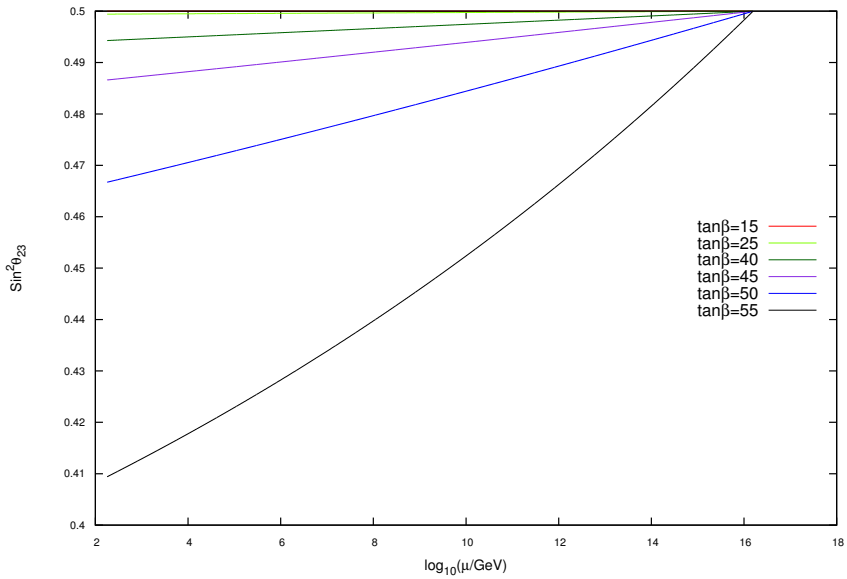

Figure 4.9: Evolution of $\sin^2\theta_{23}$ for tanβ=15, 25, 40, 45, 50, 55 for IH using input values given in Table 4.2

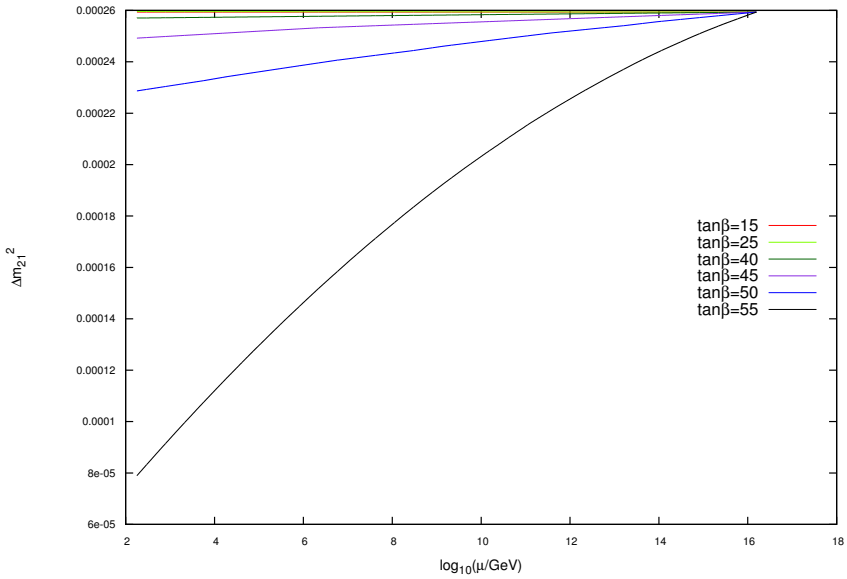

Figure 4.10: Evolution of Δm^2_{21} for tanβ=15, 25, 40, 45, 50, 55 for IH using input values given in Table 4.2

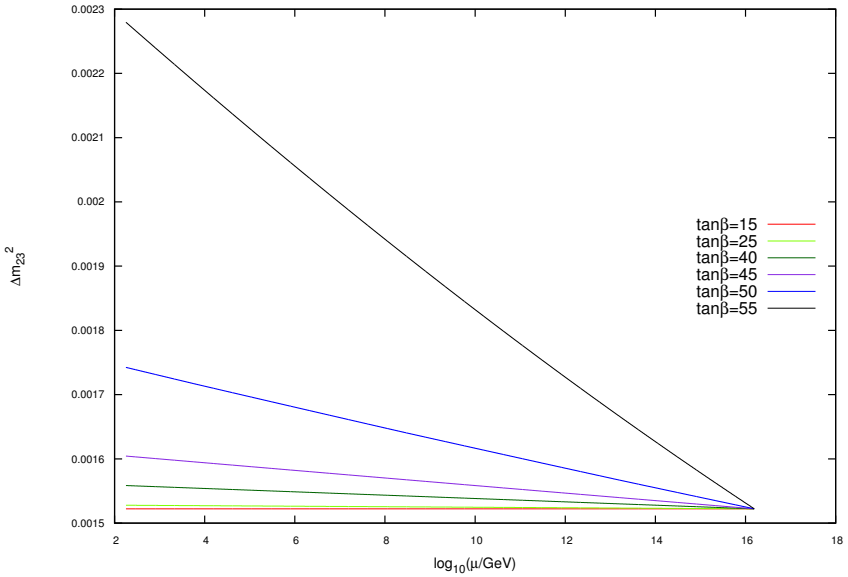

Figure 4.11: Evolution of Δm^2_{23} for tanβ=15, 25, 40, 45, 50, 55 for IH using input values given in Table 4.2

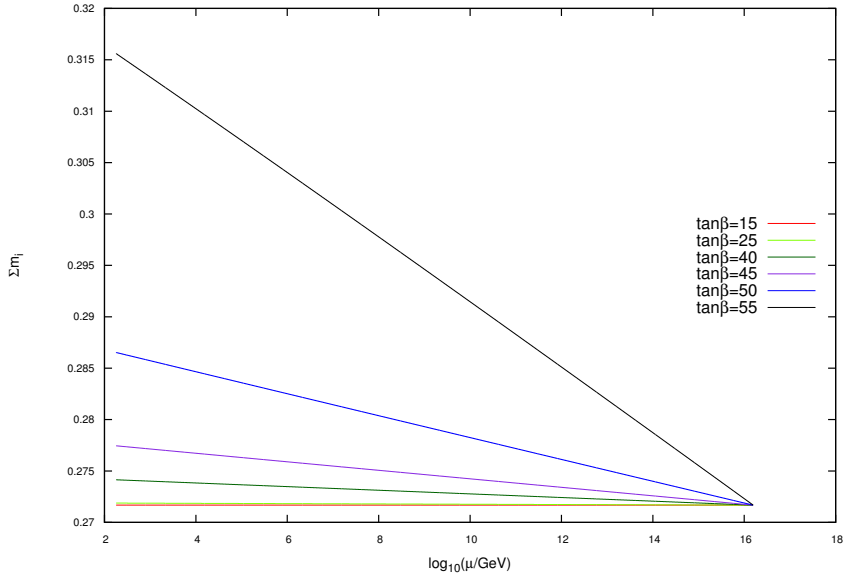

Figure 4.12: Evolution of $\sum_i |m_i|$ for tanβ=15, 25, 40, 45, 50, 55 for IH using input values given in Table 4.2

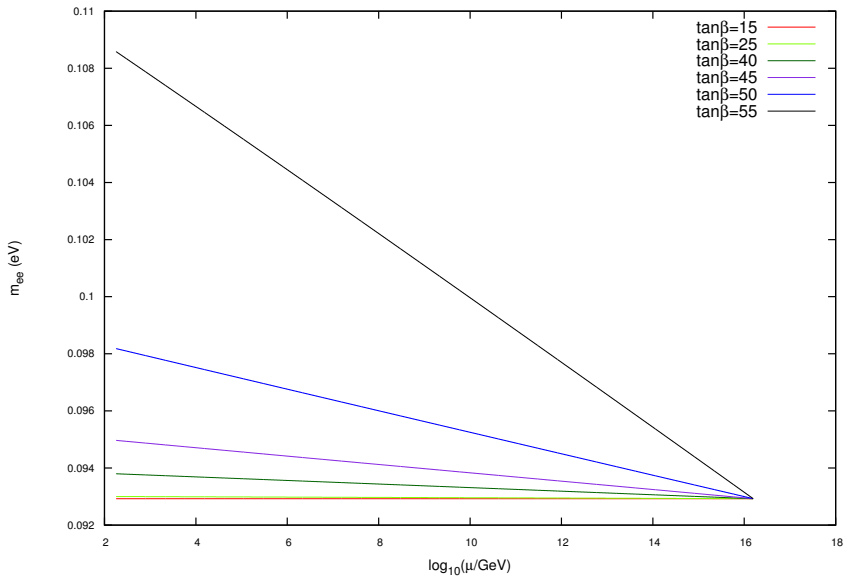

Figure 4.13: Evolution of m_{ee} for tanβ=15, 25, 40, 45, 50, 55 for IH using input values given in Table 4.2

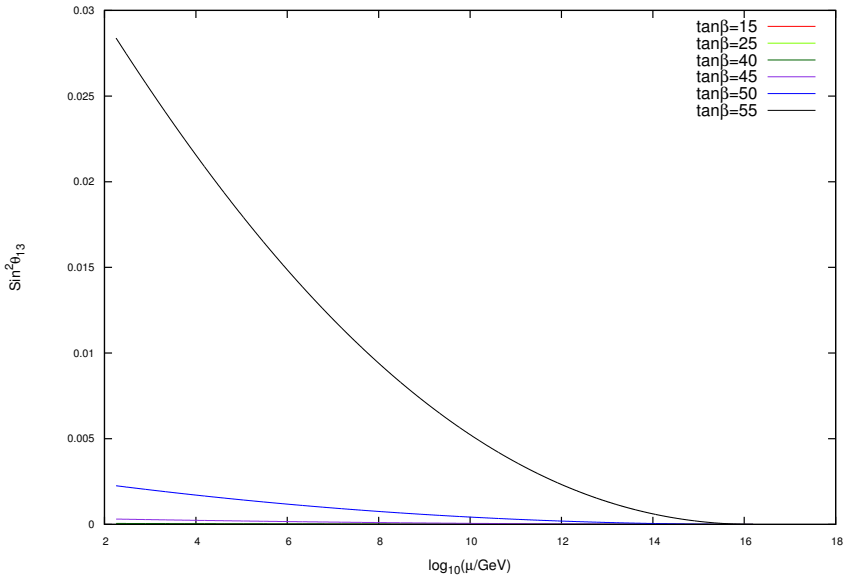

Figure 4.14: Radiative generation of $\sin^2\theta_{13}$ for tanβ=15, 25, 40, 45, 50, 55 for NH using input values given in Table 4.3

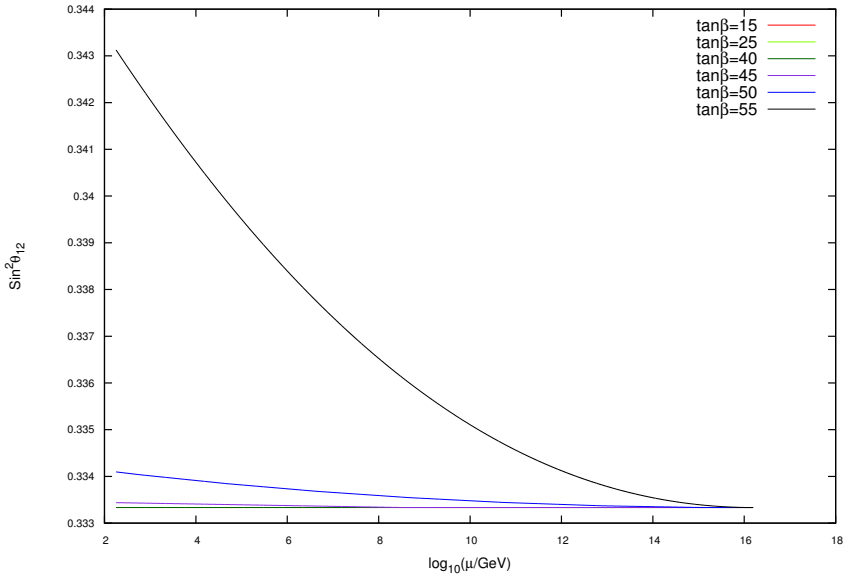

Figure 4.15: Evolution of $\sin^2\theta_{12}$ for tanβ=15, 25, 40, 45, 50, 55 for NH using input values given in Table 4.3

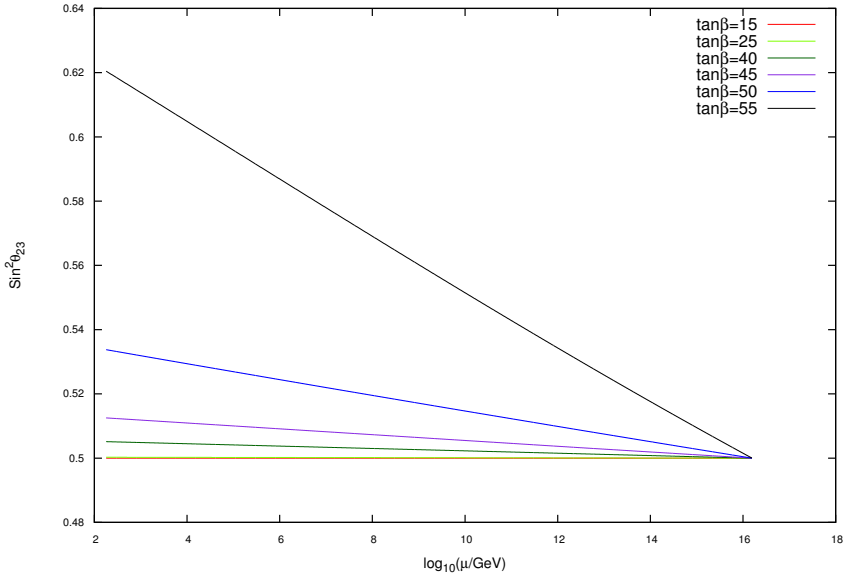

Figure 4.16: Evolution of $\sin^2\theta_{23}$ for tanβ=15, 25, 40, 45, 50, 55 for NH using input values given in Table 4.3

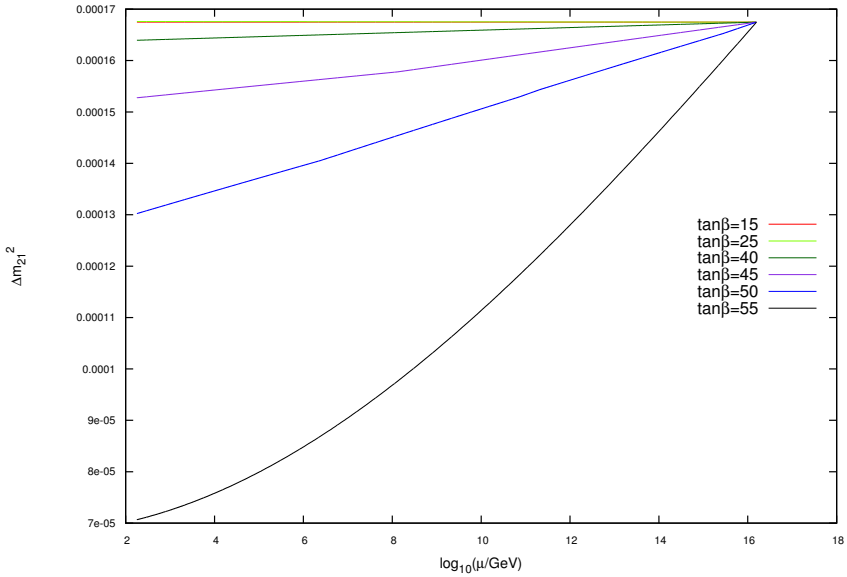

Figure 4.17: Evolution of Δm^2_{21} for tanβ=15, 25, 40, 45, 50, 55 for NH using input values given in Table 4.3

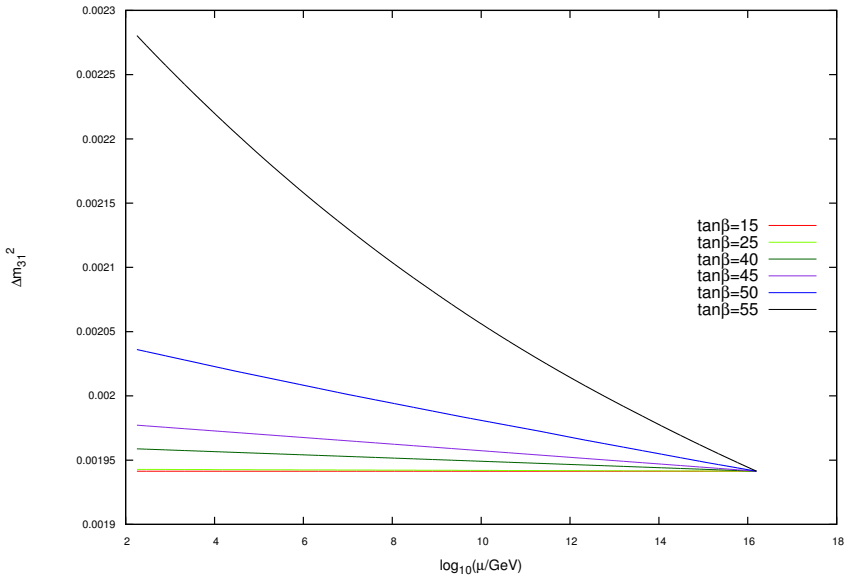

Figure 4.18: Evolution of Δm^2_{31} for tanβ=15, 25, 40, 45, 50, 55 for NH using input values given in Table 4.3

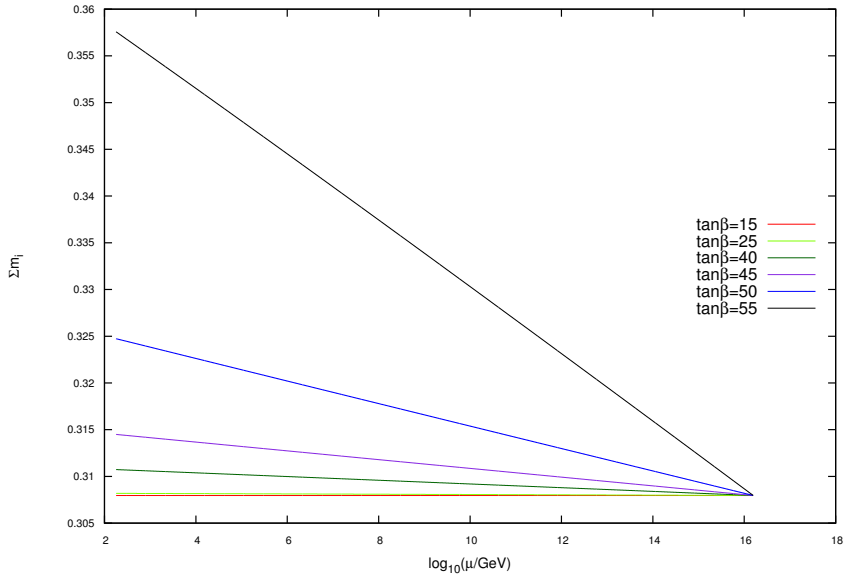

Figure 4.19: Evolution of $\sum_i |m_i|$ for tanβ=15, 25, 40, 45, 50, 55 for NH using input values given in Table 4.3

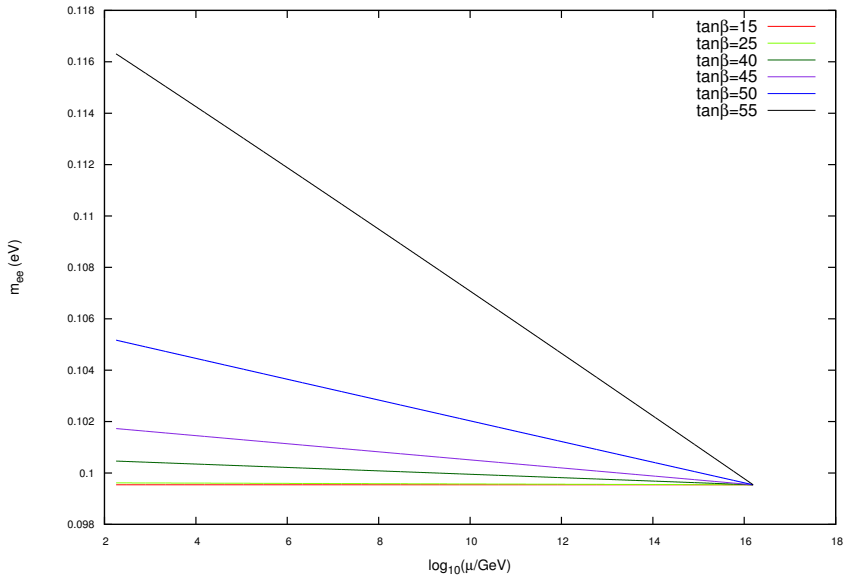

Figure 4.20: Evolution of m_{ee} for tanβ=15, 25, 40, 45, 50, 55 for NH using input values given in Table 4.3

4.5 Conclusion

We have studied the effect of RGE's on neutrino masses and mixing in MSSM with $\mu - \tau$ symmetric neutrino mass model giving TBM type mixing at high energy scale. We incorporate an additional flavor symmetry A_4 at high scale to achieve the desired structure of the neutrino mass matrix. The RGE equations for different neutrino parameters are numerically solved simultaneously for different values of $\tan\beta$ ranging from 15 to 55. We take the three neutrino mass eigenvalues at high energy scale as free parameters and determine the parameter space that can give rise to correct values of neutrino oscillation parameters at low energy. We find that only very mild hierarchy produces correct values of oscillation parameters at low enrgy when the values of $\tan\beta$ is close to 55. We also find that there are no such significant effects on the running of $\sin^2\theta_{23}$, $\sin^2\theta_{12}$ with $\tan\beta$. Similarly, we observe that the sum of the absolute neutrino mass lie above the plank upper bound $\Sigma|m_i| < 0.23$ eV [31].

Bibliography

[1] Fukuda, S., et al. Constraints on neutrino oscillations using 1258 days of Super-Kamiokande solar neutrino data, *Phys. Rev. Lett.*, **86**(25), 5656–5660, 2001.

[2] Ahmad, Q. R., et al. Direct evidence for neutrino flavor transformation from neutral-current interactions in the Sudbury Neutrino Observatory, *Phys. Rev. Lett.*, **89**(1), 011301, 2002.

[3] Ahmad, Q. R., et al. Measurement of day and night neutrino energy spectra at SNO and constraints on neutrino mixing parameters, *Phys. Rev. Lett.*, **89**(1), 011302, 2002.

[4] Bahcall, J. N., & Pena-Garay, C. Solar models and solar neutrino oscillations, *New Journal of Physics*, **6**(1), 63, 2004.

[5] Nakamura, K., et al. Review of particle physics, *J. Phys. G: Nucl. and Part. Phys.*, **37**(7A), 075021, 2010.

[6] Abe, K., et al. Indication of electron neutrino appearance from an accelerator-produced off-axis muon neutrino beam, *Phys. Rev. Lett.*, **107**(4), 041801, 2011.

[7] Abe, Y., et al. Indication of reactor ν_e disappearance in the Double Chooz experiment, *Phys. Rev. Lett.*, **108**(13), 131801, 2012.

[8] An, F. P., et al. Observation of electron-antineutrino disappearance at Daya Bay, *Phys. Rev. Lett.*, **108**(17), 171803, 2012.

[9] Ahn, J. K., et al. Observation of reactor electron antineutrinos disappearance in the RENO experiment, *Phys. Rev. Lett.*, **108**(19), 191802, 2012.

[10] Gonzalez-Garcia, M. C., et al. Global fit to three neutrino mixing: critical look at present precision, *JHEP*, **2012**(12), 1–24, 2012.

[11] Fogli, G. L., et al. Global analysis of neutrino masses, mixings, and phases: Entering the era of leptonic C P violation searches, *Phys. Rev. D*, **86**(1), 013012, 2012.

[12] Borah, D., & Das, M. K. Neutrino masses and mixings with non-zero θ_{13} in type I+ II seesaw models, *Nucl. Phys. B*, **870**(3), 461–476, 2013.

[13] Das, M. K., Borah, D., & Mishra, R. Quasidegenerate neutrinos in type II seesaw models, *Phys. Rev. D*, **86**(9), 095006, 2012.

[14] BenTov, Y., He, X., & Zee, A. An $A_4 \times Z_4$ model for neutrino mixing, *JHEP*, **2012**(12), 1–23, 2012.

[15] Altarelli, G., et al. Discrete flavour groups, θ_{13} and lepton flavour violation, *JHEP*, **2012**(8), 1–43, 2012.

[16] Altarelli, G., & Feruglio, F. Neutrino masses and mixings: A Theoretical perspective, *Phys. Rep.*, **320**(1), 295–318, 1999.

[17] Shimizu, Y., Tanimoto, M., & Watanabe, A. Breaking tri-bimaximal mixing and large θ_{13}, *Prog. Th. Phys.*, **126**(1), 81–90, 2011.

[18] Datta, A., Everett, L., & Ramond, P. Cabibbo haze in lepton mixing, *Phys. Lett. B*, **620**(1), 42–51, 2005.

[19] King, S. F. Tri-bimaximal-Cabibbo mixing, *Phys. Lett. B*, **718**(1), 136–142, 2012.

[20] Duarah, C., Das, A., & Singh, N. N. Charged lepton contributions to bimaximal and tri-bimaximal mixing for generating and, *Phys. Lett. B*, **718**(1), 147–152, 2012.

[21] Francis, N. K., & Singh, N. N. Validity of quasi-degenerate neutrino mass models and their predictions on baryogenesis, *Nucl. Phys. B*, **863**(1), 19–32, 2012.

[22] Brahmachari, B., & Raychaudhuri, A. Perturbative generation of θ_{13} from tribimaximal neutrino mixing, *Phys. Rev. D*, **86**(5), 051302, 2012.

[23] Goswami, S., et al. Large U_{e3} and tribimaximal mixing, *Phys. Rev. D*, **80**(5), 053013, 2009.

[24] Lin, Y., Merlo, L. & Paris, A. Running effects on lepton mixing angles in flavour models with type I seesaw, *Nucl. Phys. B*, **835**(1), 238–261, 2010.

[25] Harrison, P. F., Perkins, D. H., & Scott, W. G. Tri-bimaximal mixing and the neutrino oscillation data, *Phys. Lett. B*, **530**(1), 167–173, 2002.

[26] Harrison, P. F., & Scott, W. G. Symmetries and generalisations of tri-bimaximal neutrino mixing, *Phys. Lett. B*, **535**(1), 163–169, 2002.

[27] Xing, Z. Z. Nearly tri-bimaximal neutrino mixing and CP violation, *Phys. Lett. B*, **533**(1), 85–93, 2002.

[28] Harrison, P. F., & Scott, W. G. $\mu - \tau$ reflection symmetry in lepton mixing and neutrino oscillations, *Phys. Lett. B*, **547**(3), 219–228, 2002.

[29] Harrison, P. F., & Scott, W. G. Permutation symmetry, tri-bimaximal neutrino mixing and the $S3$ group characters, *Phys. Lett. B*, **557**(1), 76–86, 2003.

[30] Harrison, P. F., & Scott, W. G. The simplest neutrino mass matrix, *Phys. Lett. B*, **594**(3), 324–332, 2004.

[31] Ade, P. A. R., et al. Planck 2013 results. XVI, Cosmological parameters, *Astronomy & Astrophysics*, **571**, A16, 2014.

[32] Ishimori, H., et al. Non-Abelian discrete symmetries in particle physics, *Prog. Theor. Phys. Suppl.*, **183**(1), 1–163, 2010.

[33] Grimus, W., & Ludl, P. Finite flavour groups of fermions, *J. Phys. A: Mathematical and Theoretical*, **45**(23), 233001, 2012.

[34] King, S. F., & Luhn, C. Neutrino mass and mixing with discrete symmetry, *Rept. Prog.Phys.*, **76**(5), 056201, 2013.

[35] Altarelli, G., & Feruglio, F. Tri-bimaximal neutrino mixing, $A4$ and the modular symmetry, *Nucl. Phys. B*, **741**(1), 215–235, 2006.

[36] Ma, E., & Wegman, D. Nonzero θ_{13} for neutrino mixing in the context of A_4 symmetry, *Phys. Rev. Lett.*, **107**(6), 061803, 2011.

[37] Gupta, S., Joshipura, A. S., & Patel, K. M. Minimal extension of tribimaximal mixing and generalized $Z_2 \times Z_2$ symmetries, *Phys. Rev. D*, **85**(3), 031903, 2012.

[38] Dev, S., Gautam, R. R., & Singh, L. Broken S_3 symmetry in the neutrino mass matrix and non-zero θ_{13}, *Phys. Lett. B*, **708**(3), 284–289, 2012.

[39] Gu, P., and He, H. Neutrino mass and baryon asymmetry from Dirac seesaw, *JCAP*, **2006**(12), 1–10, 2006.

[40] He, H. J., & Xu, X. J. Octahedral symmetry with geometrical breaking: New prediction for neutrino mixing angle θ_{13} and CP-violation, *Phys. Rev. D*, **86**(11), 111301, 2012.

[41] Branco, G. C., et al. Spontaneous leptonic CP violation and nonzero θ_{13}, *Phys. Rev. D*, **86**(7), 076008, 2012.

[42] Ma, E. Near tribimaximal neutrino mixing with $\Delta(27)$ symmetry, *Phys. Lett. B*, **660**(5), 505–507, 2008.

[43] Plentinger, F., Seidl, G., & Winter, W. Group space scan of flavor symmetries for nearly tribimaximal lepton mixing, *JHEP*, **2008**(04), 077, 2008.

[44] Haba, N., et al. Tribimaximal mixing from cascades, *Phys. Rev. D*, **78**(11), 113002, 2008.

[45] Ge, S.F., Dicus, D. A., & Repko, W. W. Residual symmetries for neutrino mixing with a large θ_{13} and nearly maximal δ_D, *Phys. Rev. D*, **108**(4), 041801, 2012.

[46] Ma, E., and Rajasekaran, G. Softly broken A_4 symmetry for nearly degenerate neutrino masses, *Phys. Rev. D*, **64**(11), 113012, 2001.

[47] Ma, E. A_4 symmetry and neutrinos with very different masses, *Phys. Rev. D*, **70**(3), 031901, 2004.

[48] Araki, T., & Li, Y. F. Q_6 flavor symmetry model for the extension of the minimal standard model by three right-handed sterile neutrinos, *Phys. Rev. D*, **85**(6), 065016, 2012.

[49] Xing, Z.Z. Implications of the Daya Bay observation of θ_{13} on the leptonic flavor mixing structure and CP violation, *Chin. Phys. C*, **36**(4), 281–297, 2012.

[50] Xing, Z. Z. A shift from democratic to tri-bimaximal neutrino mixing with relatively large θ_{13}, *Phys. Lett. B*, **696**(3), 232–236, 2011.

[51] Dev, P. S. B, et al. θ_{13} and proton lifetime in a minimal $SO(10) \times S_4$ model of flavor, *Phys. Rev. D*, **86**(3), 035002, 2012.

[52] Adhikary, B., et al. A_4 symmetry and prediction of U_{e3} in a modified Altarelli–Feruglio model, *Phys. Lett. B*, **638**(4), 345–349, 2006.

[53] Altarelli, G, & Feruglio, F. Discrete flavor symmetries and models of neutrino mixing, *Rev. Mod. Phys.*, **82**(3), 2701–2729, 2010.

[54] Parattu, K. M., & Wingerter, A. Tribimaximal mixing from small groups, *Phys. Rev. D*, **84**(1), 013011, 2011.

[55] Felipe, R. G., Serôdio, H., & Silva, J. P. Neutrino masses and mixing in A_4 models with three Higgs doublets, *Phys. Rev. D*, **88**(1), 015015, 2013.

[56] Altarelli, G., & Feruglio, F. Tri-bimaximal neutrino mixing from discrete symmetry in extra dimensions, *Nucl. Phys. B*, **720**(1), 64–88, 2005.

[57] Altarelli, G., & Meloni, D. A simplest $A4$ model for tri-bimaximal neutrino mixing, *J. Phys. G: Nucl. and Part. Phys.*, **36**(8), 085005, 2009.

[58] Altarelli, G., et al. Discrete flavour groups, θ_{13} and lepton flavour violation, *JHEP*, **2012**(8), 1–43, 2012.

[59] Chankowski, P. H., & Pluciennik, Z. Renormalization group equations for seesaw neutrino masses, *Phys. Lett. B*, **316**(2), 312–317, 1993.

[60] Babu, K. S., Leung, C. N., & Pantaleone, J. Renormalization of the neutrino mass operator, *Phys. Lett. B*, **319**(1), 191–198, 1993.

[61] Antusch, S., et al. Neutrino mass operator renormalization revisited, *Phys. Lett. B*, **519**(3), 238–242, 2001.

[62] Antusch, S., et al. Neutrino mass operator renormalization in two Higgs doublet models and the MSSM, *Phys. Lett. B*, **525**(1), 130–134, 2002.

[63] King, S. F., & Singh, N. N. Renormalisation group analysis of single right-handed neutrino dominance, *Nucl. Phys. B*, **591**(1), 3-25, 2000.

[64] King, S. F., & Singh, N. N. Inverted hierarchy models of neutrino masses, *Nucl. Phys. B*, **596**(1), 81–98, 2001.

[65] B. Pontecorvo, Inverse β processes and nonconsevation of lepton charge,*Sov. Phys. JETP*, **7**, 172, 1958.

[66] Maki, Z., Nakagawa, M., & Sakata, S. Remarks on the unified model of elementary particles, *Prog. Th. Phys.*, **28**(5), 870–880, 1962.

[67] Chankowski, P. H., Krolikowski, W., & Pokorski, S. Fixed points in the evolution of neutrino mixings, *Phys. Lett. B*, **473**(1), 109–117, 2000.

[68] Parida, M. K., & Singh, N. N. Low-energy formulas for neutrino masses with tan β-dependent hierarchy, *Phys. Rev. D*, **59**(3), 32001, 1999.

[69] Singh, N. N. Effects of the scale-dependent vacuum expectation values in the renormalisation group analysis of neutrino masses, *EPJC*, **19**(1), 137–141, 2001.

[70] Joshipura, A. S. Radiative origin of solar scale and U_{e3}, *Phys. Lett. B*, **543**(3), 276–282, 2002.

[71] Joshipura, A. S., & Rindani, S. D. Radiatively generated ν_e oscillations: General analysis, textures, and models, *Phys. Rev. D*, **67**(7), 073009, 2003.

[72] Antusch, S., et al. Running neutrino masses, mixings and CP phases: Analytical results and phenomenological consequences, *Nucl. Phys. B*, **674**(1), 401–433, 2003.

[73] Giusarma, E., et al. Constraints on neutrino masses from Planck and Galaxy Clustering data, *Phys. Rev. D*, **88**(6), 063515, 2013.

[74] Hu, J., et al. Cosmological parameter estimation from CMB and X-ray cluster after Planck, *JCAP*, **2014**(05), 020, 2014.

[75] Giusarma, E., et al. Relic neutrinos, thermal axions, and cosmology in early 2014, *Phys. Rev. D*, **90**(4), 043507, 2014.

[76] Bastero-Gil, M., & Brahmachari, B. Two-loop renormalization group analysis of supersymmetric $SO(10)$ models with an intermediate scale, *Nucl. Phys. B*, **482**(1), 39–58, 1996.

[77] Kielanowski, P. Theorems on the renormalization group evolution of quark Yukawa couplings and CKM matrix, *Phys. Lett. B*, **479**(1), 181–189, 2000.

[78] Ray, S., Rodejohann, W., & Schmidt, M. A. Lower bounds on the smallest lepton mixing angle, *Phys. Rev. D*, **83**(3), 033002, 2011.

Chapter 5

Conclusion and Future Scope

In this chapter, we outlines the major conclusions drawn from the above phenomenological studies which deals with the study of different $\mu - \tau$ symmetric neutrino mass models relationg to the origin of non-zero θ_{13}, the study of one-zero and two zero texture in terms of baryogenesis and the evolution of non-zero θ_{13} using renormalization group equation (RGE). We also discuss the various possible scopes of research in the above mentioned fields in future.

5.1 Conclusion

The significant conclusions as achieved from the present study are summarized chapterwise in the subsections 5.1.1, 5.1.2 and 5.1.3 respectively.

5.1.1 Chapter 2

In chapter 2, we try to generate nonzero θ_{13} by adding a perturbative term to the $\mu - \tau$ symmetric mass matrix using type II seesaw. Here, we consider four different

types of $\mu - \tau$ symmetric mass matrices bimaximal, tribimaximal, hexagonal and golden ratio mixing respectively. We find that

- Except golden ratio mixing with IH and $m_3 = 0.001$ eV, all other mixing patterns give rise to correct θ_{13}.

- We also calculate the other neutrino parameters Δm^2_{21}, Δm^2_{23} (IH), Δm^2_{31} (NH), $\sin^2\theta_{23}$ and $\sin^2\theta_{12}$ and plot them against the type II seesaw strength w. We find that bimaximal mixing with IH, tribimaximal mixing with both IH and NH and hexagonal mixing with $m_3 = 0.001$ give rise to correct values of all the neutrino parameters in 3σ range.

- We then compute baryogenesis through the process of leptogenesis. We observed that bimaximal mixing and tribimaximal mixing with IH and $m_3 = 0.001$ can produce correct baryon asymmetry in 1 flavor and 2 flavor regimes. The values of Dirac CP-phase δ which give rise to exact baryon asymmetry for TBM with IH and $m_3 = 0.001$ ranges from $0.003298676 - 0.0043982297$ & $3.1376656 - 3.13860814$ (1 flavor regime) and 3014190681 (2 flavor regime). For BM with IH and $m_3 = 0.001$, we get the values of δ as 0.000314159, 1.40711935, 4.8754376 (1 flavor regime) and 0.0001570769 (2 flavor regime). Moreover, tribimaximal mixing and hexagonal mixing with NH and $m_1 = 0.0001$ show proper baryon asymmetry in the 1 flavor regime. For these two cases, we get approximately same values of δ. The range of δ for TBM(NH) with $m_1 = 0.0001$ are 3.14269221-3.14300637 & 6.282085749-6.282242829 and for HEX(NH) it is 3.182276-3.1981413 & 6.28020079-6.2808291.

- The golden ratio mixing is disfavored in our framework for both IH and NH cases.

5.1.2 Chapter 3

In chapter 3, we study different possible one-zero and two-zero texture Majorana mass matrices allowed from neutrino oscillation data. For the case of onbe-zero texture, we assume the two Majorana phases to be equal and then calculate it as a function of Dirac CP phase. For two-zero texture case, we calculate all the three CP phases and the lightest neutrino mass separately. Then we adopt a type I seesaw framework, we evaluate the baryon asymmetry through the mechanism of leptogenesis for all possible texture zero mass matrices. The results are pointed below:

- In case of one-zero texture with IH, the patterns G_1 and G_2 do not have real solutions to the lightest neutrino mass and hence they are excluded in calculating baryon asymmetry. Only the patterns $G_{3,4,5,6}$ have solutions. G_3 can produce correct baryogenesis in one and two flavor regime. In our study, only the case G_4 and G_6 (IH) can generate the required baryogenesis in all flavor regimes. The pattern G_5 shows good agreement in one and three flavor regimes.

- Similarly, for one-zero texture with NH, the patterns $G_{1,2,3}$ have real solutions to the lightest neutrino mass and therefore only these cases are taken into account for the study of baryogenesis. We find that G_1 can produce correct baryogenesis in all flavor regimes whereas G_2 and G_3 can produce exact baryogenesis in one flavor regime only.

- For two-zero texture case, all the patterns $A_{1,2}, B_{1,2,4}$ except B_3 can give rise to correct Y_B in one flavor regime depending on the neutrino mass hierarchy. For two flavor regime, only $B_{2,3,4}$ with IH can produce the required baryon asymmetry. Similarly, in three flavor regime B_2 with both IH & NH and $B_{3,4}$ with only IH can give rise to correct Y_B. This implies that if the lightest right-handed neutrino mass $M_1 < 10^{12}$ GeV, then among the six allowed two-zero

textures, only three of them respectively $B_{2,3,4}$ are favored in the light of baryon asymmetry.

5.1.3 Chapter 4

In chapter 4, we study the effect of RGE's on neutrino masses and mixing in MSSM with $\mu - \tau$ symmetric neutrino mass model giving rise to TBM type of mixing in the higher energy scale. We solve the RGE equations for both neutrino masses and mixing angles for different values of $\tan\beta$ ranging from 15 to 55. We choose the three neutrino mass eigenvalues as free parameters at high energy scale and calculate all the neutrino parameter space that can give rise to correct values of oscillation parameters at low energy scale. The results are itemized below:

- Moderate or large hierarchy (both normal and inverted) of neutrino masses at high energy scale does not give rise to correct output at low energy scale.
- Very mild hierarchy (with all neutrino mass eigenvalues having same order of magnitude values and $|m_{1,2,3}| = 0.08-0.12$ eV) give correct results at low energy provided the $\tan\beta$ values are kept high, close to 55. Such a preference towards large mass eigenvalues with all eigenvalues having same order of magnitude values can have tantalizing signatures at oscillation as well as neutrino-less double beta decay experiments.
- No significant changes in running of $\sin^2\theta_{23}$, $\sin^2\theta_{12}$ with $\tan\beta$ are observed.
- Sum of absolute neutrino masses at low energy lie above the Planck upper bound $\Sigma|m_i| < 0.23$ eV hinting towards non-standard cosmology to accommodate a larger $\Sigma|m_i|$ or more relativistic degrees of freedom.
- The preference for high $\tan\beta$ regions of MSSM could go through serious tests at collider experiments pushing the model towards verification or falsification.

5.2 Future Prospects

The thesis mainly consists of study on different neutrino mass models in different prospects to give a rough idea about which hierarchy pattern is most favorable. Since the degenerate hierarchy is already discarded by the oscillation data and hence we constrain our study with NH and IH patterns only. In the present thesis, we discuss different neutrino mass models, different Majorana texture zero mass matrices and evolution of neutrino parameters using RGE considering both type of hierarchies and summarize our results regarding which hierarchy pattern give us better aggrement with the oscillation data. However, it can be made comment easily that we can expand our work by incorporating different approach.

- In our first study, we consider different $\mu - \tau$ symmetric neutrino mass matrices and evalute the neutrino parameters after adding a $\mu - \tau$ symmetry breaking type II seesaw perturbative term. Here, we also study baryogenesis through the mechanism of leptogenesis arising from the decay of lightest right-handed neutrino by considering the presence of both type I and type II seesaws. This work can be further extended by using different perturbative terms which fit under the theory. Again, more precise experimental data from the neutrino oscillation experiments can able to falsify or verify some of the models discussed in this work.

- In our second work, we make a systematic study on one-zero and two-zero Majorana textures and lastly we end with the evaluation of baryon asymmetry considering both NH and IH patterns. We make our final conclusions in the basis of which texture pattern exactly can produce correct baryogenesis depending on the neutrino mass hierarchy. Similar work can be done if we consider the hybrid texture, a combination of both one and two-zero texture. Moreover,

one can also expand studies by incorporating the different Yukawa texture zero patterns.

- In the last chapter, our study is mainly based on RGE effects on the neutrino masses and mixing in MSSM. Here we have not considered the CP phases. This work will be more interesting if the running of the Dirac and Majorana CP phases is taken into account. This work can be further studied by adding the seesaw threshold effects and considering all the right handed neutrinos to decouple at the same high energy scale. Such threshold effects could be important for large values of $\tan\beta$.

LIST OF PUBLICATIONS

In refereed journals:

1. M. Borah, D. Borah, M. K. Das, S. Patra, Perturbations to the $\mu-\tau$ symmetry, leptogenesis, and lepton flavor violation with the type II seesaw mechanism, **Phy. Rev. D**, 90.9 (2014): 095020.

2. M. Borah, D. Borah, M. K. Das, Discriminating Majorana Neutrino Textures in the light of Baryon Asymmetry, **Phy. Rev. D**, 91 (2015), 113008.

3. M. Borah, D. Borah, M. K. Das, Radiative generation of non-zero θ_{13} in MSSM with broken A_4 flavor symmetry, **Nucl. Phys. B**, 885 (2014): 76–96.

Papers presented in conferences:

1. M. Borah, B. Sharma and M. K. Das, **National Conference on Theoretical Physics (NCTP-2013)**, Tezpur University, Napaam, Tezpur, India, 08-12 Feb, 2013.

2. M. Borah and M. K. Das, **National Seminar on Current Trends in Physics Research (NSCTPR-2014)**, Department of Physics, Darrang College, Tezpur, Assam, India, 30th January-1st February, 2014.

3. M. Borah, D. Borah and M. K. Das, **IXth National Conference of Physics Acadamy of North-East (PANE-2014)**, Department of Physics, NERIST, Nirjuli, Arunachal Pradesh, India, 18th – 20th Dec.